NASA/TM—2004-213113

An Experiment on the Near Flow Field of the GE/ARL Mixer Ejector Nozzle

K.B.M.Q. Zaman
Glenn Research Center, Cleveland, Ohio

July 2004

The NASA STI Program Office . . . in Profile

Since its founding, NASA has been dedicated to the advancement of aeronautics and space science. The NASA Scientific and Technical Information (STI) Program Office plays a key part in helping NASA maintain this important role.

The NASA STI Program Office is operated by Langley Research Center, the Lead Center for NASA's scientific and technical information. The NASA STI Program Office provides access to the NASA STI Database, the largest collection of aeronautical and space science STI in the world. The Program Office is also NASA's institutional mechanism for disseminating the results of its research and development activities. These results are published by NASA in the NASA STI Report Series, which includes the following report types:

- TECHNICAL PUBLICATION. Reports of completed research or a major significant phase of research that present the results of NASA programs and include extensive data or theoretical analysis. Includes compilations of significant scientific and technical data and information deemed to be of continuing reference value. NASA's counterpart of peer-reviewed formal professional papers but has less stringent limitations on manuscript length and extent of graphic presentations.

- TECHNICAL MEMORANDUM. Scientific and technical findings that are preliminary or of specialized interest, e.g., quick release reports, working papers, and bibliographies that contain minimal annotation. Does not contain extensive analysis.

- CONTRACTOR REPORT. Scientific and technical findings by NASA-sponsored contractors and grantees.

- CONFERENCE PUBLICATION. Collected papers from scientific and technical conferences, symposia, seminars, or other meetings sponsored or cosponsored by NASA.

- SPECIAL PUBLICATION. Scientific, technical, or historical information from NASA programs, projects, and missions, often concerned with subjects having substantial public interest.

- TECHNICAL TRANSLATION. English-language translations of foreign scientific and technical material pertinent to NASA's mission.

Specialized services that complement the STI Program Office's diverse offerings include creating custom thesauri, building customized databases, organizing and publishing research results . . . even providing videos.

For more information about the NASA STI Program Office, see the following:

- Access the NASA STI Program Home Page at ***http://www.sti.nasa.gov***

- E-mail your question via the Internet to help@sti.nasa.gov

- Fax your question to the NASA Access Help Desk at 301–621–0134

- Telephone the NASA Access Help Desk at 301–621–0390

- Write to:
  NASA Access Help Desk
  NASA Center for AeroSpace Information
  7121 Standard Drive
  Hanover, MD 21076

NASA/TM—2004-213113

An Experiment on the Near Flow Field of the GE/ARL Mixer Ejector Nozzle

K.B.M.Q. Zaman
Glenn Research Center, Cleveland, Ohio

National Aeronautics and
Space Administration

Glenn Research Center

July 2004

Acknowledgments

Thanks are due to Dr. Muni Majjigi of GEAE for initiating the investigation and providing guidance in the choice of the experimental parameters, and to Dr. J. M. Seiner of NASA Langley for his continued support.

Document History

This research was originally published internally as HSR040 in July 1996.

Available from

NASA Center for Aerospace Information
7121 Standard Drive
Hanover, MD 21076

National Technical Information Service
5285 Port Royal Road
Springfield, VA 22100

Available electronically at http://gltrs.grc.nasa.gov

An Experiment on the Near Flow Field of the GE/ARL Mixer Ejector Nozzle

K.B.M.Q. Zaman
National Aeronautics and Space Administration
Glenn Research Center
Cleveland, Ohio 44135

Summary

This report is a documentation of the results on flowfield surveys for the GE/ARL mixer-ejector nozzle carried out in an open jet facility at NASA Glenn Research Center. The results reported are for cold (unheated) flow without any surrounding co-flowing stream. Distributions of streamwise vorticity as well as turbulent stresses, obtained by hot -wire anemometry, are presented for a low subsonic condition. Pitot probe survey results are presented for nozzle pressure ratios up to 3.5. Flowfields both inside and outside of the ejector are considered. Inside the ejector, the mean velocity distribution exhibits a cellular pattern on the cross sectional plane, originating from the flow through the primary and secondary chutes. With increasing downstream distance an interchange of low velocity regions with adjacent high velocity regions takes place due to the action of the streamwise vortices. At the ejector exit, the velocity distribution is nonuniform at low and high pressure ratios but reasonably uniform at intermediate pressure ratios. The effects of two chevron configurations and a tab configuration on the evolution of the downstream jet are also studied. Compared to the baseline case, minor but noticeable effects are observed on the flowfield.

Introduction

In order to achieve jet noise reduction goals for the High Speed Civil Transport (HSCT) aircraft, currently under development, various designs of a mixer-ejector nozzle have been under consideration. Its basic feature includes a two dimensional primary nozzle with multiple chutes which is surrounded by an ejector of rectangular cross section. An earlier model of the nozzle was tested extensively in the Aerodynamic Research Laboratory (ARL) of General Electric Aircraft Engines Company in Cincinnati. Laser doppler velocimeter data for the flowfield and data for the radiated noise field were obtained; these results were summarized in an earlier report (Majjigi, R.K., Brausch, J.F., Askew, J.W., Shin, H., Mengle, V., and Balan, C., "Low Noise Exhaust Nozzle Technology Development", Report on Grant NAS3–25415, April, 1996, not published). While the noise reduction goal continues to be pursued through testing with later generations of the nozzle, the earlier model was brought to Glenn to carry out relatively fundamental measurements in an effort to further understand the flow mechanisms. The immediate goal in the Glenn study has been to obtain complementary, further details of the flowfield with and without noise suppression devices such as chevrons and tabs. The overall goal has been to look for clues that could lead to improved mixing within the ejector and further spreading of the jet downstream which are thought to hold keys for the desired noise suppression. So far measurements have been conducted with a fixed geometry of the chutes and the ejector, with and without the chevrons and tabs, and the purpose of this report is to document those results.

The specific objectives in the measurements were as follows. (A) For the baseline configuration perform hot-wire surveys for an incompressible flow case inside and outside of the ejector (mean velocity, vorticity and turbulent stresses.). (B) For the baseline configuration perform Pitot probe surveys at various nozzle pressure ratios inside and outside of the ejector (flow uniformity, pumping, jet spreading, etc.). (C) Study effects of "chevrons" and "tabs" on the downstream evolution of the jet.

The main results are presented with composite plots and perspective views of the velocity and vorticity distributions, in figures V.1 to V.15, without any details of the quantitative information. A discussion of each of these figures is listed in the Results section. Details of the data are included in the appendix as contour plots. With the help of the nomenclature section and the annotations on the margin of the appendix figures one should be able to obtain all pertinent details. For cross reference, the corresponding appendix figure numbers are listed in parentheses on each of figures V.1 to V.15.

Nomenclature

D	Equivalent diameter of ejector exit (4.07 in.)
$\dot{m}$	Mass flow rate ($\dot{m}_I$ from flow meter, other data from Pitot probe survey)
M	Mach number
NPR	Nozzle pressure ratio, P_0/P_A
P	Static pressure
P_T	Total pressure
u,v,w	Streamwise and transverse velocity components (upper case for mean values)
x,y,z	Coordinates with origin at ejector exit center (z along long axis of the ejector cross section)
ω_x	Streamwise vorticity ($\partial V/\partial z - \partial W/\partial y$)

Subscripts

A	Ambient conditions
I	Conditions at primary nozzle exit
J	Conditions at ejector exit
0	Plenum chamber conditions
MAX	Maximum value at a given x

Measurement Conditions and Procedure

The measurements were conducted for the nozzle configuration with suppressor area ratio (SAR) of 2.8 and mixing area ratio (MAR) of 1.0. The "long ejector" was used together with the "flush inlet." MAR = 1 implied that the cross sectional area of the ejector (5.005 in. × 2.600 in.) was constant throughout its length. The long ejector had a length of 9.705 in. downstream of the primary nozzle exit. SAR denoted the ratio of the ejector area to the primary nozzle exit area which was 4.649 in.^{2}. The hot-wire data were obtained at NPR = 1.07 (P_0 = 1 psig, M_I = 0.32). The Pitot probe data were obtained covering an NPR range of 1 to 3.5. The effect of chevrons and tabs were studied mostly at NPR = 2.5. Standard measurement techniques were employed with computer controlled probe traversing and data acquisition. For details of the Pitot probe measurements reference 1 may be consulted, while details of the hot-wire measurements are discussed in reference 2.

The Mach number values in appendix figures B1 to B22 are approximate especially far inside the ejector. Only total pressure was measured and the Mach number was calculated assuming static pressure to be equal to that outside in the ambient. Furthermore, Pitot probe errors were large just downstream of the primary nozzle due to flow angularity. The errors were also large on the periphery of the downstream jet (figs. C1 to C16) where the velocity was small and dominated by the entrainment component. (No significance should be attached to the small "negative" Mach numbers in those regions which, for ease of analysis, were calculated simply by using the absolute values of the measured negative total pressures.) The hot-wire measurements similarly had errors in the same regions due to flow angularity. Further discussion of the errors can be found in references 1 and 2.

Figure P.1 shows an end view of the nozzle mounted in the jet facility. The lower half of the primary nozzle chutes can be seen. The upper and lower chutes were aligned. Figure P.2 shows a close up view of the nozzle mounted in the jet facility. Here, the ejector end is fitted with the large chevrons. Figure P.3 shows another view of the facility where the ejector end is fitted with the tabs. A three element Pitot probe rake mounted on the probe traversing unit can be seen in the foreground. (Chevrons and tabs are described further with figures V.11(A) and (B).) Figure P.4, reproduced from reference 3, shows schematic views of the nozzle and the chutes.

Results

Figure V.1.—Longitudinal mean velocity distributions at five x-locations inside the ejector; M_I = 0.32. The box outlines the ejector, with the primary nozzle exit located on the left end.

Figure V.2.—Streamwise vorticity distribution within the ejector shown by two iso-surfaces. The data are based on measurements at the five stations of figure V.1. The outer vortex strands appear broken because measurement range was smaller farther inside.

Figure V.3.—Sense of the streamwise vortex pairs originating from the chutes, as inferred from the ω_x data.

Figure V.4.—The data of figure V.1 shown as contour plots at four stations. The switchover of the high-low-high velocity regions to low-high-low velocity regions from x/D = –2 to x/D = –1 is clearly shown. This occurs because the streamwise vortex pairs continually transport fluid in the lateral direction.

Figure V.5.—Downstream evolution of the jet shown by data at x/D = 0, 1, 2, 4, and 8; $M_I = 0.32$.

Figure V.6.—Streamwise vorticity distribution corresponding to the measurement range of figure V.5. Note that the iso-surface levels are ten times lower than those in figure V.2.

Figure V.7.—Mach number distributions within the ejector obtained from Pitot probe surveys. (A), (B) and (C) are for indicated values of NPR and M_I. Note that the distribution at the exit plane is nonuniform and similar at $M_I = 0.34$ and 1.21 but more uniform at $M_I = 0.70$.

Figure V.8.—The switchover of the high and low velocity regions, as in figure V.4, is shown by total pressure variations measured downstream of a primary and an adjacent secondary chute. Data are shown for 11 values of NPR in (a) and (b). The pair of traces for each NPR are normalized by P_{T_O} which is the measured total pressure at x = –9.5 in., y = 0.8 in., z = 0. Successive pairs are staggered by one major ordinate division. Switchover occurs at all values of NPR, more than once in certain cases. No systematic trend in the first switchover location can be discerned.

Figure V.9.—Mach number distributions at the exit plane of the ejector obtained from Pitot probe surveys. The cellular patterns occur at low and high values of NPR, but the flow is more uniform at NPR = 1.36 ($M_I = 0.68$).

Figure V.10.—Ratio of mass flow rate at ejector exit, obtained by integration of data as in figure V.9, to the mass flow rate through primary nozzle measured by a flow meter.

Figure V.11.—Sketch of the chevrons and tabs. The large chevrons in (a) are approximately similar in geometry as used with a larger model of the nozzle in Cell 41 of GEAE, Cincinnati. Chevrons are mounted on the ejector outer surface (see fig. P.2). They are bent by about 10º so that the surface exposed to the flow is parallel to the streamwise direction. Tabs are of same size as the small chevrons. Ten tabs are used (see fig. P.3), each located downstream of the secondary flow chutes. This configuration was chosen, on the basis of the measured streamwise vorticity distribution (fig. V.3), in order to augment the strength of the vortices.

Figure V.12.—Downstream evolution of the jet based on Pitot probe surveys at $M_I \simeq 1.23$ (NPR $\simeq$ 2.5) for the chevron and the tab cases. No dramatic difference in jet spreading is observed. However, noticeable changes in the jet cross sectional shape can be observed upon close inspection.

Figure V.13.—Maximum Mach number and mass flow rate variation with streamwise distance, obtained from data of figure V.12. The solid symbols are for a free rectangular jet with aspect ratio of 3:1 (ref. 2). Note that the comparison of the free rectangular jet data in figure V.13(b) should be interpreted with caution, as D is equivalent diameter of the nozzle in that case but it is equivalent diameter of the ejector in the present case.

Figure V.14.—Jet cross sectional shape at x/D = 4, at NPR = 2.5 and 3.5, for: (a) baseline, (b) tab, and (c) large chevron cases. Flutter at NPR = 3.5 did not allow measurement for the small chevron case. For the large chevron case in (c) at NPR = 3.5, probe broke off after half the field was surveyed; the full distribution is shown by assuming symmetry about y = 0 plane.

Figure V.15.—Flow unsteadiness and flutter of chevrons at NPR = 3.5 are shown by these noise spectra data measured by a microphone. With the chevrons (large and small) a rather violent

unsteadiness ensued when NPR was increased to about 3.5. It did not occur for the baseline and the tab cases. The frequency was about 400 Hz but changed for various set ups. After a sustained run, the chevrons would develop cracks (some actually fractured away) at the base along the lip of the ejector. It appeared that the unsteadiness was due to structural resonance (flutter) of the chevron pieces attached to the long edges of the ejector (fig. V.11(a)), probably instigated by unsteady shock motion.

References

1. Zaman, K.B.M.Q., "Spreading characteristics and thrust of jets from asymmetric nozzles," AIAA Paper No. 96–0200, 34th Aerospace Sciences Meeting, Reno, Nevada, January 15–18, 1996.

2. Zaman, K.B.M.Q., "Axis switching and spreading of an asymmetric jet: the role of coherent structure dynamics," J. Fluid Mechanics, vol. 316, pp. 1–27, June, 1996.

3. DeBonis, James R., "Analysis and parametric study of a mixer/ejector nozzle for application to the high speed civil transport," NASA/TM—2000-210038, April 2000 (HSR003 February, 1995).

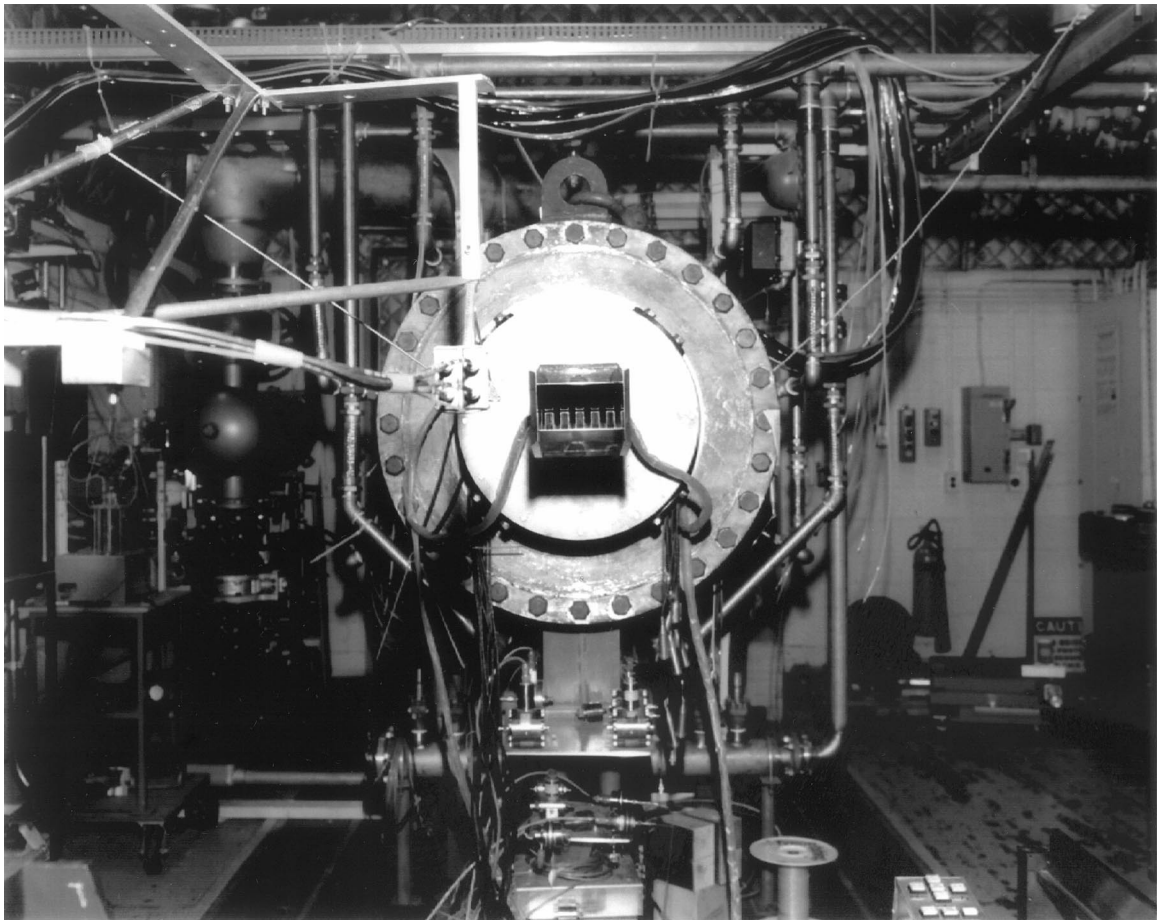

Figure P.1.—End view of the nozzle mounted in the jet facility. The lower half of the primary nozzle chutes can be seen.

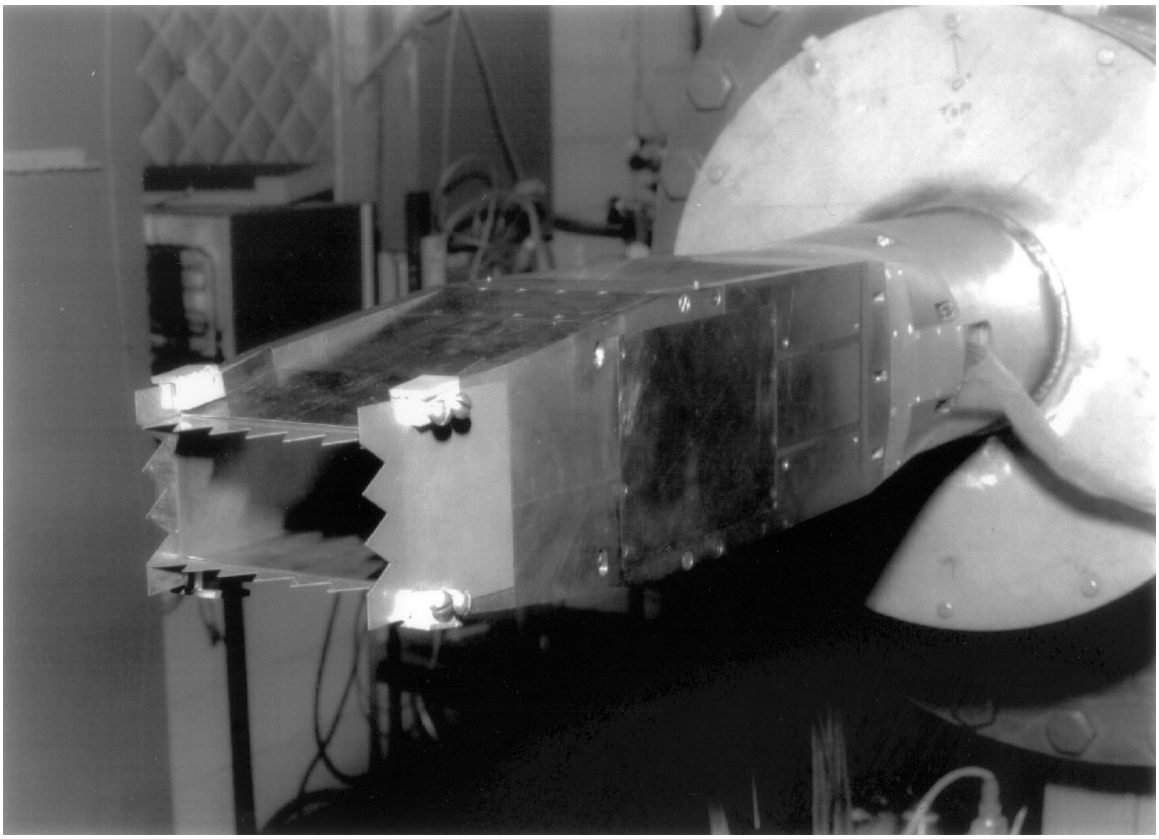

Figure P.2 .—Close up view of the nozzle mounted in the jet facility. Here, the ejector end is fitted with the large chevrons.

Figure P.3.—Another view of the facility where the ejector end is fitted with the tabs. A three element Pitot probe rake mounted on the probe traversing unit can be seen in the foreground.

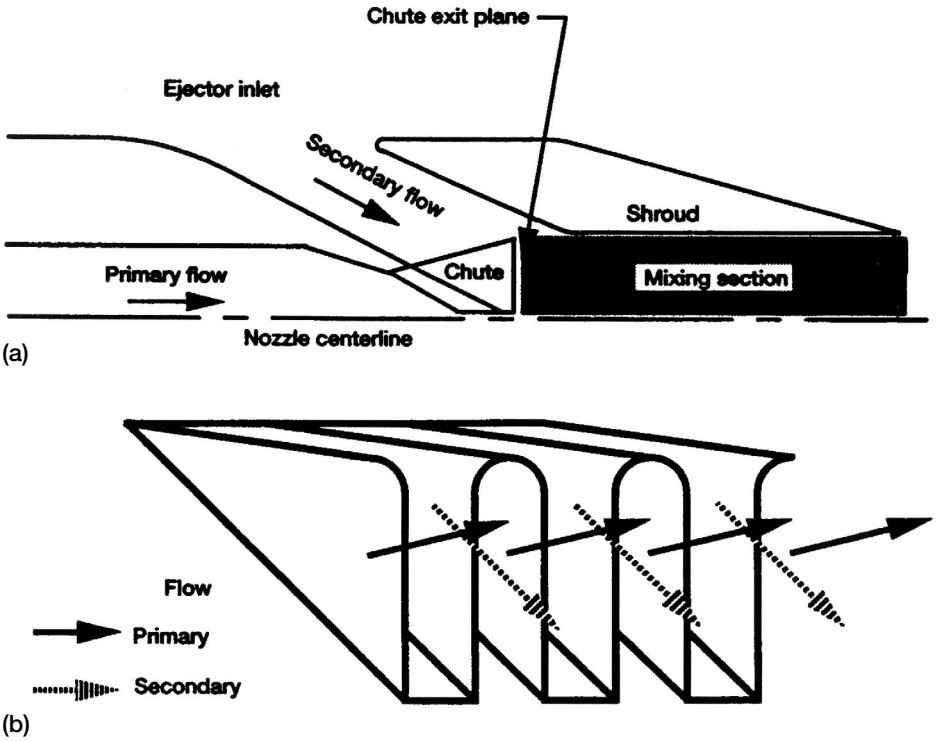

Figure P.4.—Schematic views of the nozzle and the chutes (from reference 3). (a) Schematic of nozzle. (b) Perspective view of chutes.

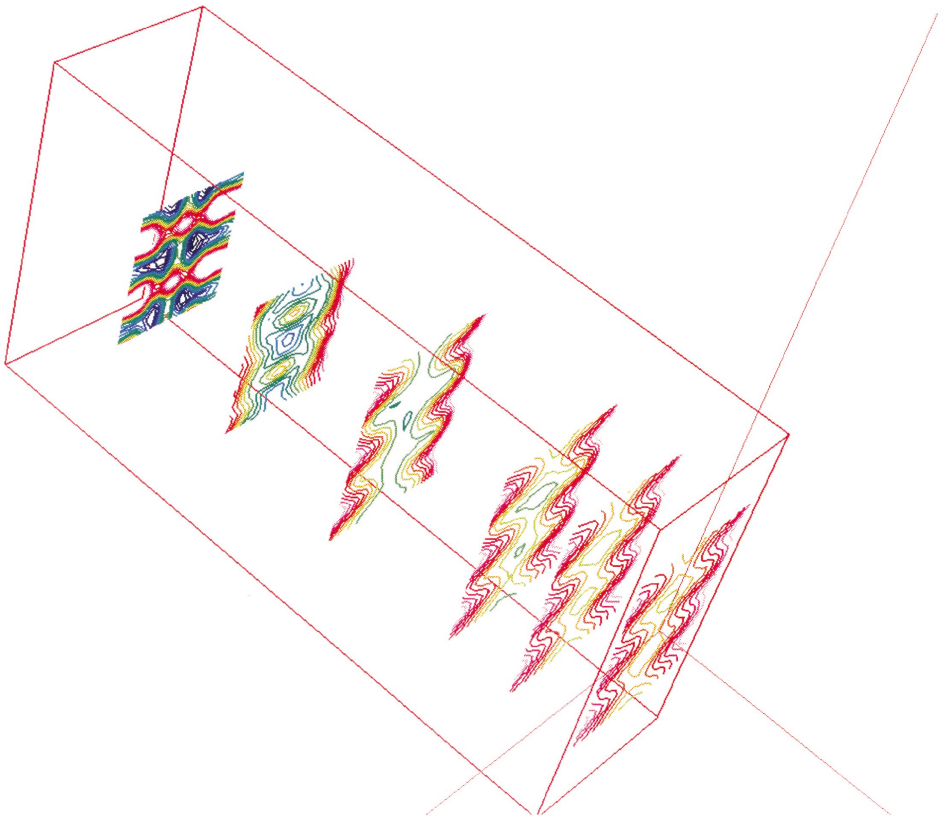

Figure V.1.—Mean velocity inside injector; x/D = –2, –1.5, –1, –0.5 and 0 (appendix figs. A1–A4).

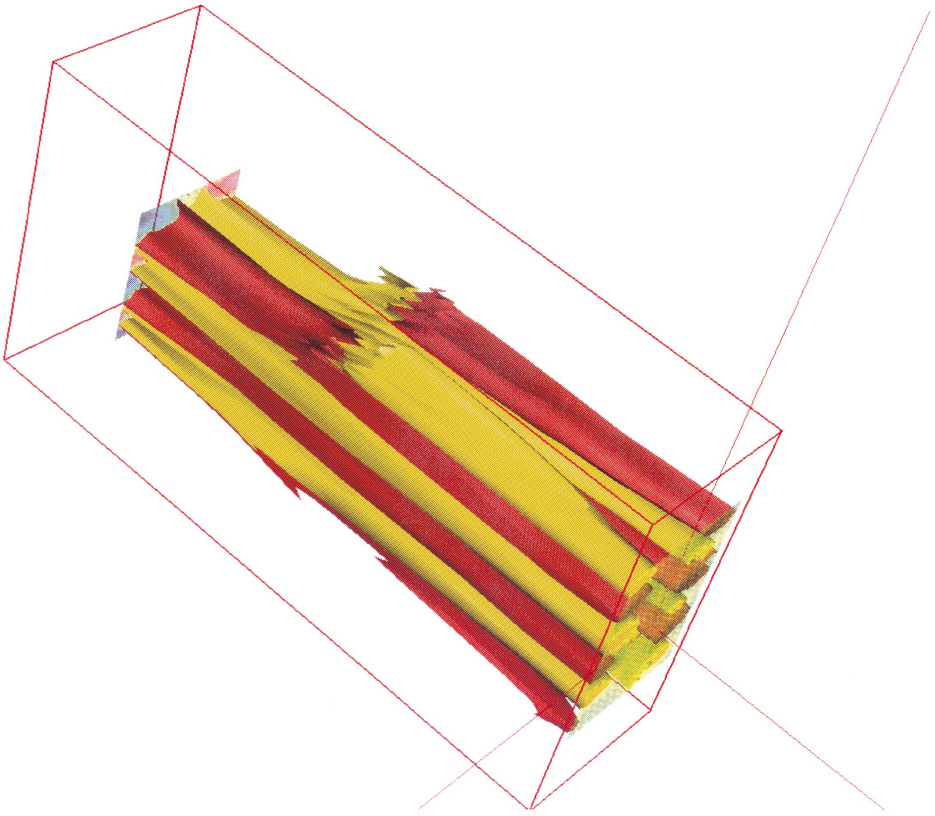

Figure V.2.—Streamwise vorticity inside injector, $\omega_x D/U_J = \pm 0.8$ iso-surfaces (appendix figs. A5–A8).

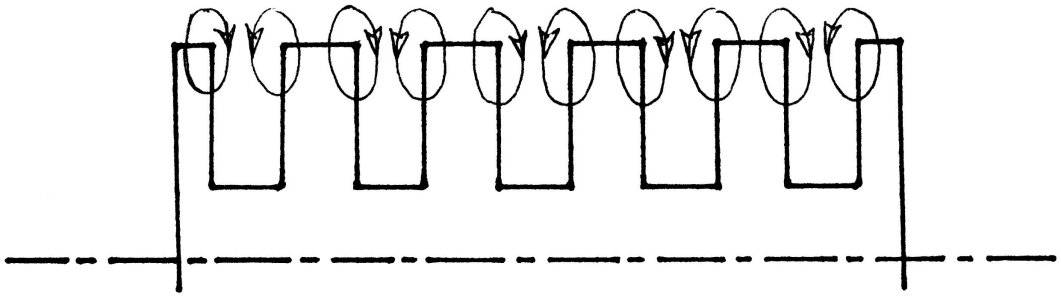

Figure V.3.—Schematic of streamwise vorticity from the chutes.

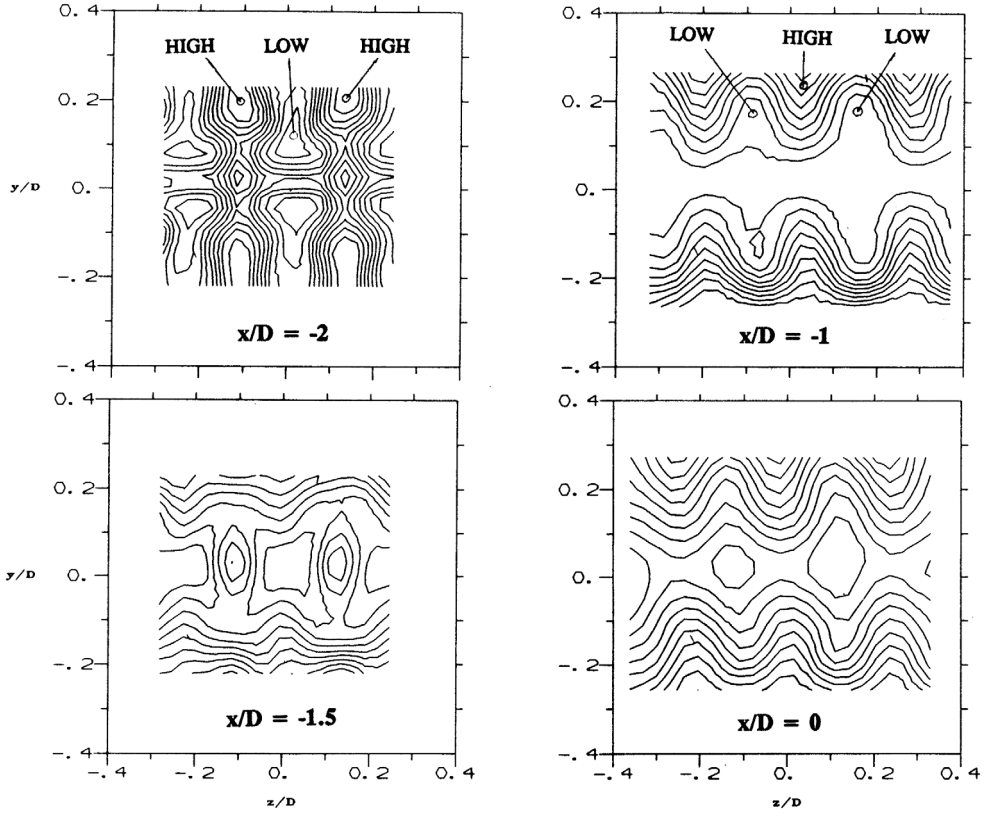

Figure V.4.—Mean velocity inside ejector. Switching of high and low velocity regions (appendix figs. A1–A4, turbulent stresses in figs. A9–A28).

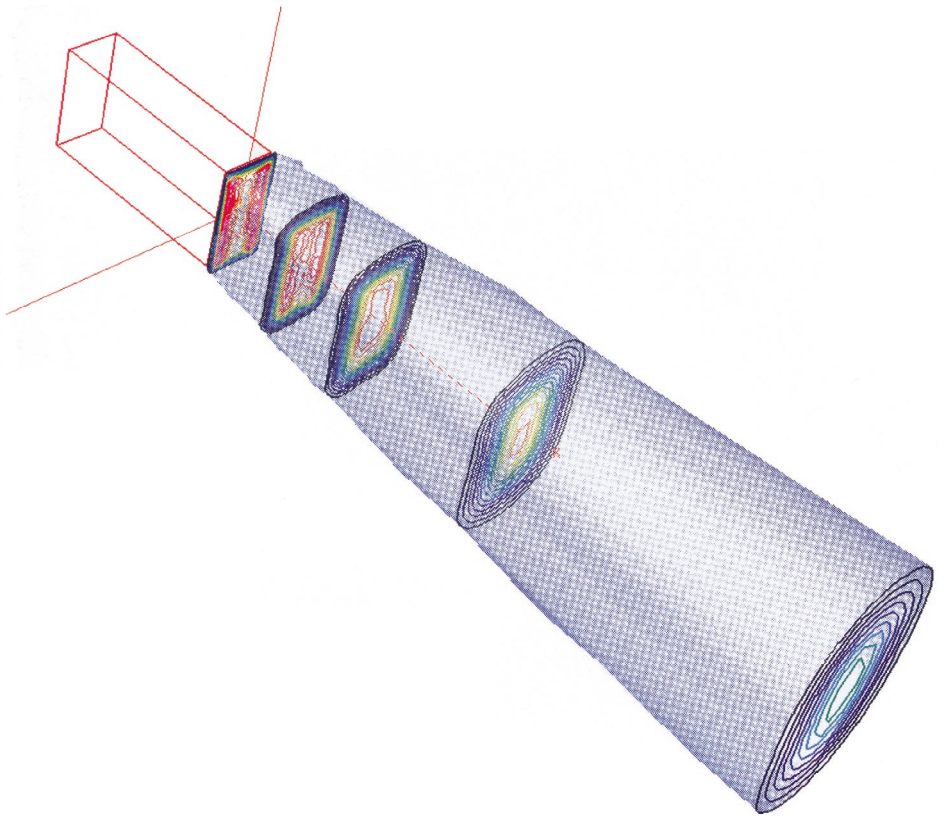

Figure V.5.—Mean velocity downstream of ejector. Blue iso-surface: $U/U_J = 0.15$ (appendix figs. A29–A32).

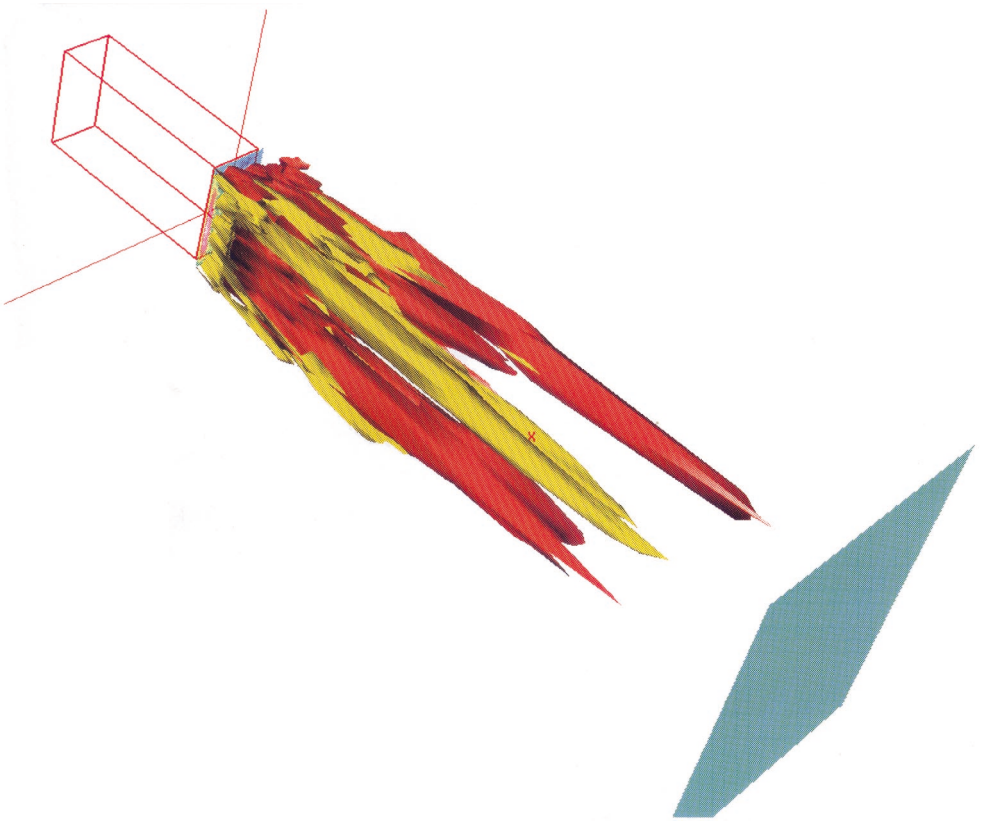

Figure V.6.—Streamwise vorticity downstream of ejector, $\omega_x D/U_J = \pm 0.08$ iso-surfaces (appendix figs. A33–A36, turbulent stresses in figs. A37–A56).

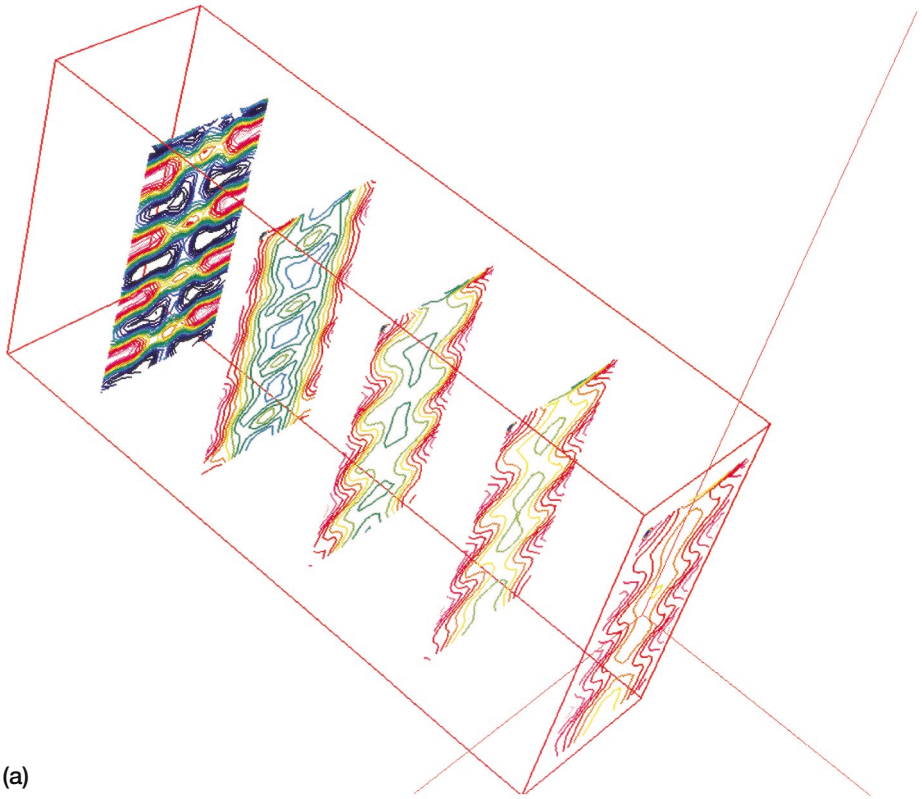

(a)

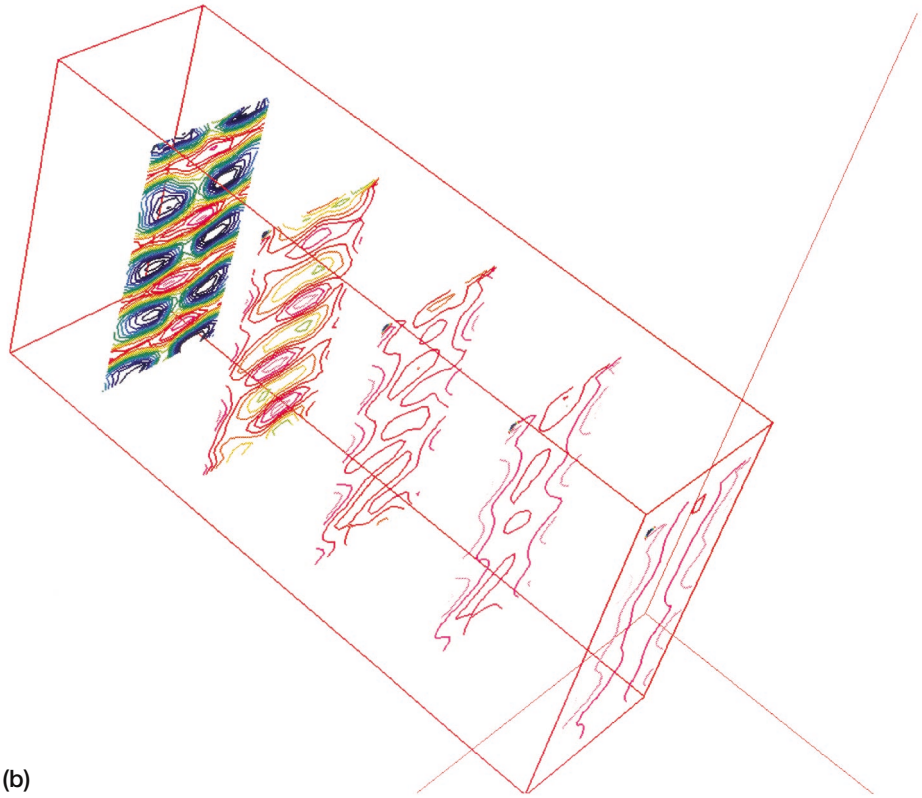

(b)

Figure V.7.—Mach number, M/M_{MAX}. (a) NPR = 1.08 (M_I = 0.34) (appendix figs. B1–B4). (b) NPR = 1.39 (M_I = 0.70) (appendix figs. B5–B8). (c) NPR = 2.46 (M_I = 1.21) (appendix figs. B9–B12).

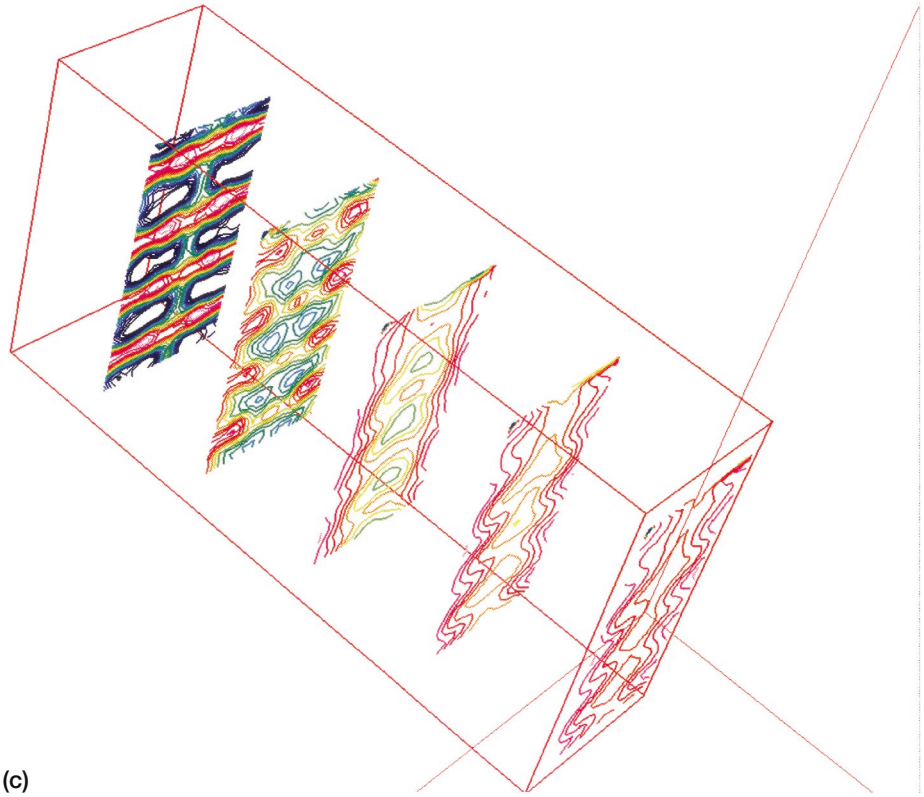

(c)

Figure V.7.—Concluded. (c) NPR = 2.46 (M_I = 1.21) (appendix figs. B9–B12).

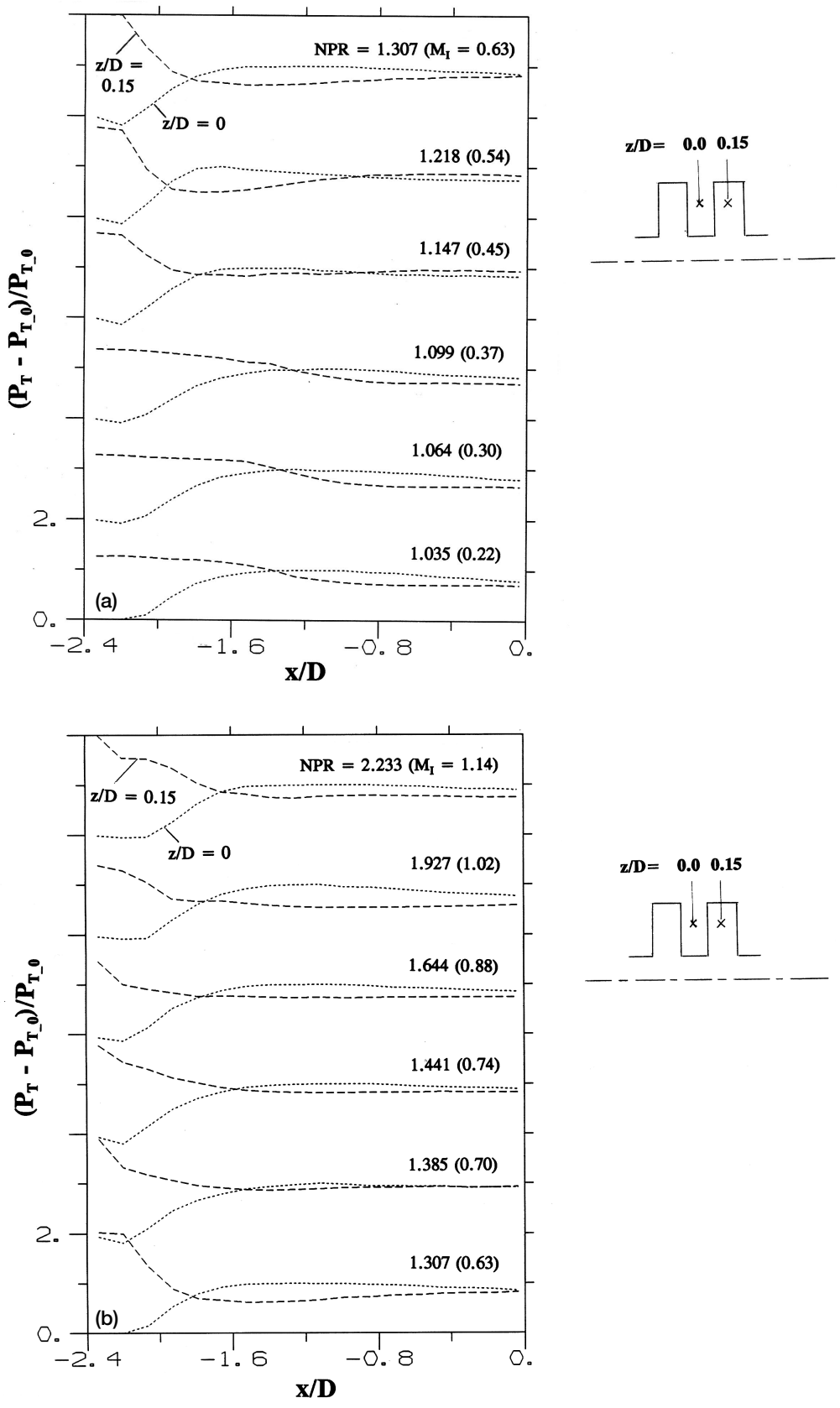

Figure V.8.—Total pressure variation inside ejector, y/D = 0.2. (a) Lower NPR. (b) Higher NPR.

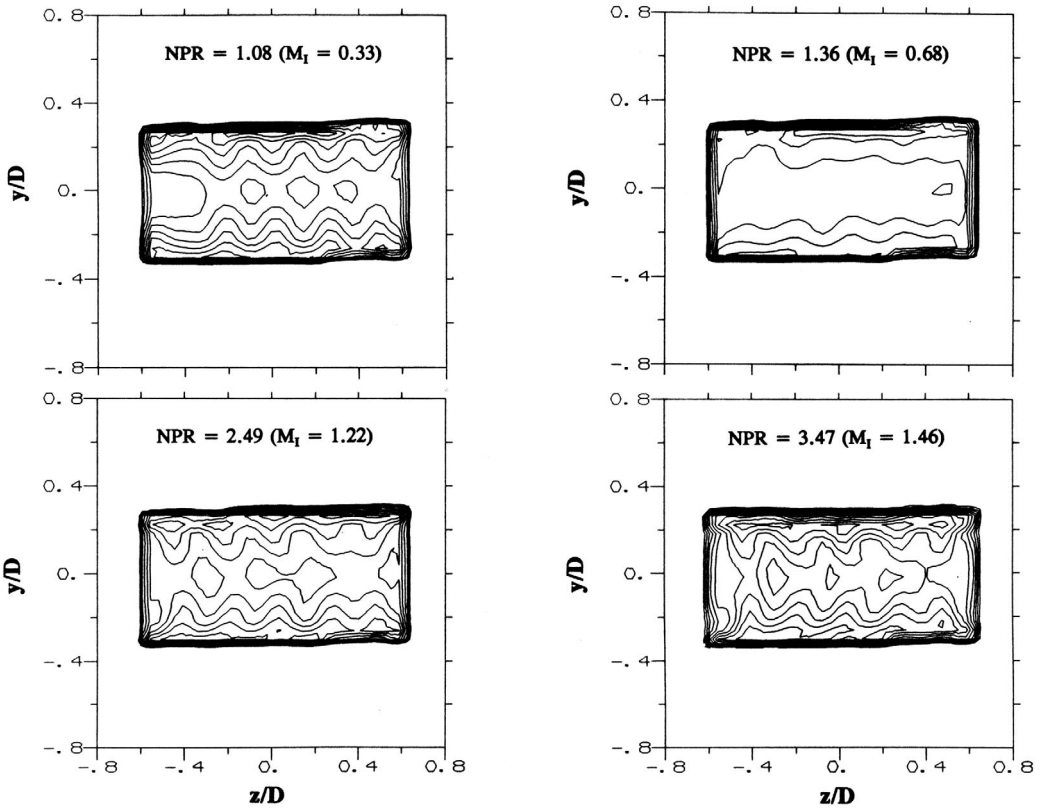

Figure V.9.—Mach number distribution at ejector exit, x/D = 0 (appendix figs. B13–B22).

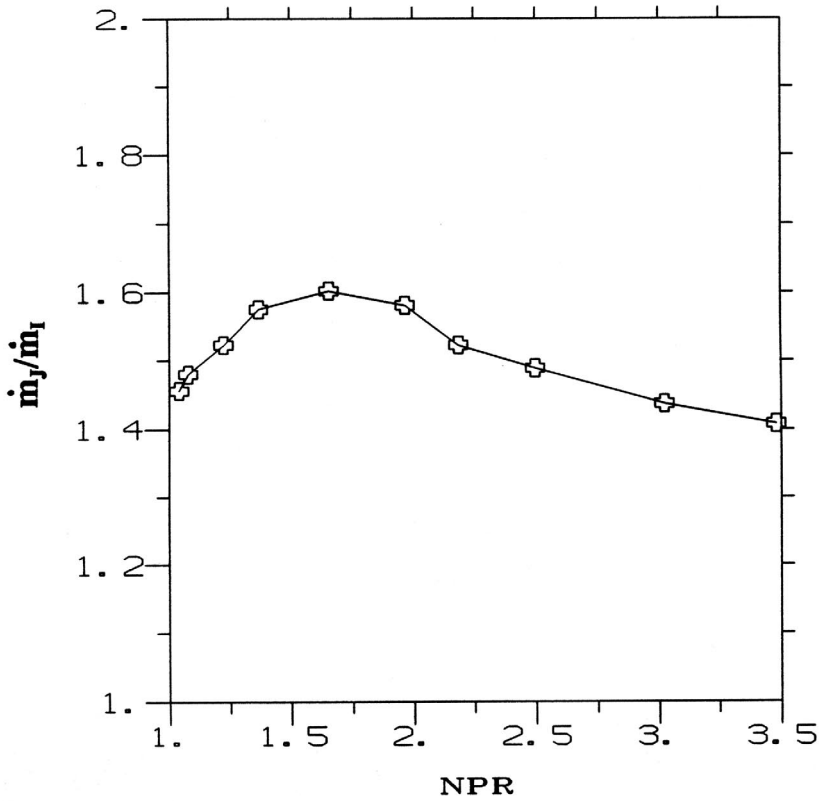

Figure V.10.—Ratio of mass flux at ejector exit and mass flux through primary nozzle (appendix figs. B13–B22).

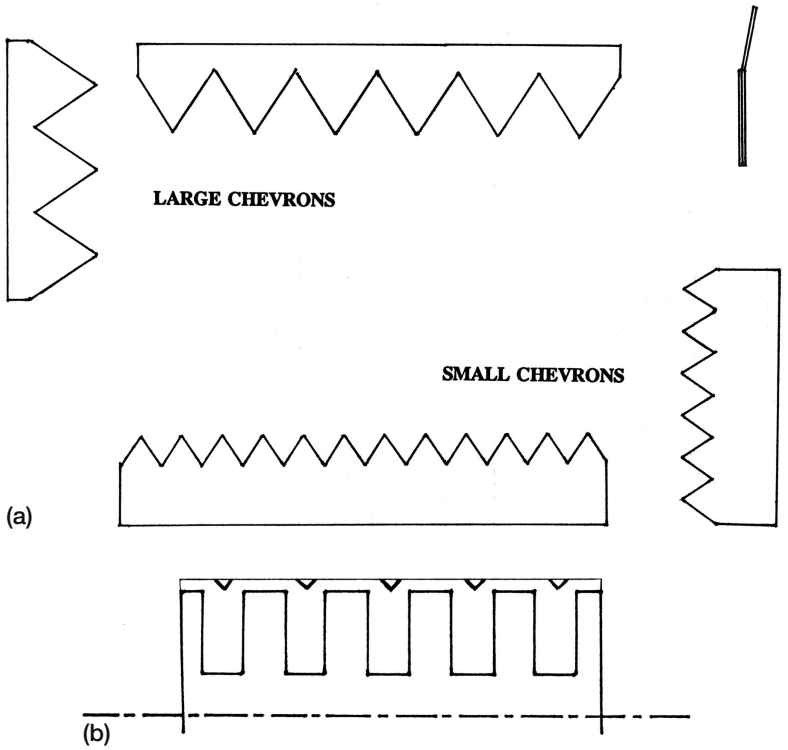

Figure V.11.—(a) Large and small chevrons. (b) Tabs are bent 35° into the flow. Area blockage is approximately 0.3% per tab.

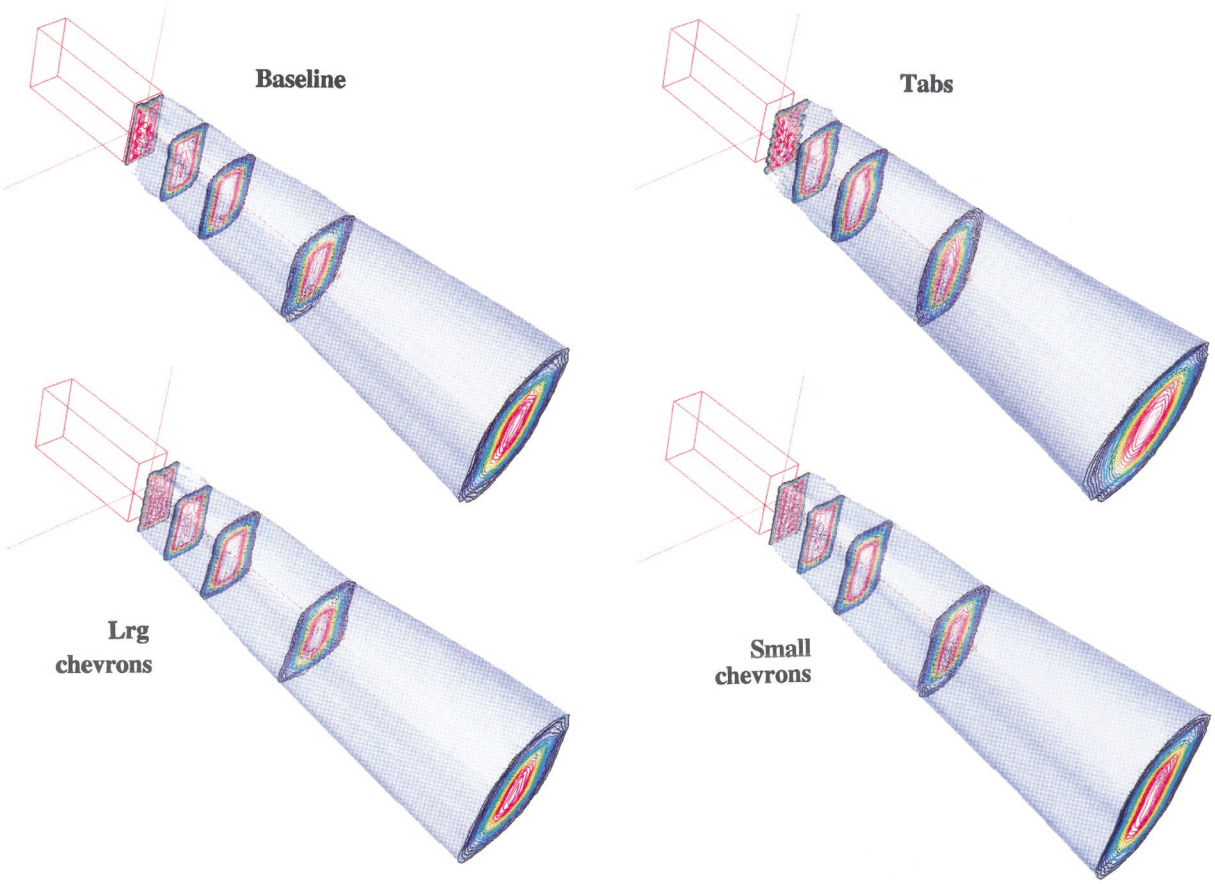

Figure V.12.—Mach number distribution, NPR = 2.5 (M_I = 1.23) (appendix figs. C1–C16).

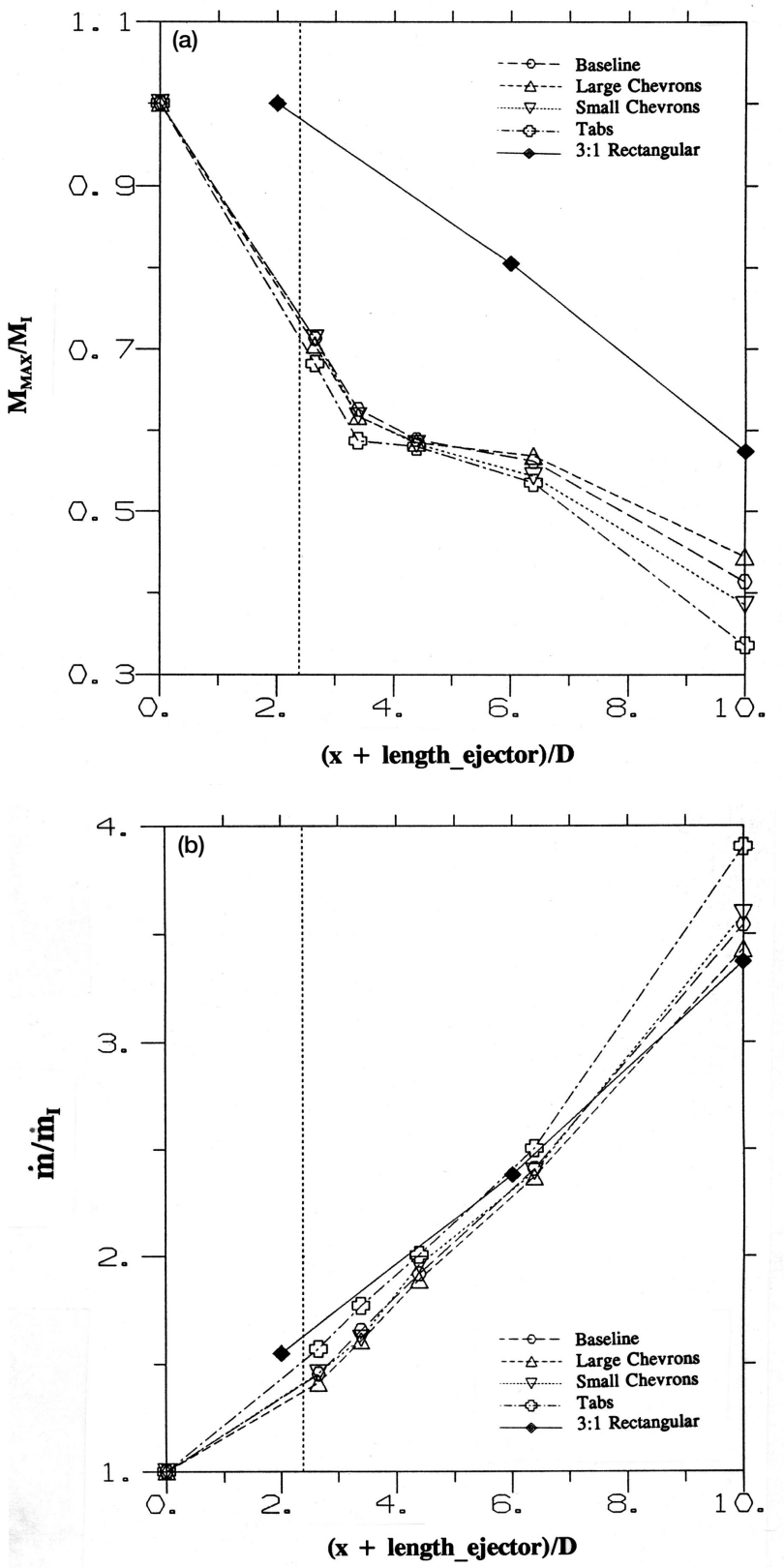

Figure V.13.—Streamwise variations of peak Mach number and mass flux, NPR = 2.5 (M_I = 1.23). (a) Peak Mach number. (b) Mass flux.

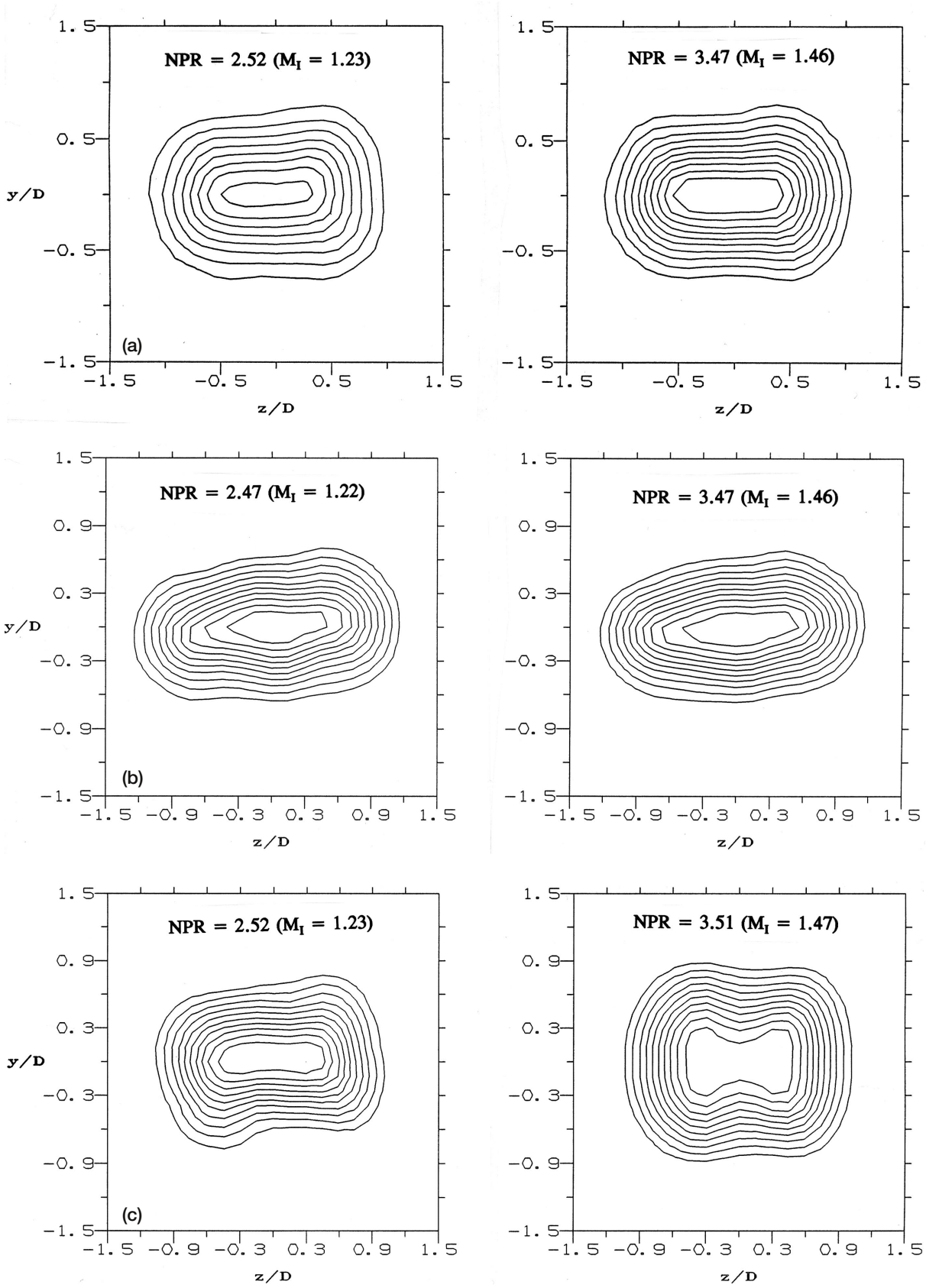

Figure V.14.—Mach number distribution, x/D = 4. (a) Baseline. (b) Tabs. (c) Large chevrons.

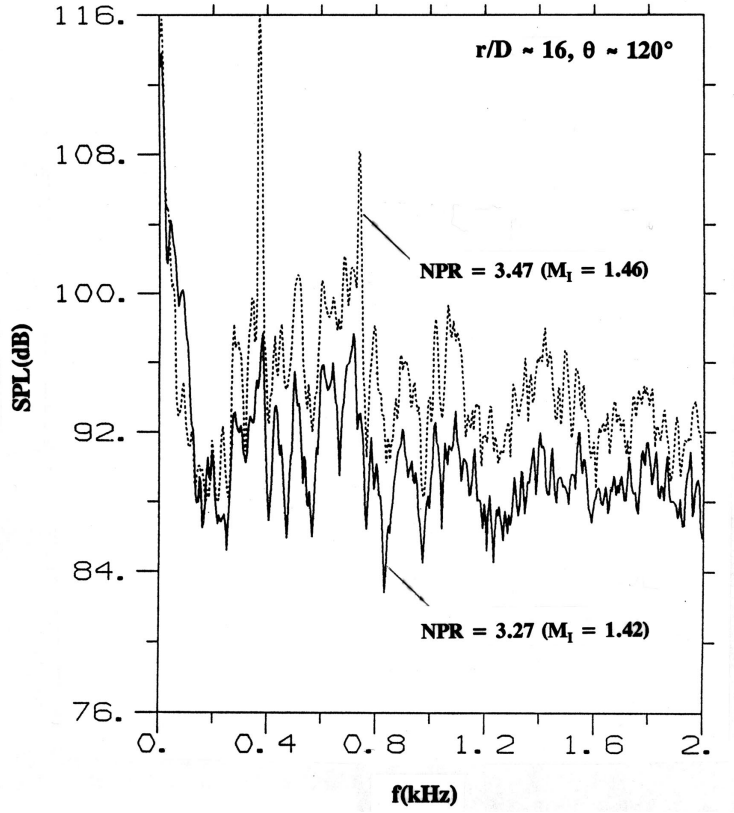

Figure V.15.—Sound pressure level spectra for the large chevron case.

Appendix

The data are presented as contour plots on the cross sectional (y, z) plane for a given x/D location indicated in the margin. Figures A1 to A56 show hot-wire data for the baseline nozzle (without tabs or chevrons). Figures B1 to B22 show Mach number contours inside and at the exit of the ejector, for various NPR. Figures C1 to C16 show Mach number contours for the baseline, chevron and tab cases in the downstream jet at NPR ≈ 2.5. Figures D1 to D14 show hot-wire data for the chevron and tab cases. Other notations used in the margin are

Min	Minimum value in the field
Max	Maximum value in the field
c_mn	Minimum contour level
c_mx	Maximum contour level
incr	Contour interval
Omega_x	ω_x
uv/Uj**2	$\overline{uv}/U_j^2$
uw/Uj**2	$\overline{uw}/U_j^2$
mi	m_I, lbs/sec
Dy, Dz	Half velocity diameters

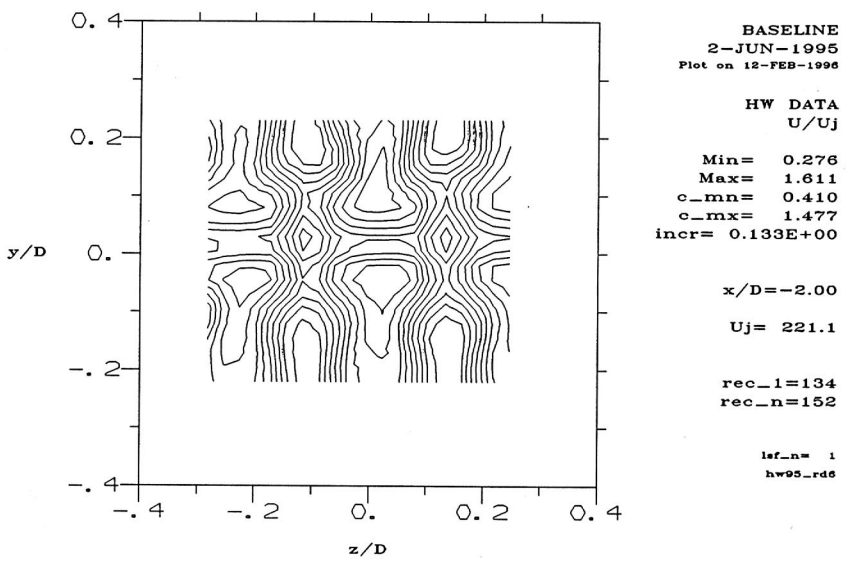

Figure A1

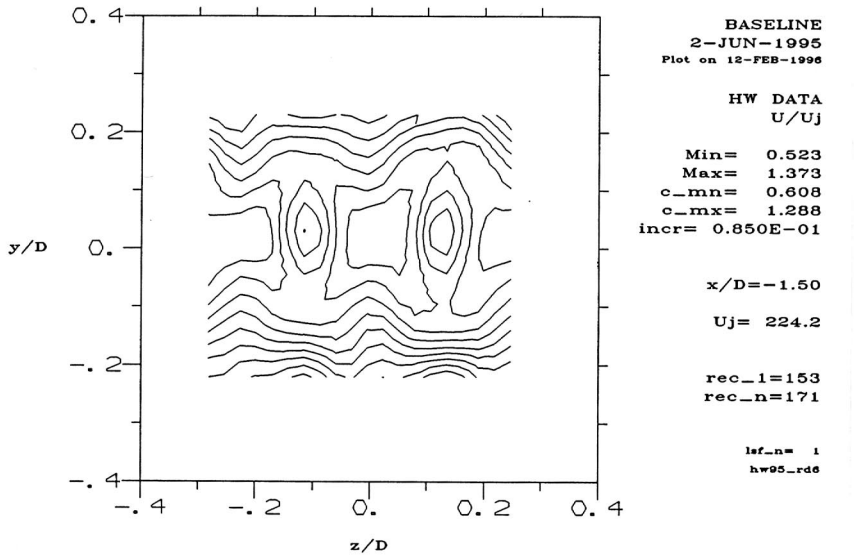

Figure A2

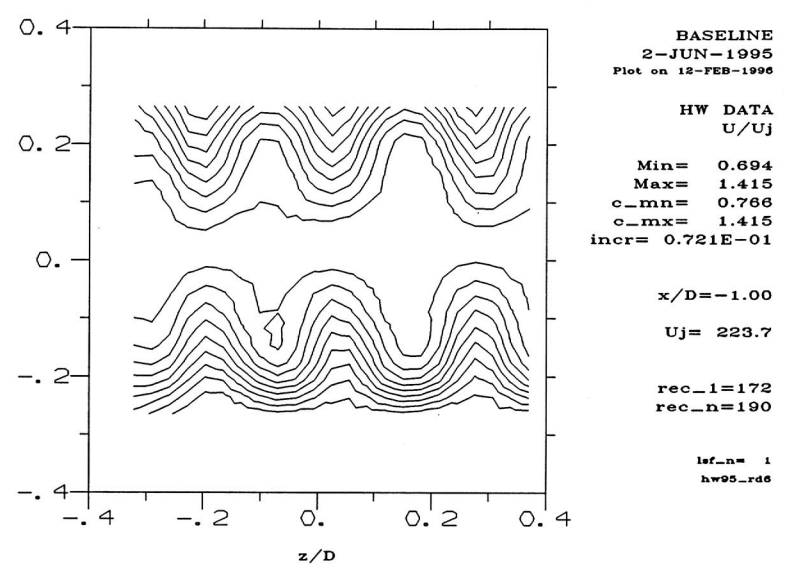

Figure A3

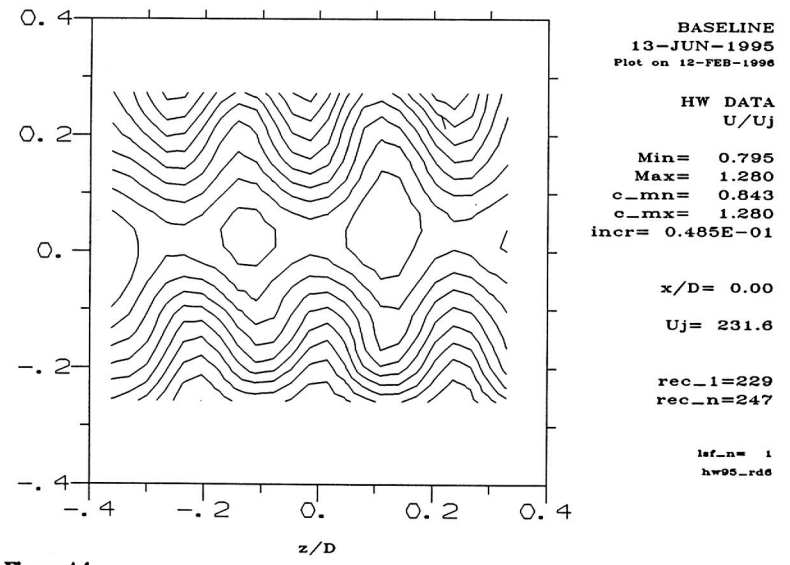

Figure A4

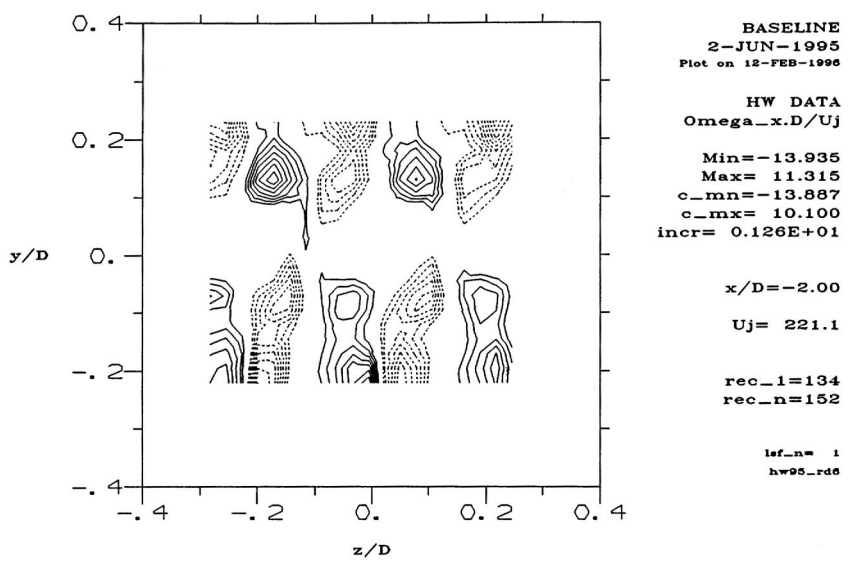

Figure A5

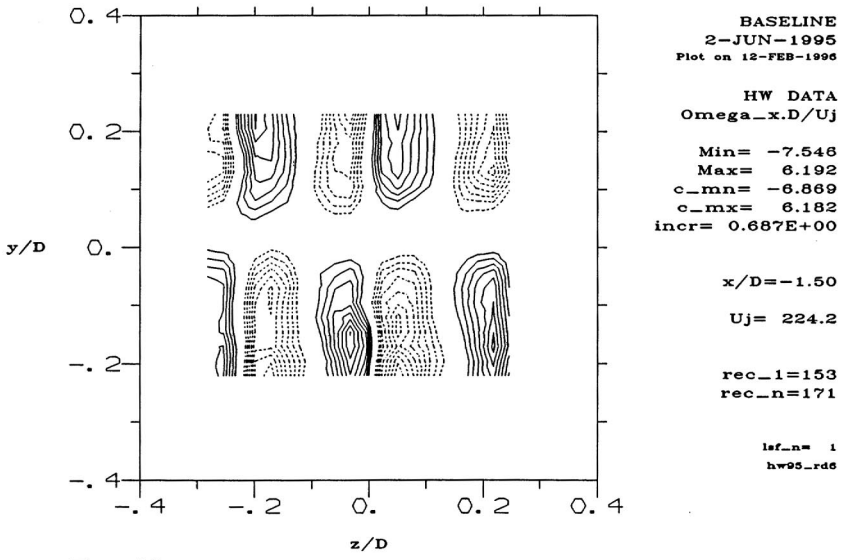

Figure A6

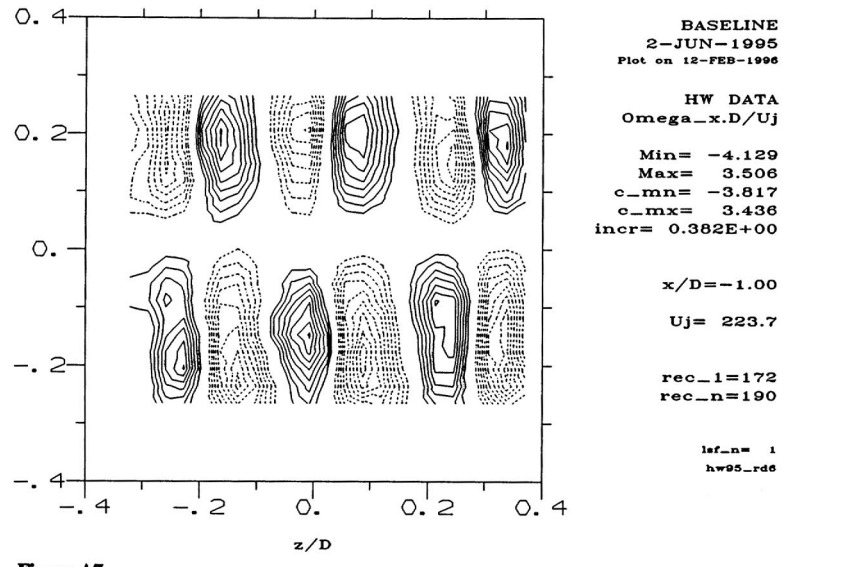

Figure A7

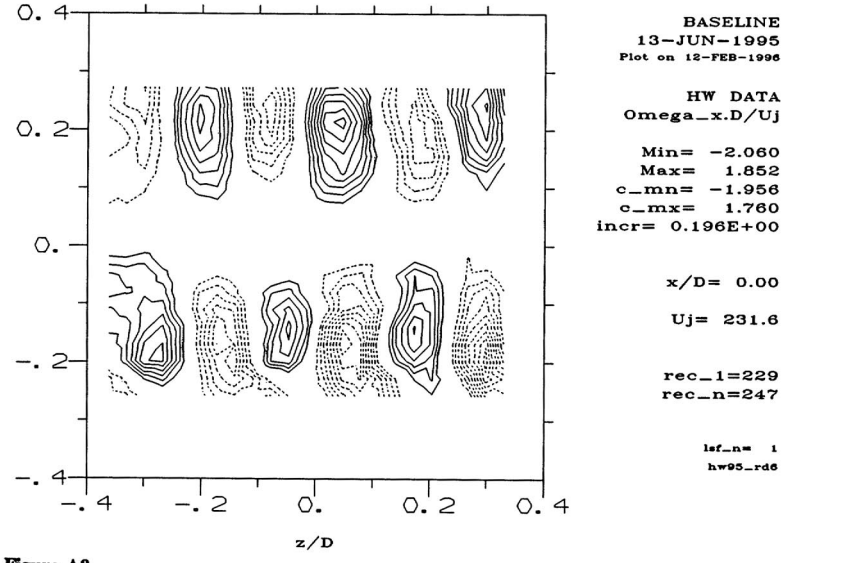

Figure A8

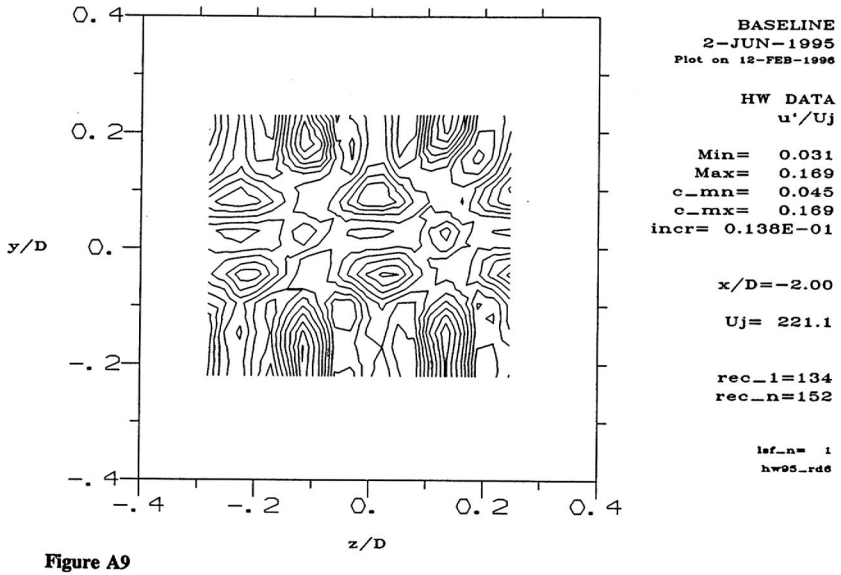

Figure A9

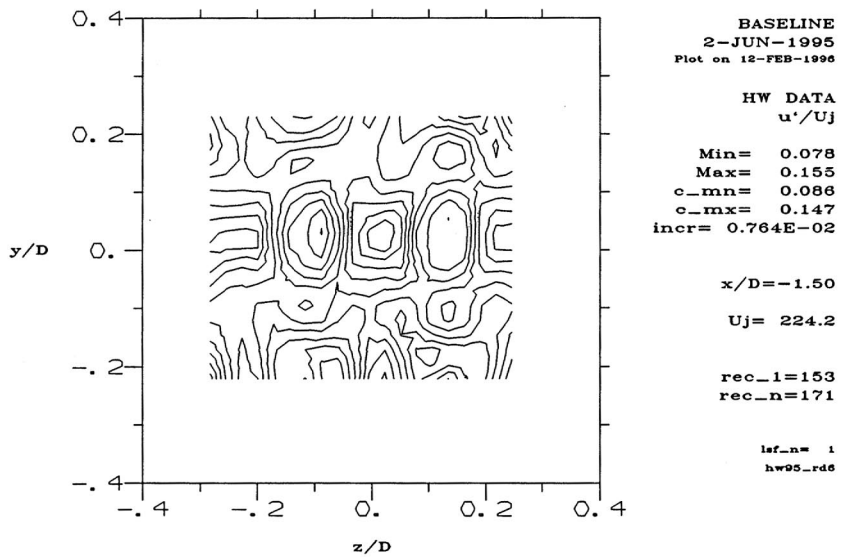

Figure A10

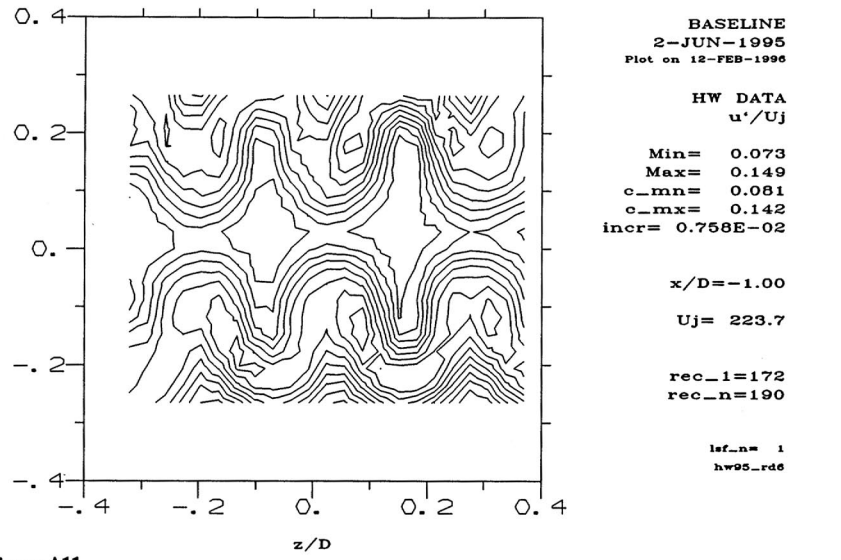

Figure A11

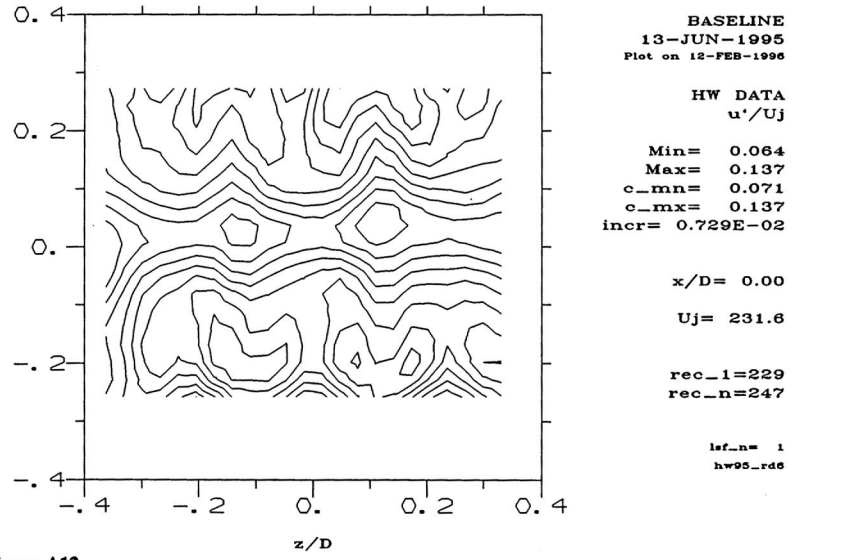

Figure A12

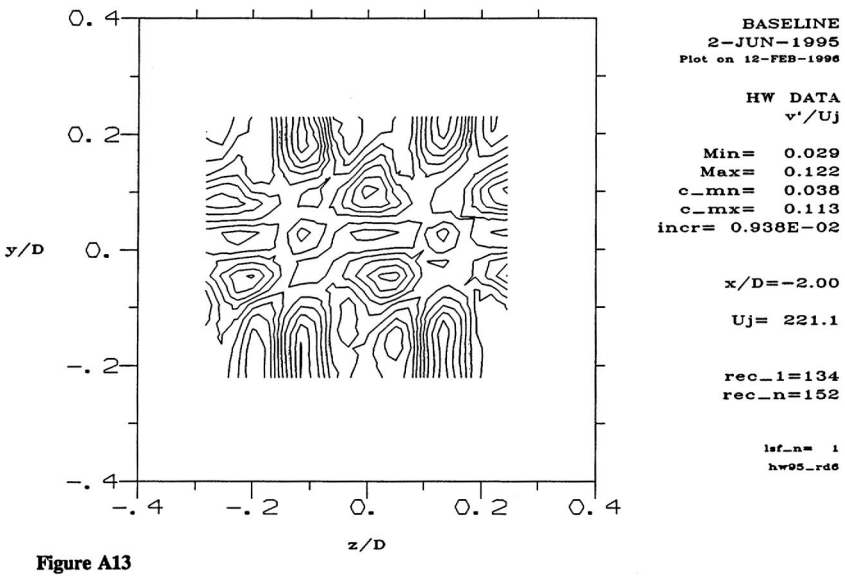

Figure A13

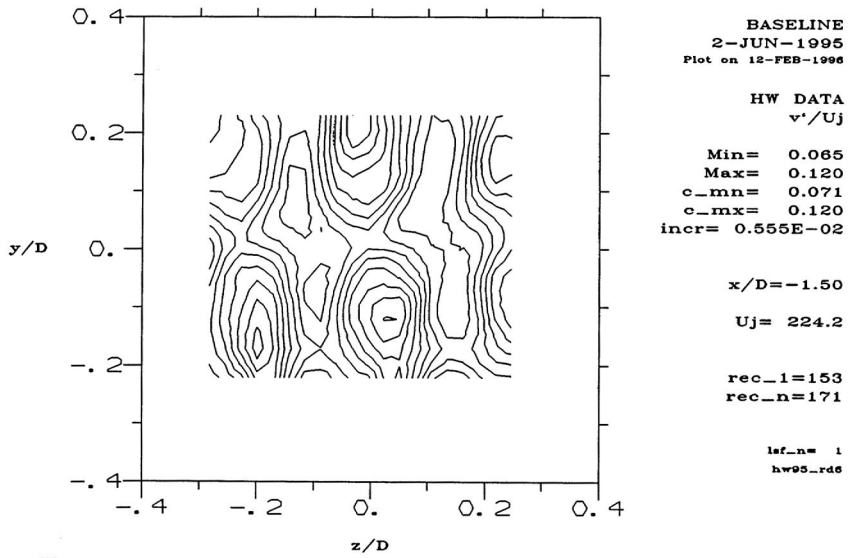

Figure A14

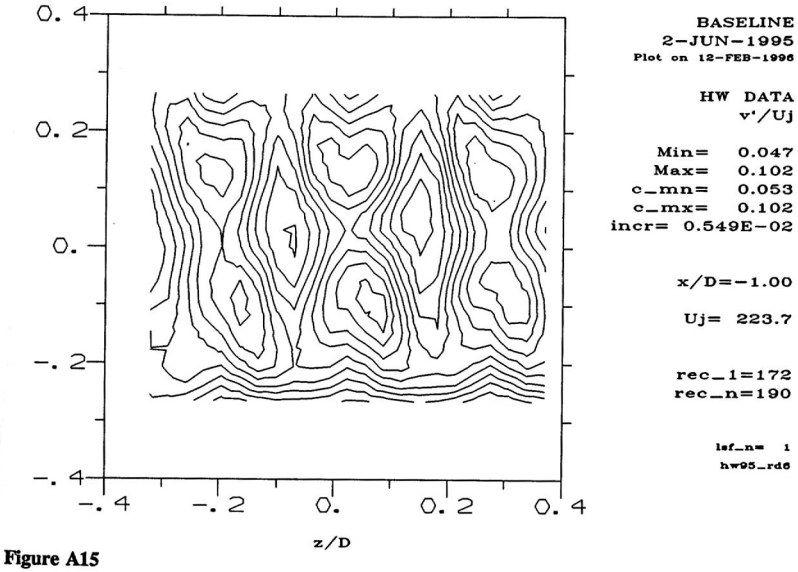

Figure A15

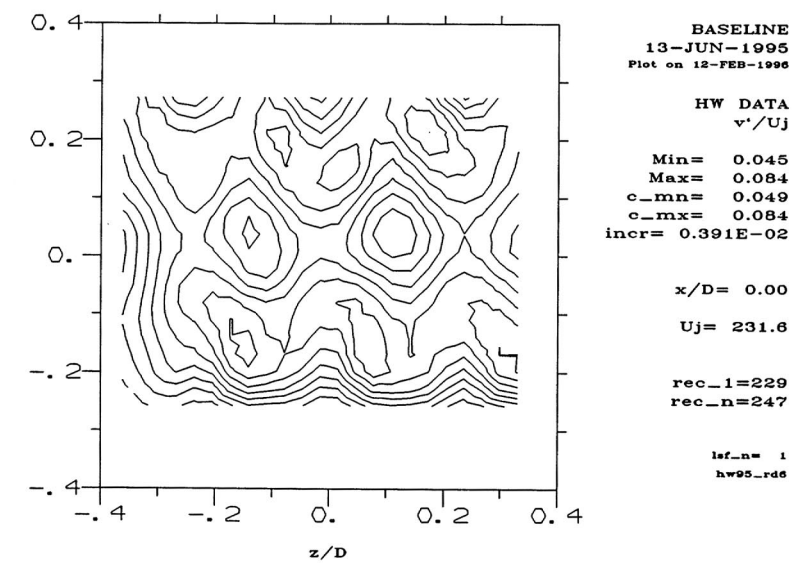

Figure A16

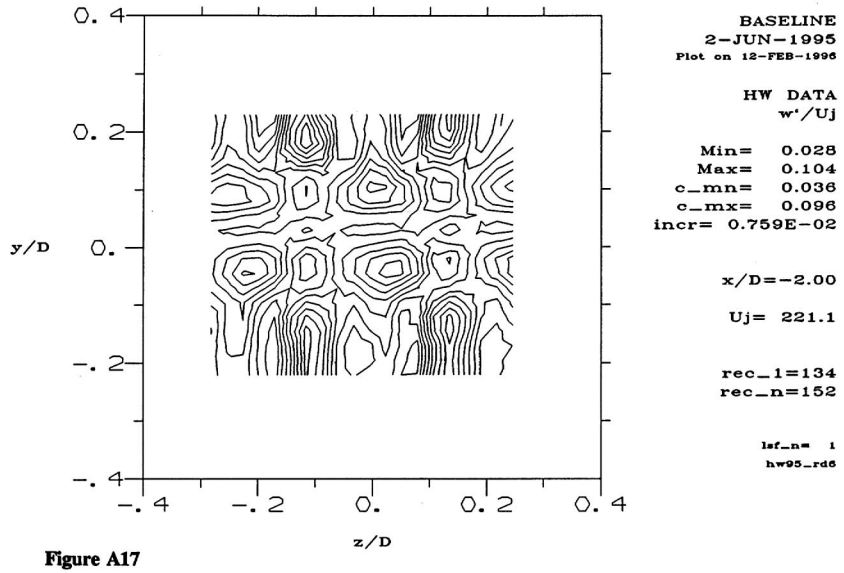

Figure A17

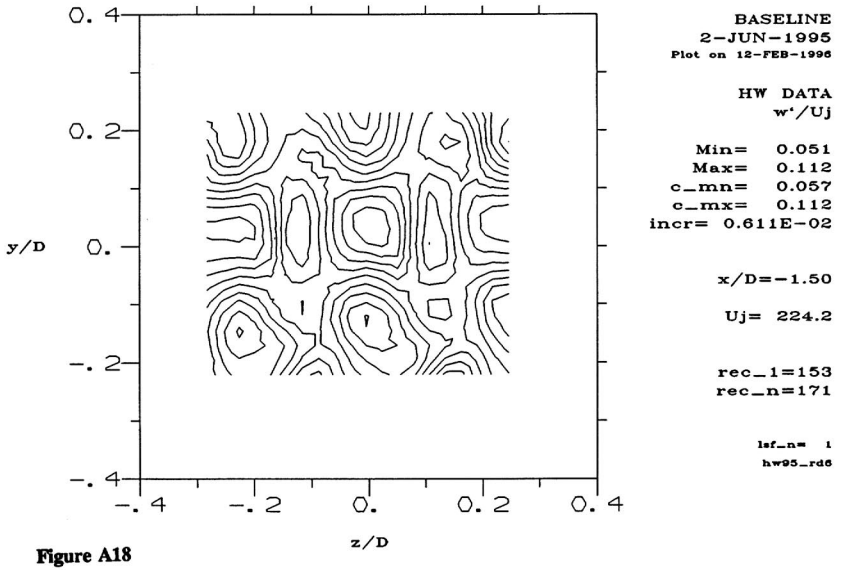

Figure A18

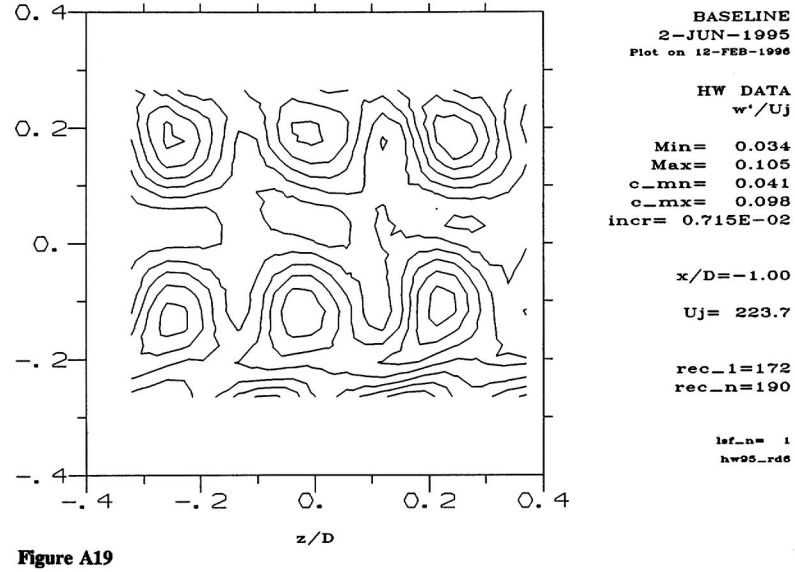

Figure A19

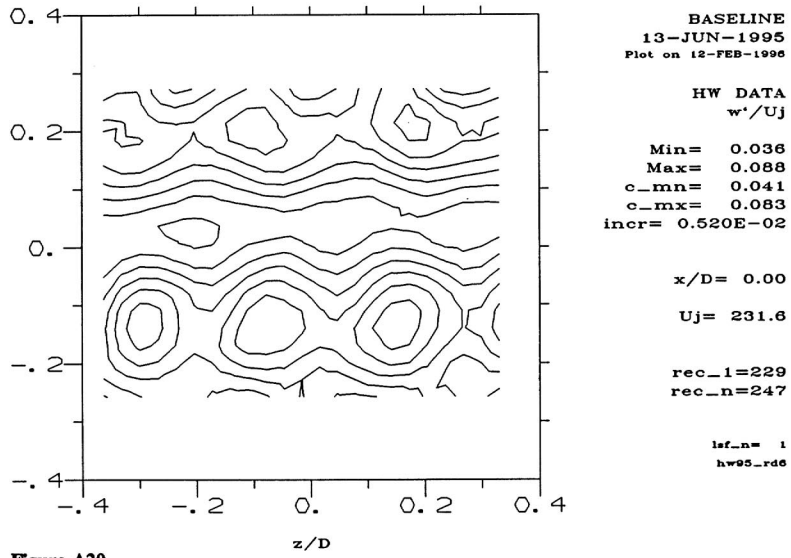

Figure A20

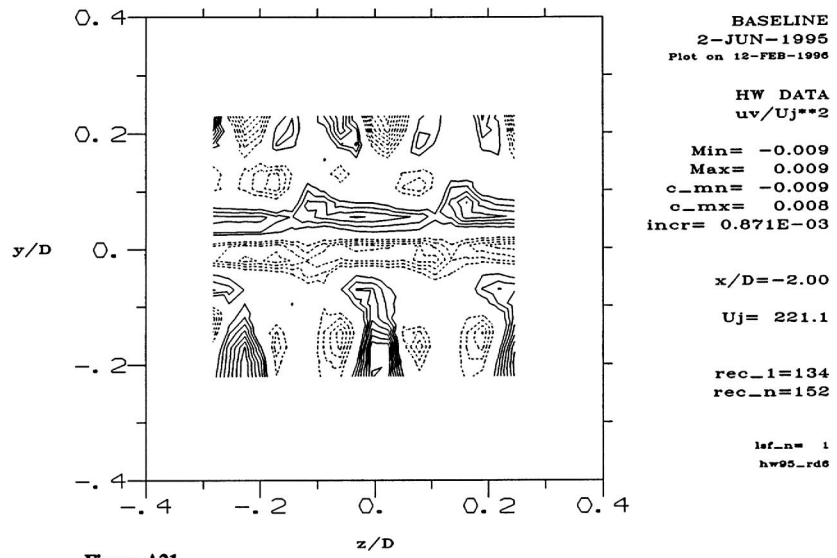

Figure A21

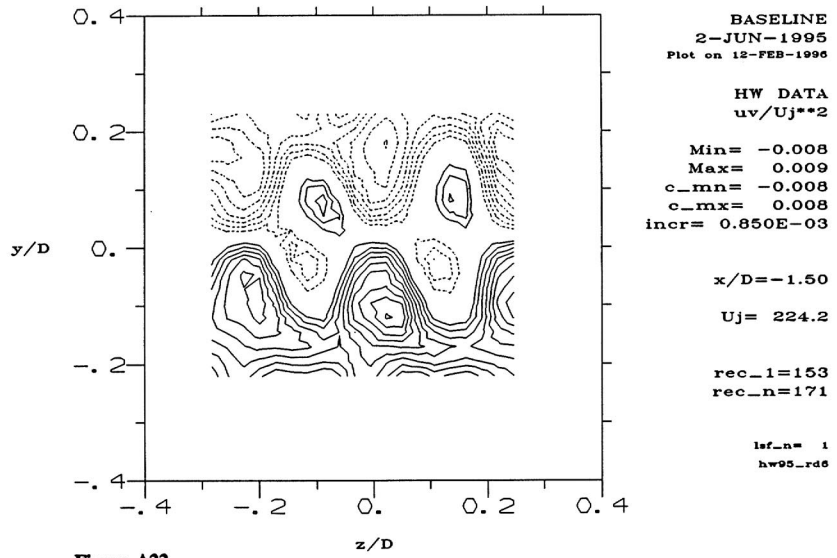

Figure A22

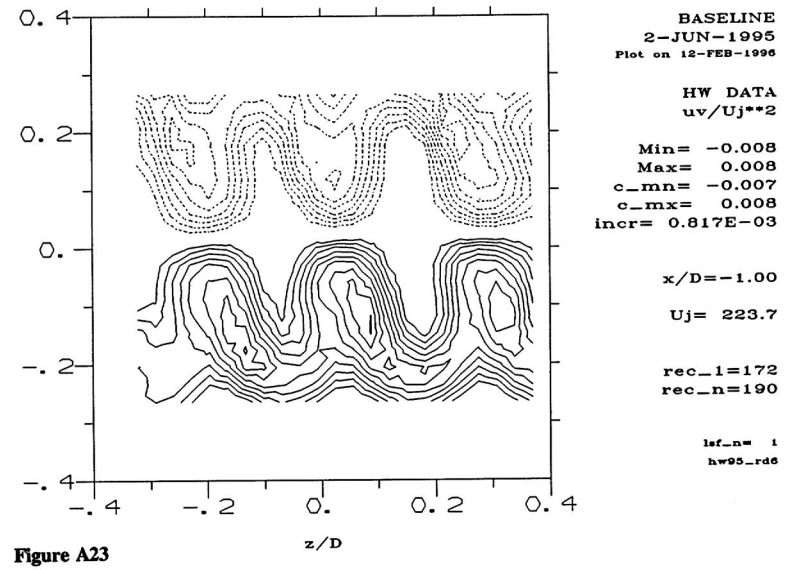

Figure A23

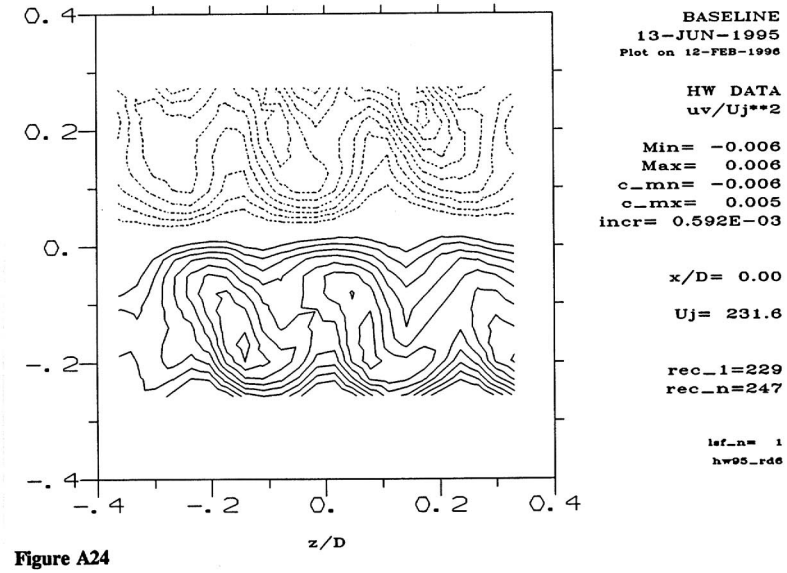

Figure A24

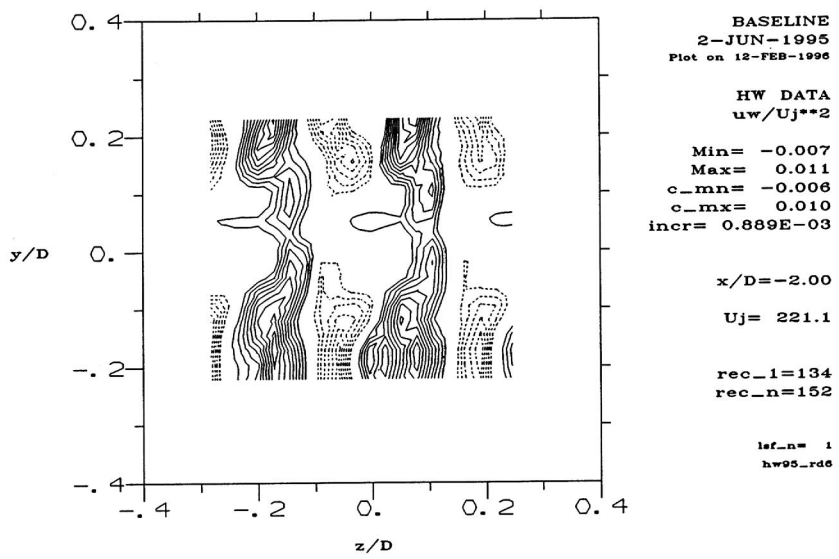

Figure A25

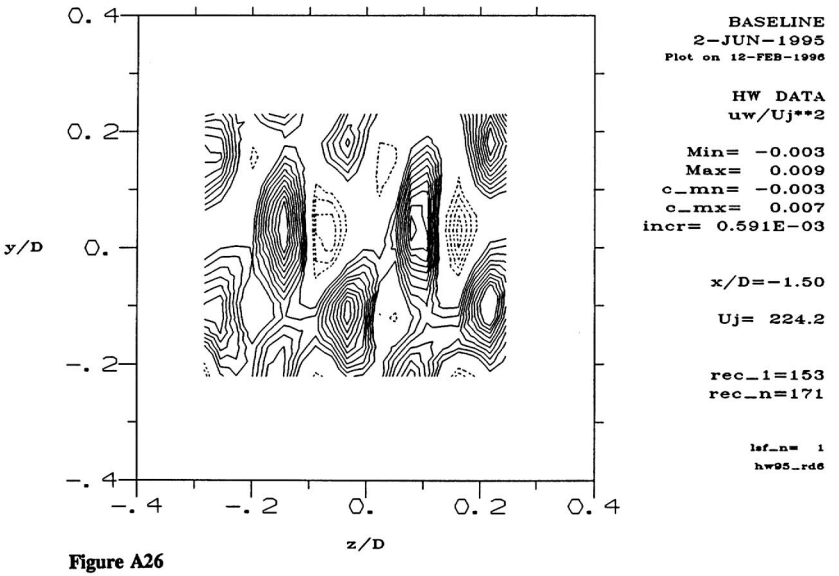

Figure A26

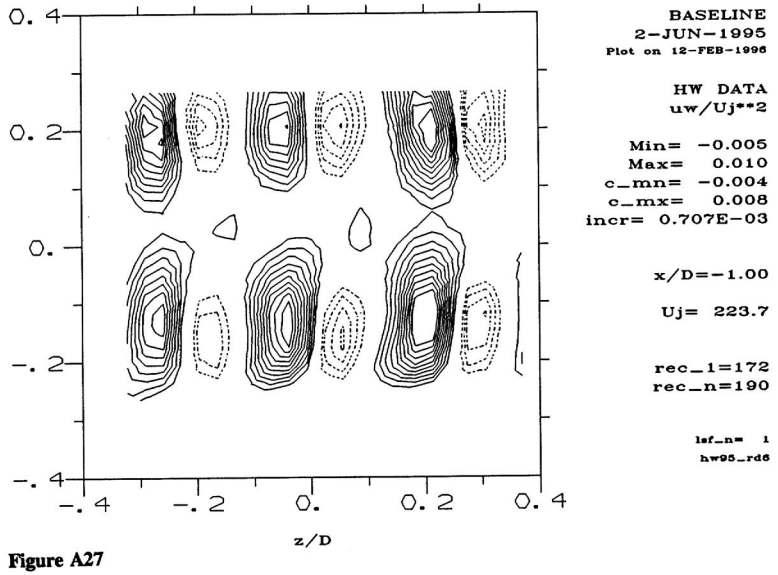

Figure A27

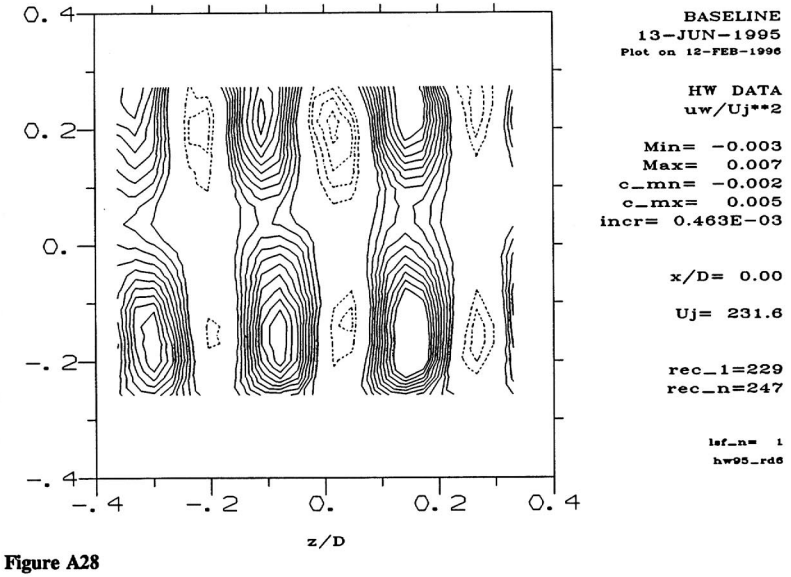

Figure A28

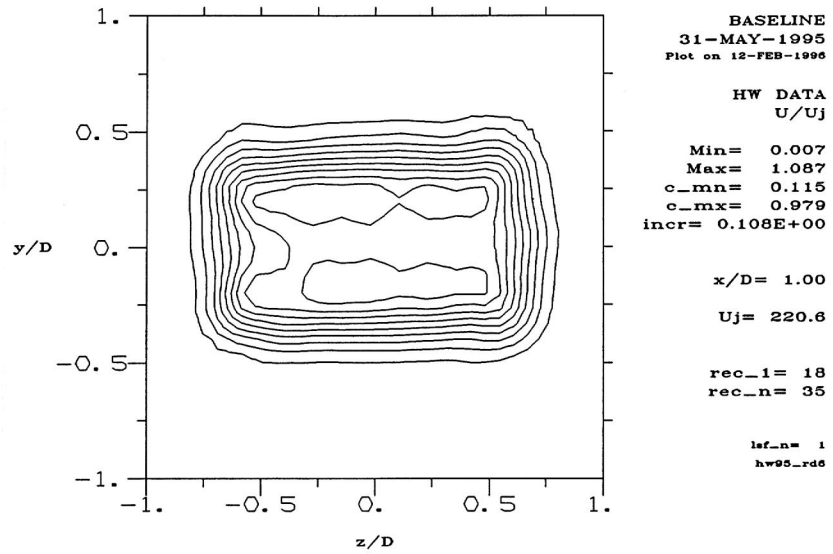

Figure A29

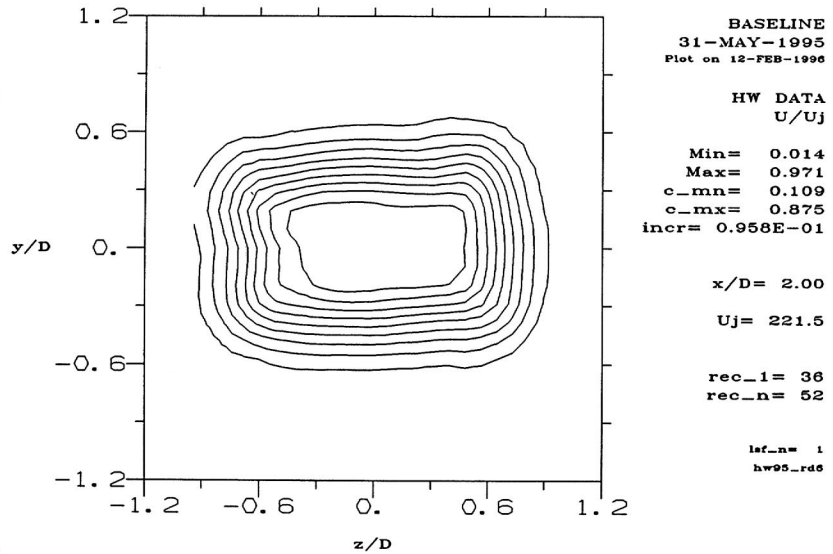

Figure A30

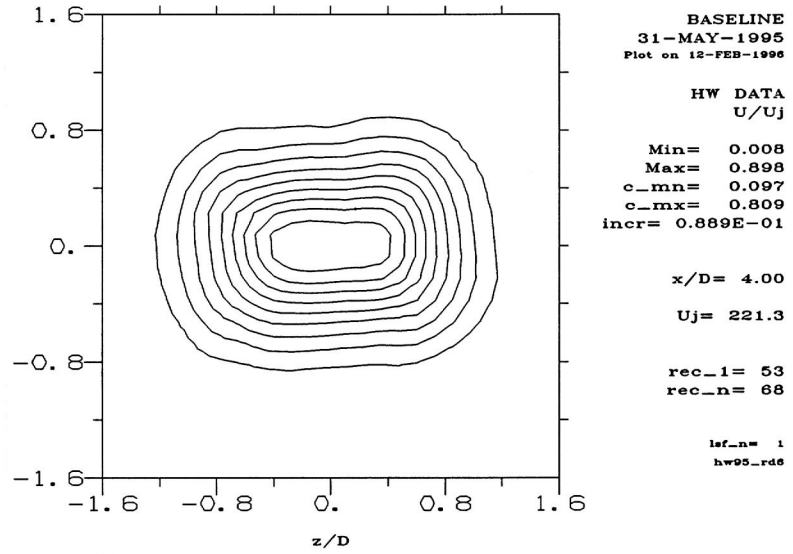

Figure A31

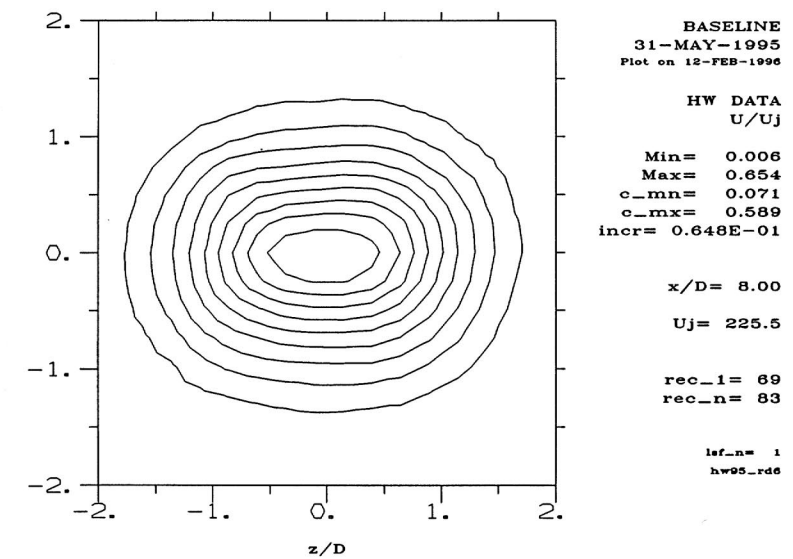

Figure A32

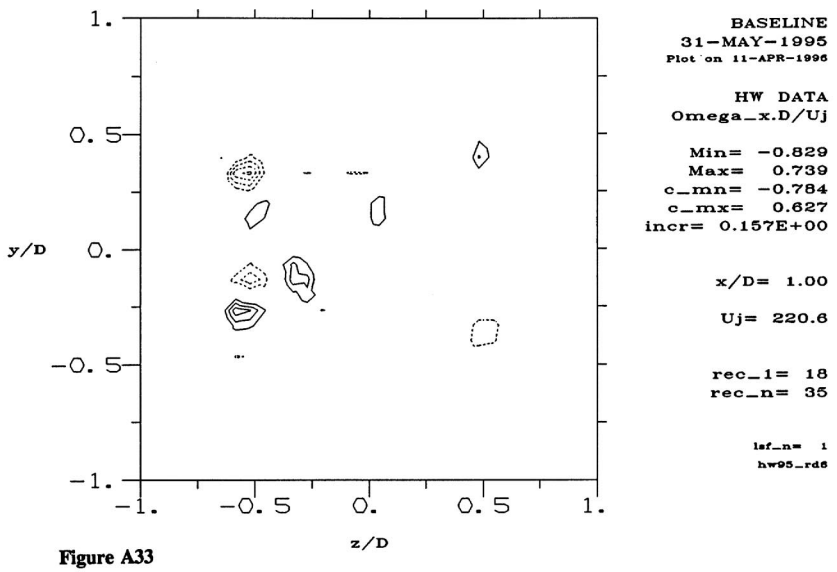

Figure A33

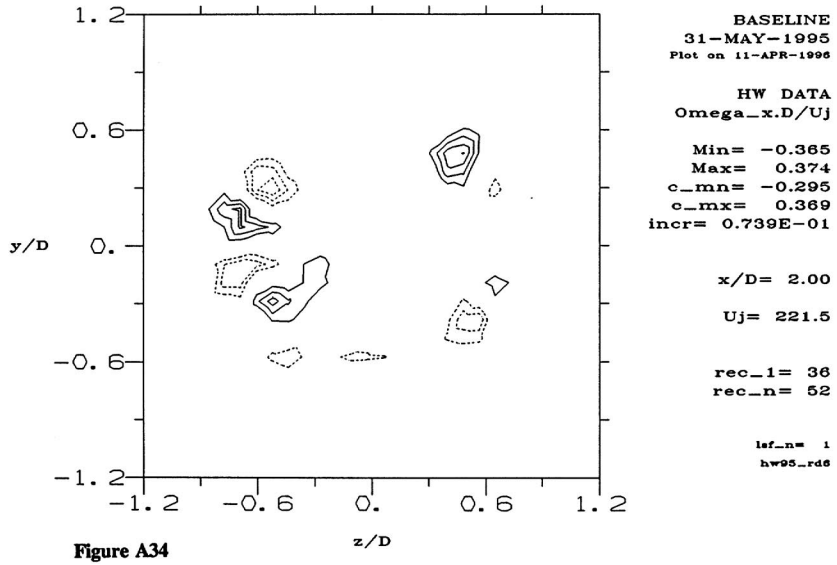

Figure A34

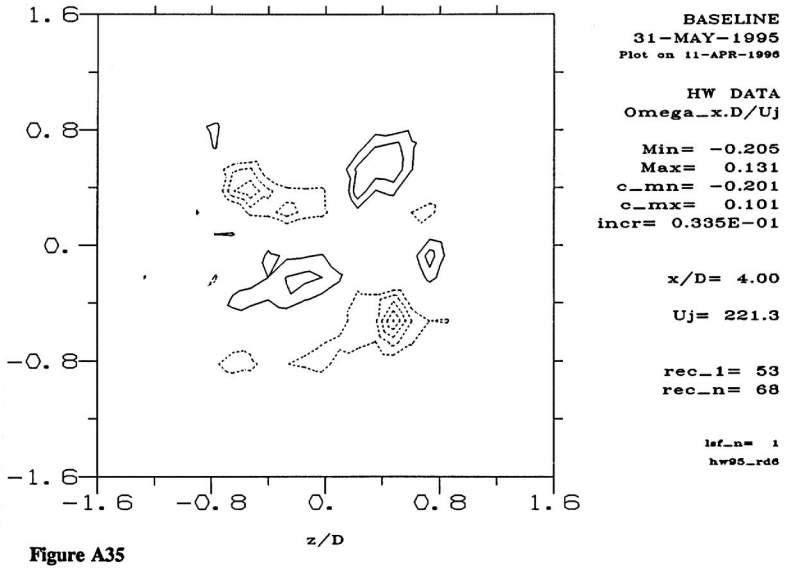

Figure A35

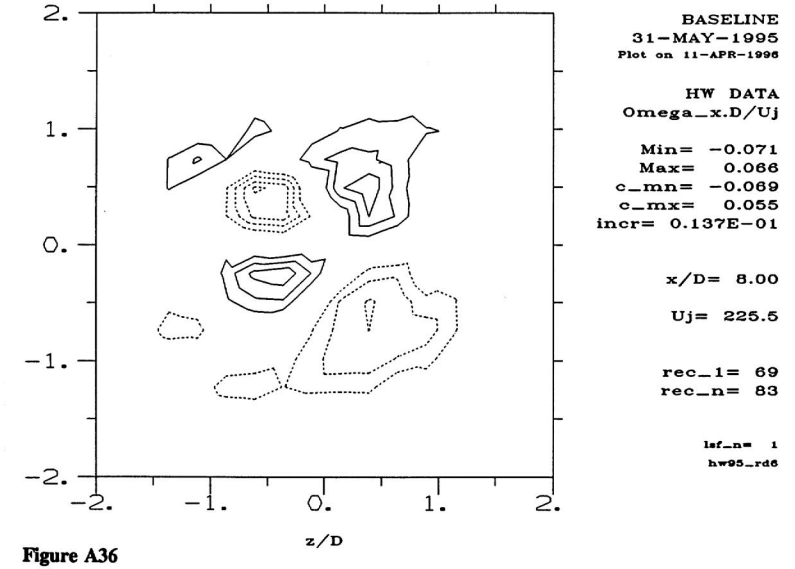

Figure A36

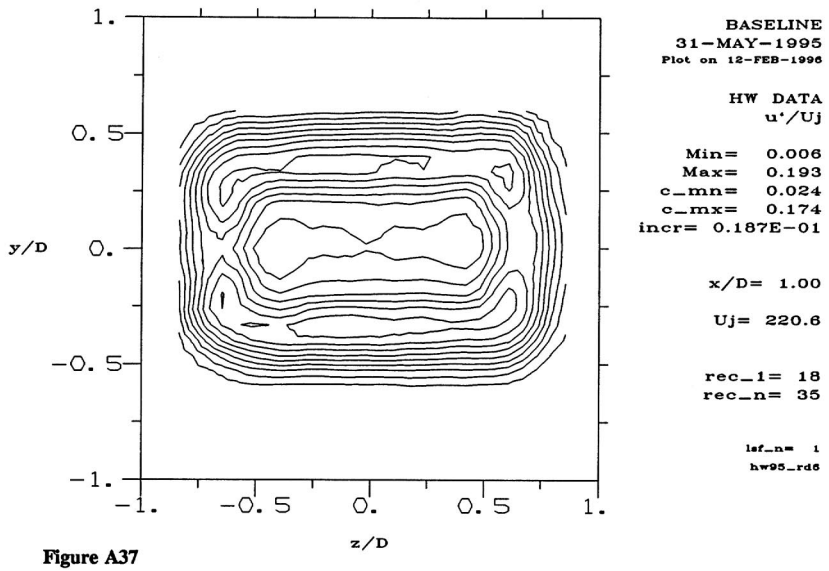

Figure A37

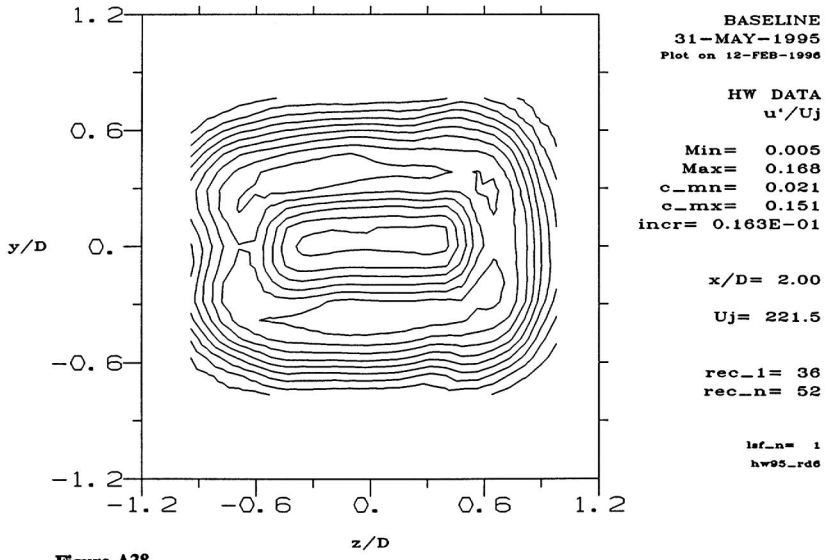

Figure A38

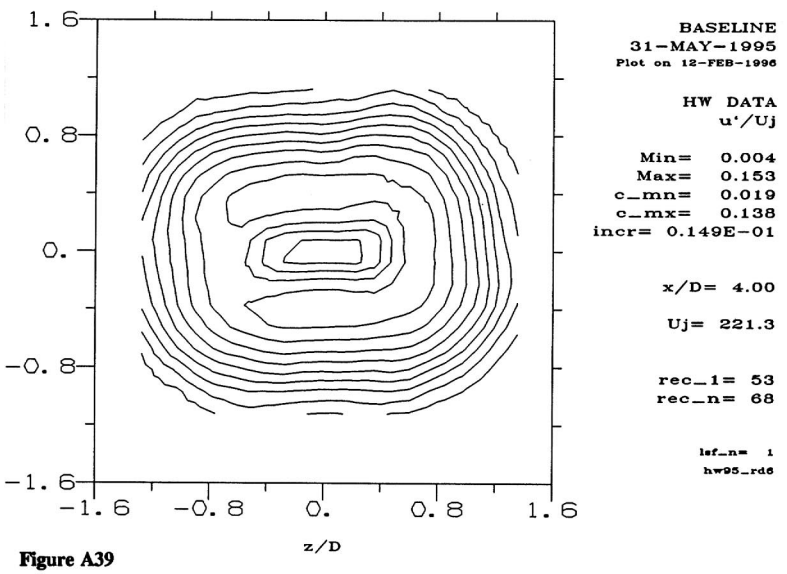

Figure A39

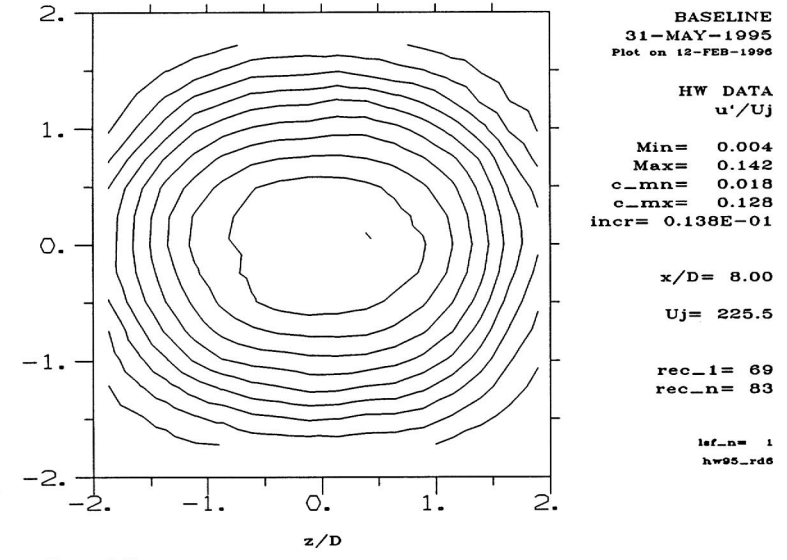

Figure A40

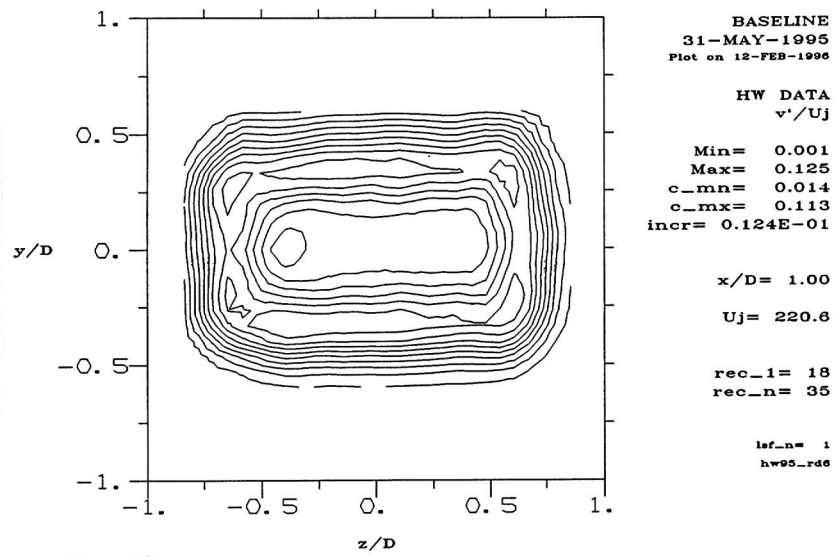

Figure A41

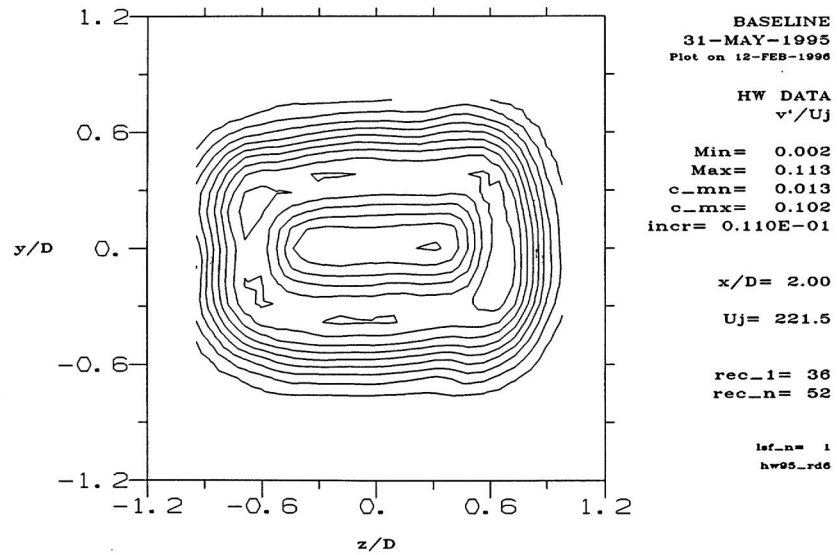

Figure A42

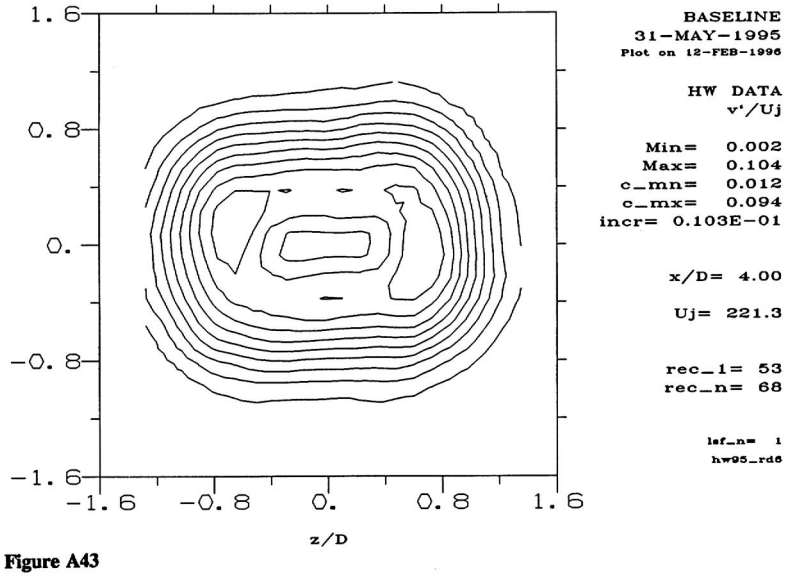

Figure A43

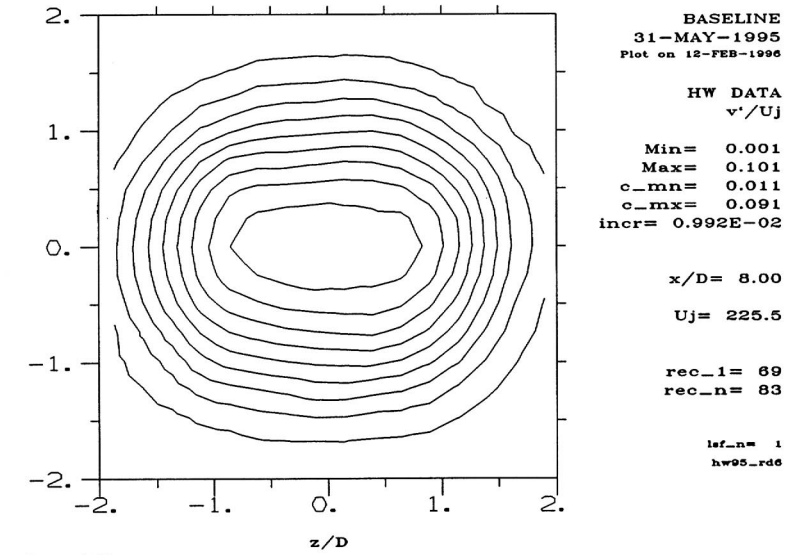

Figure A44

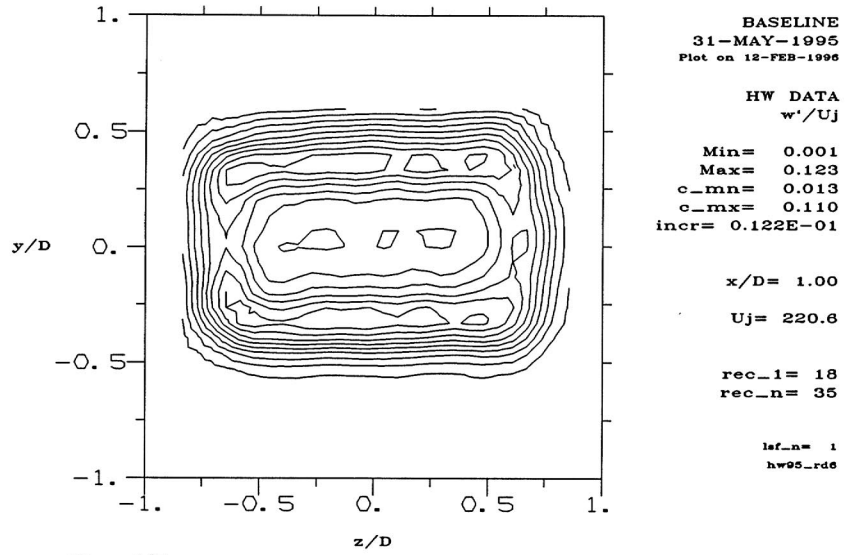

Figure A45

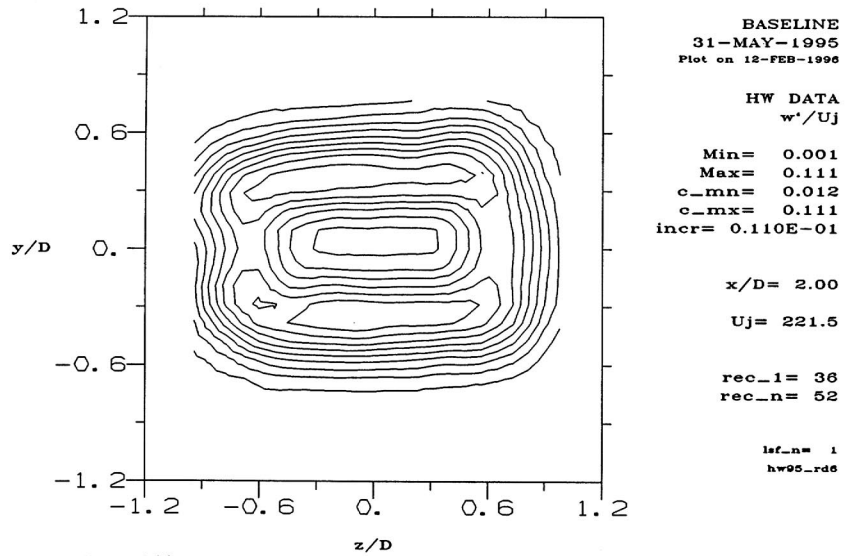

Figure A46

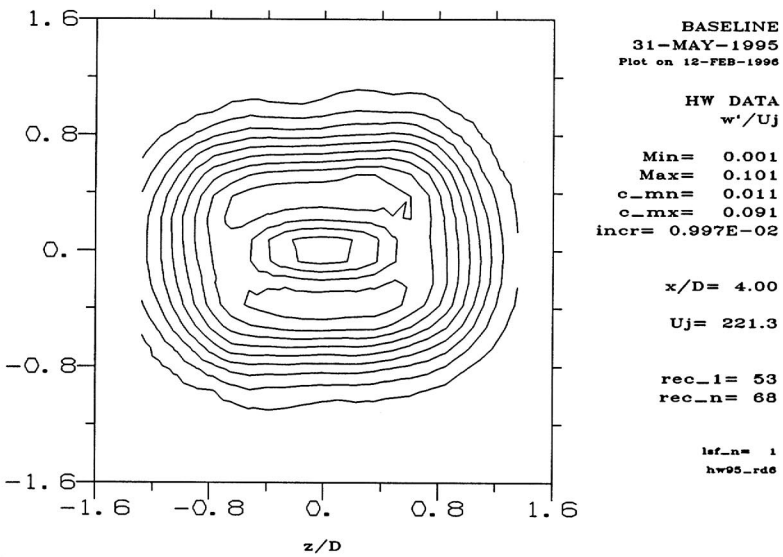

Figure A47

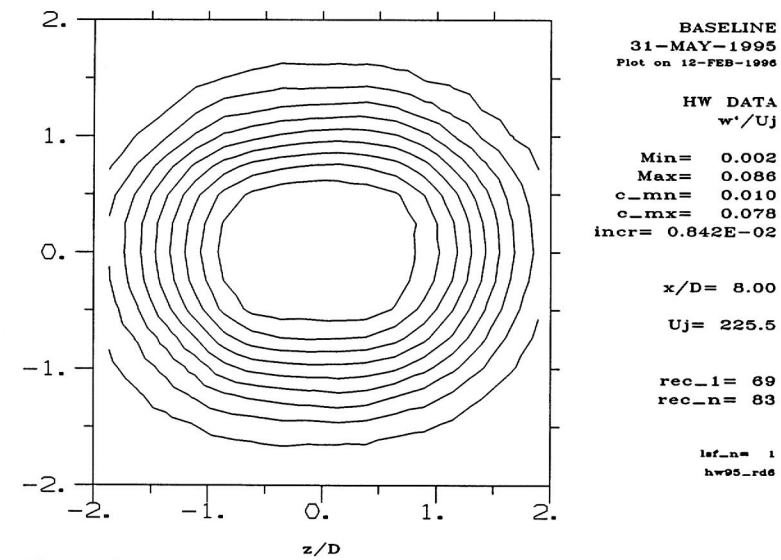

Figure A48

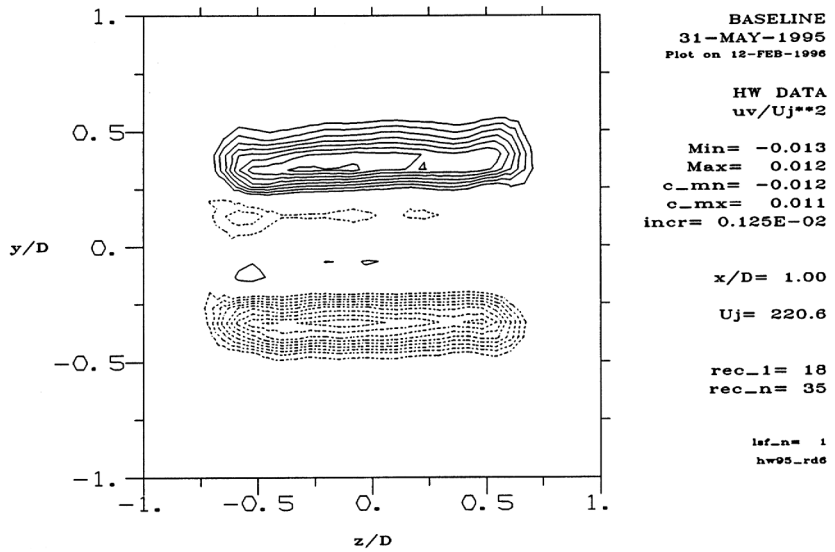

Figure A49

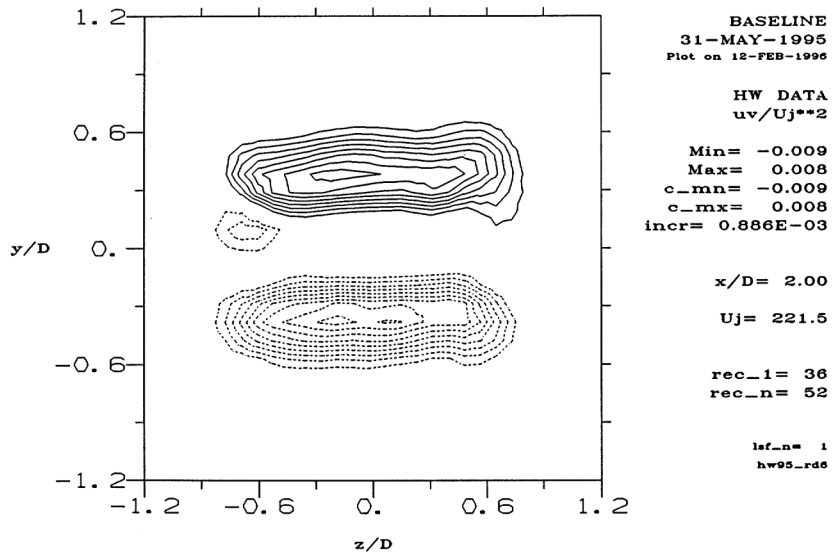

Figure A50

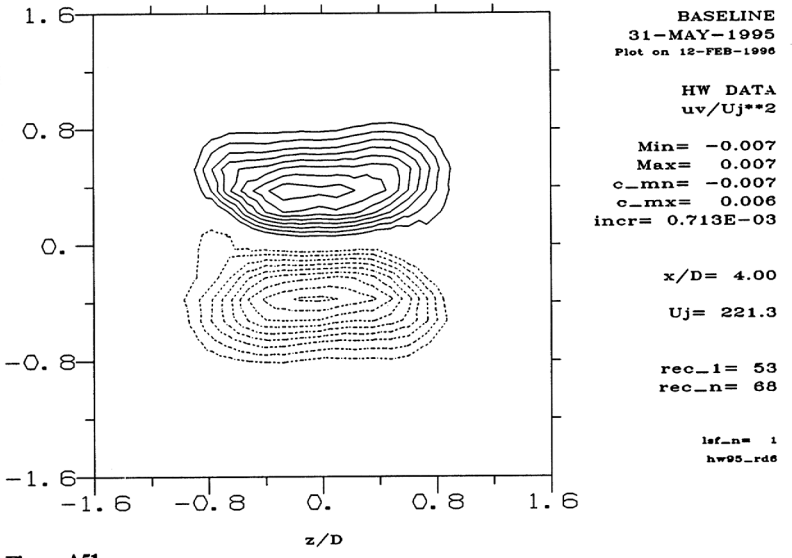

Figure A51

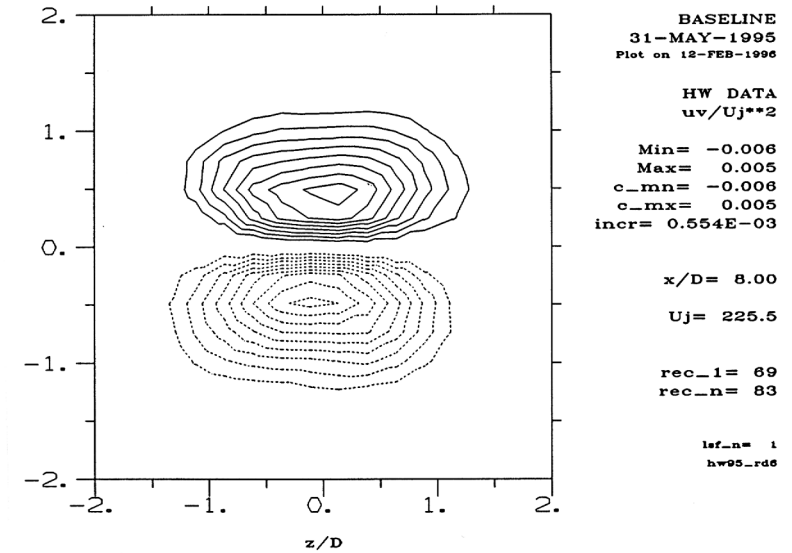

Figure A52

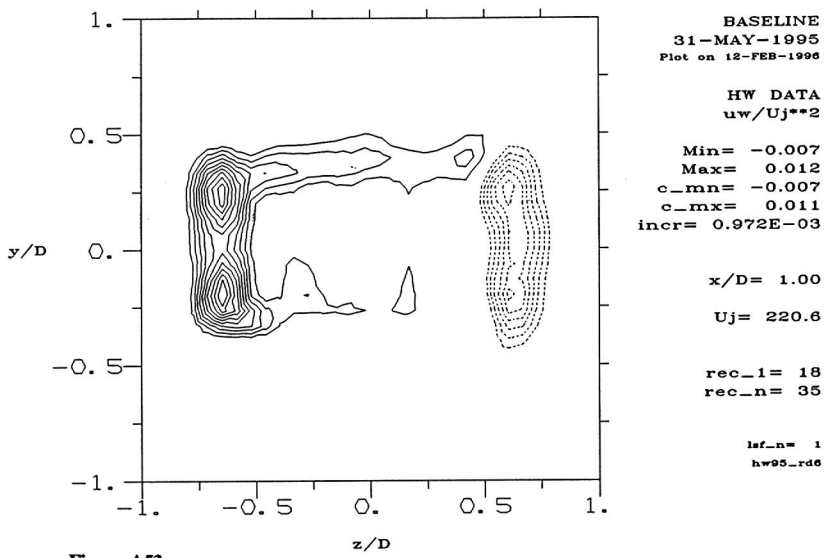

Figure A53

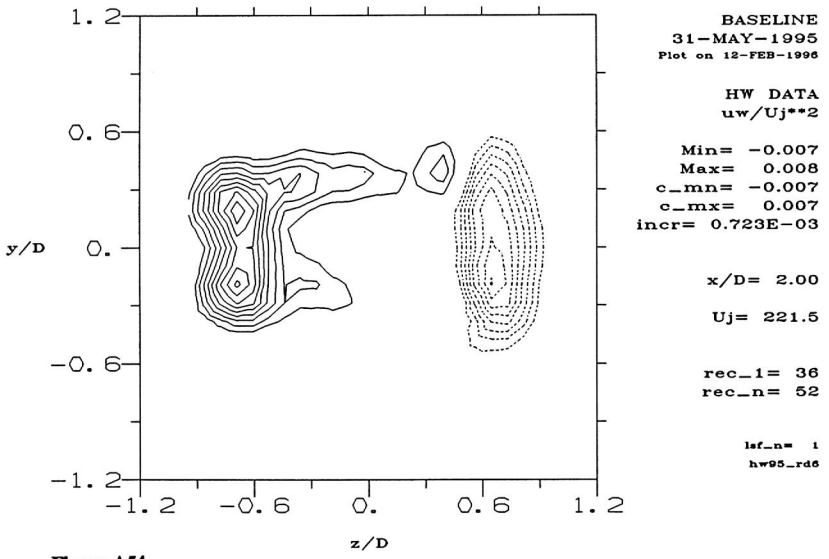

Figure A54

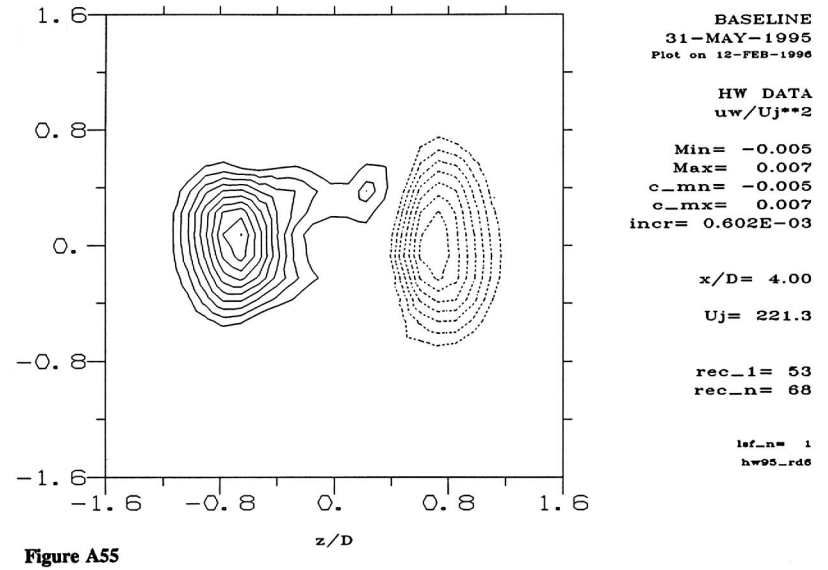

Figure A55

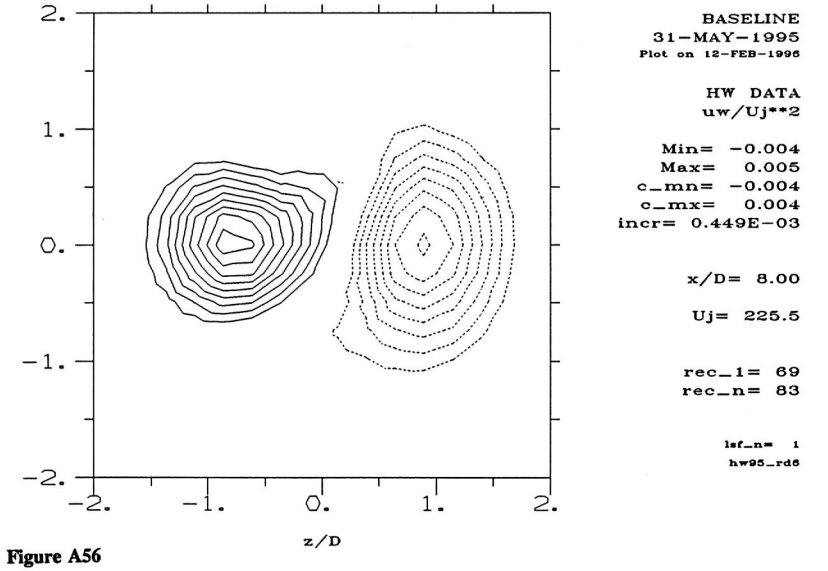

Figure A56

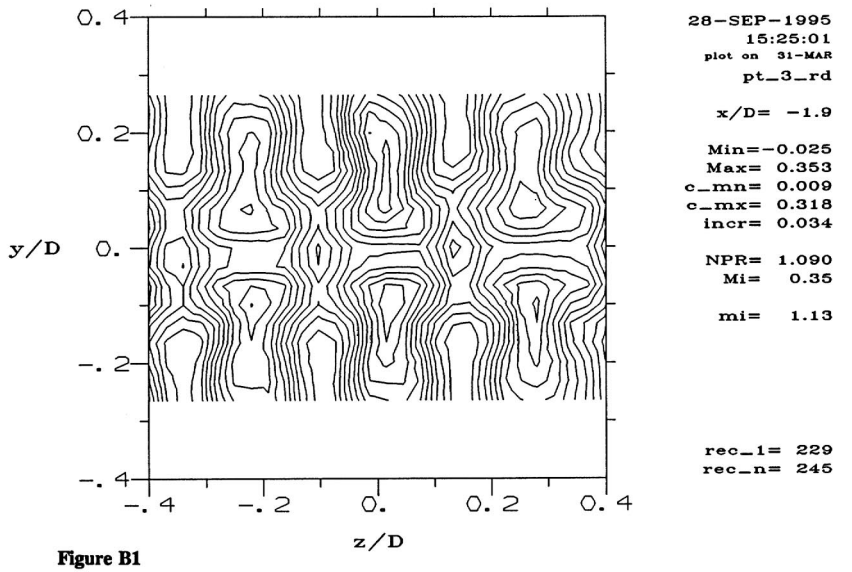

Figure B1

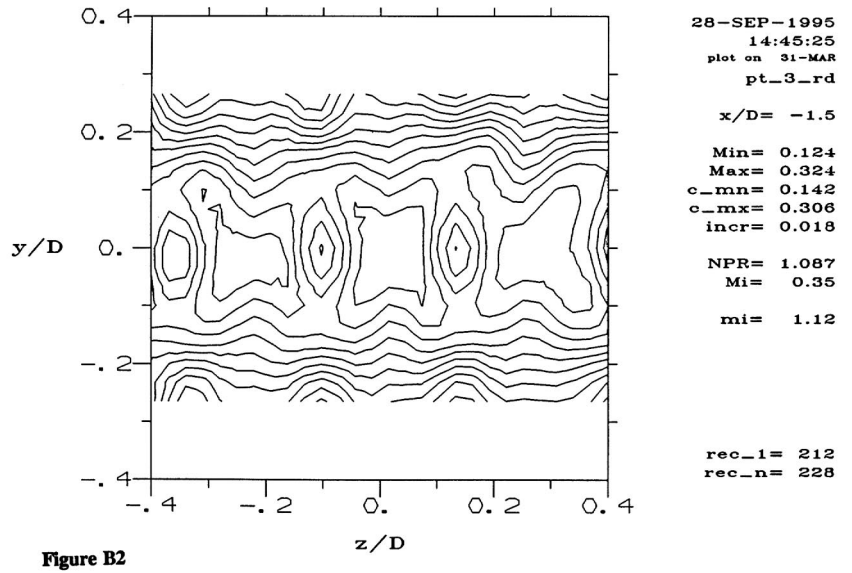

Figure B2

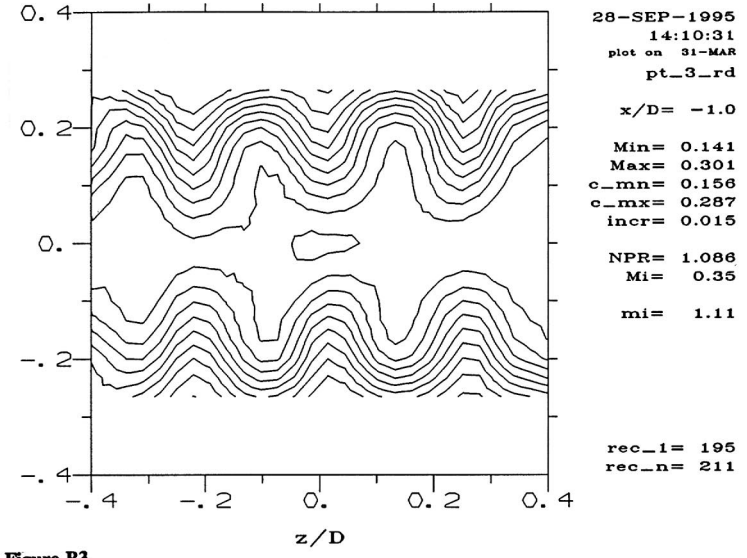

Figure B3

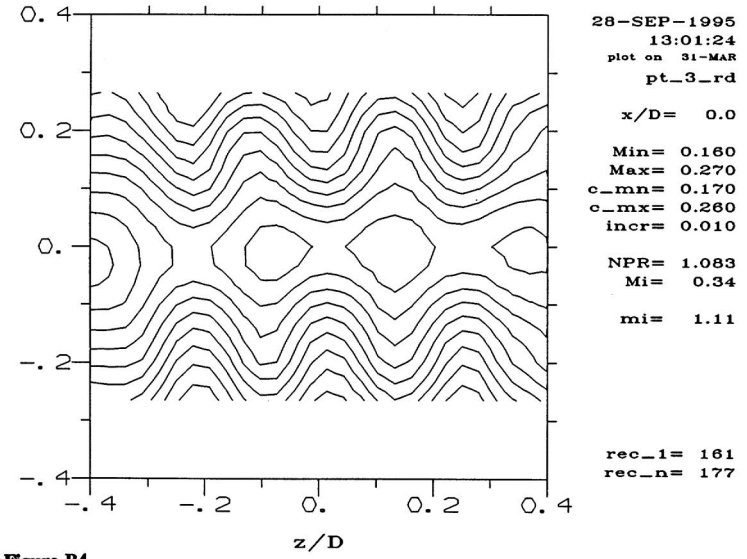

Figure B4

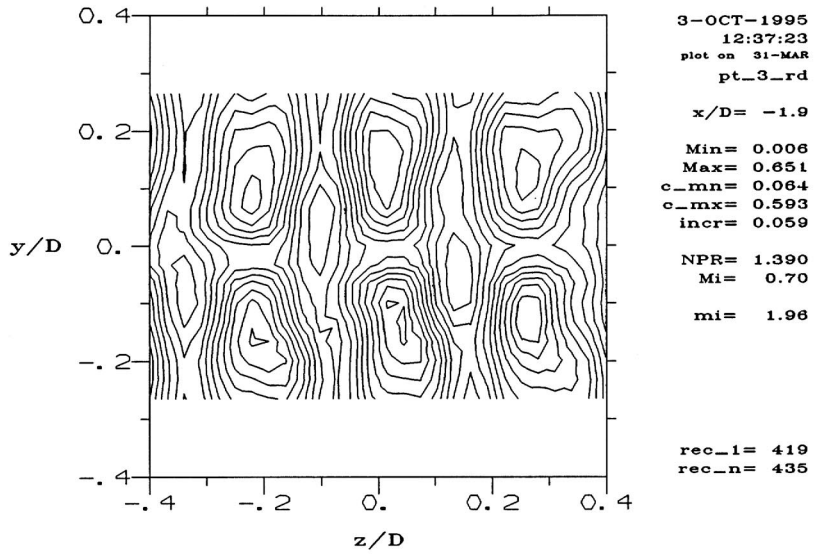

Figure B5

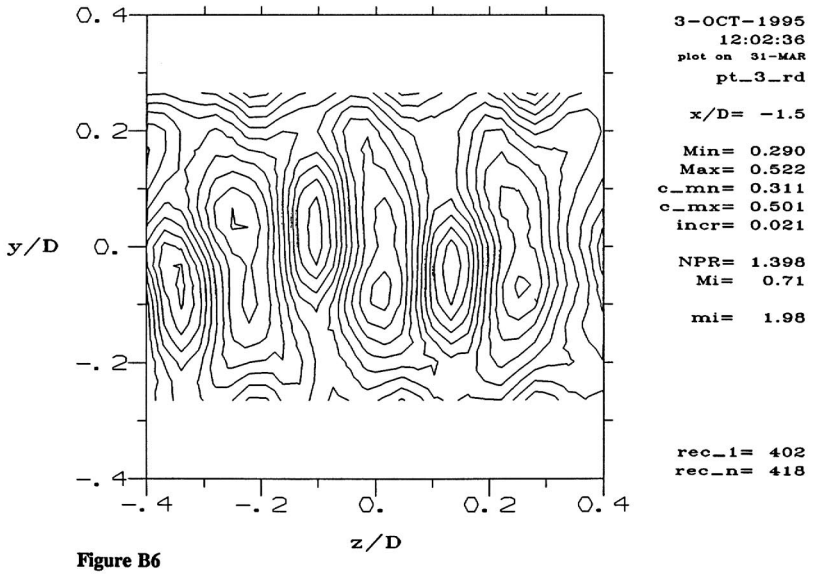

Figure B6

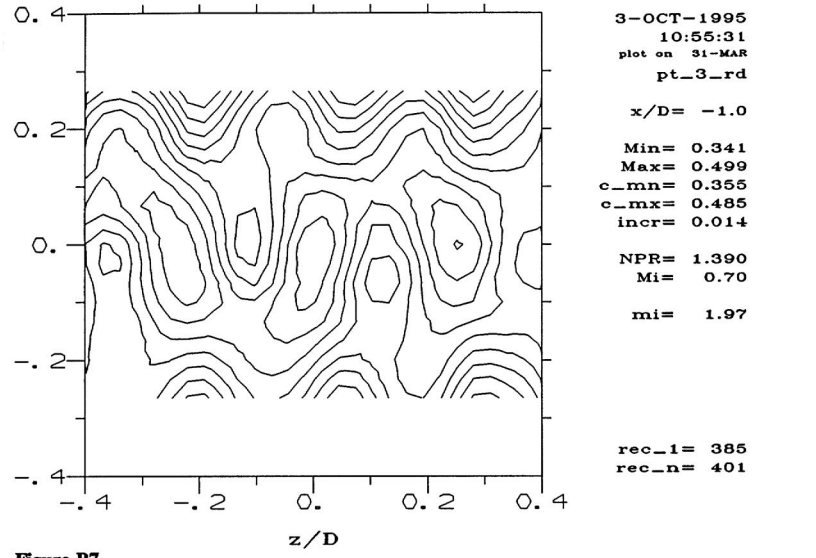

Figure B7

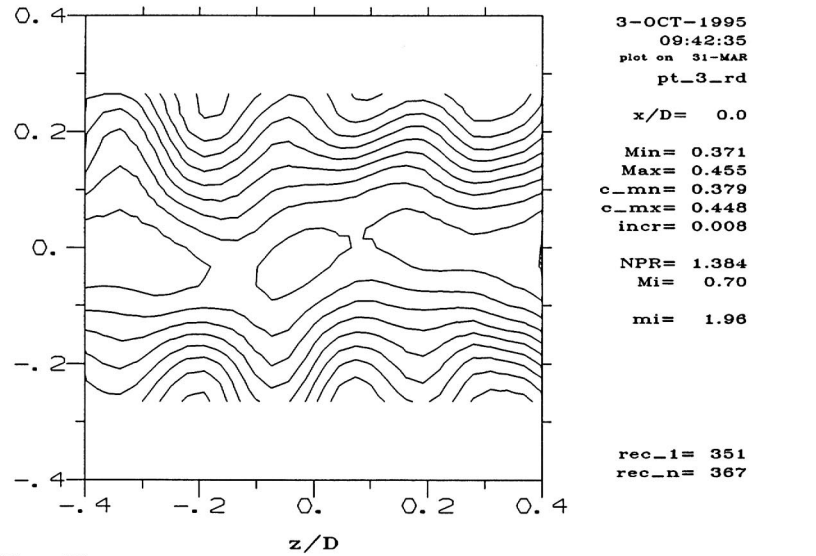

Figure B8

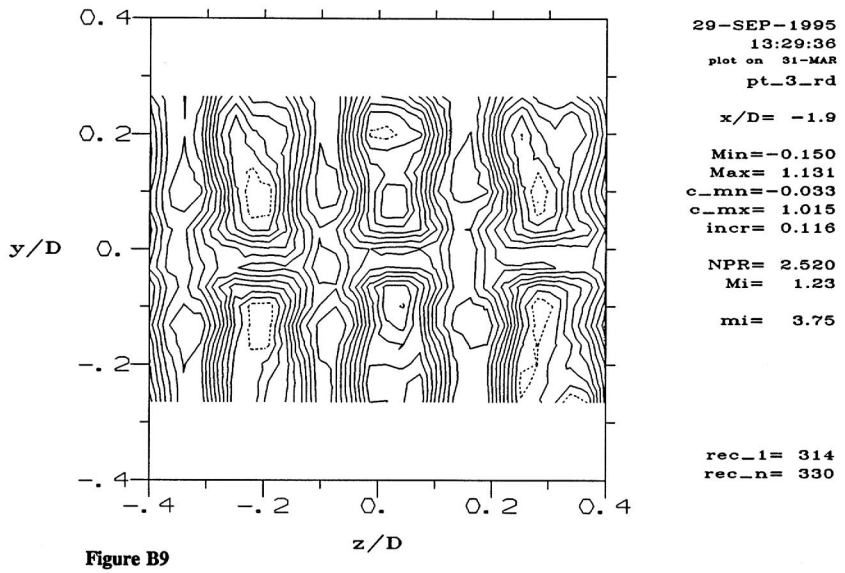

Figure B9

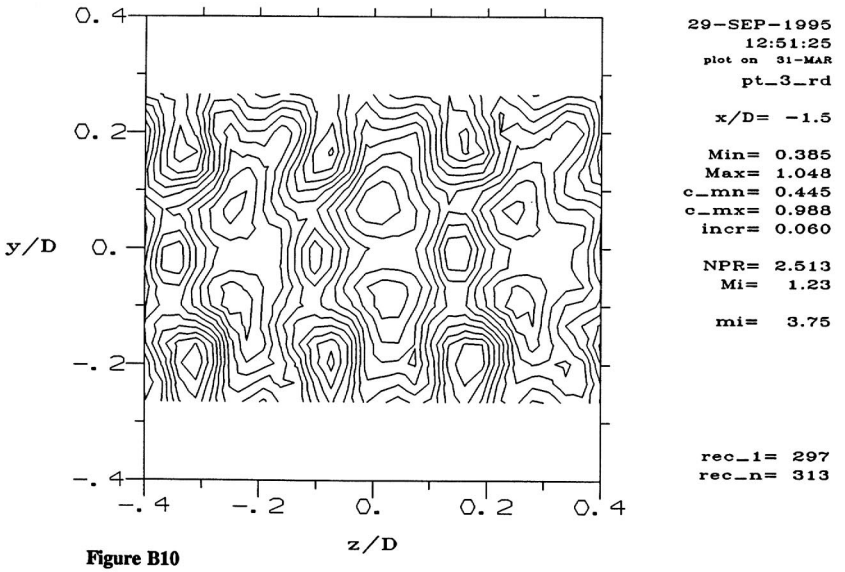

Figure B10

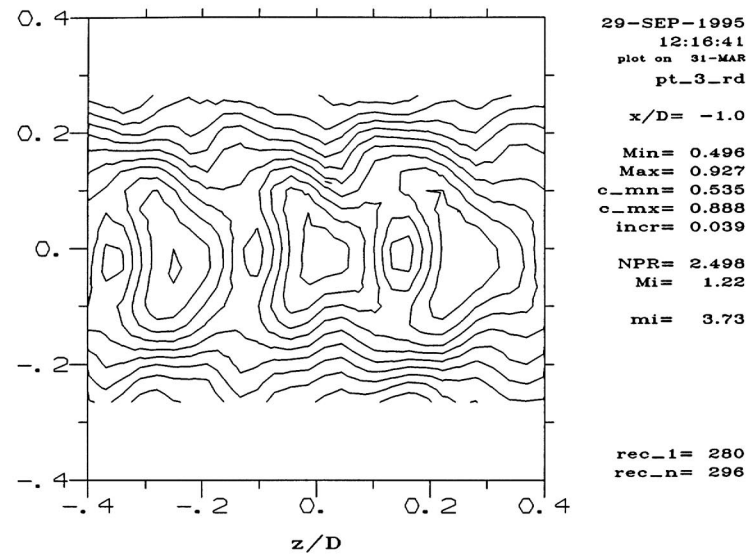

Figure B11

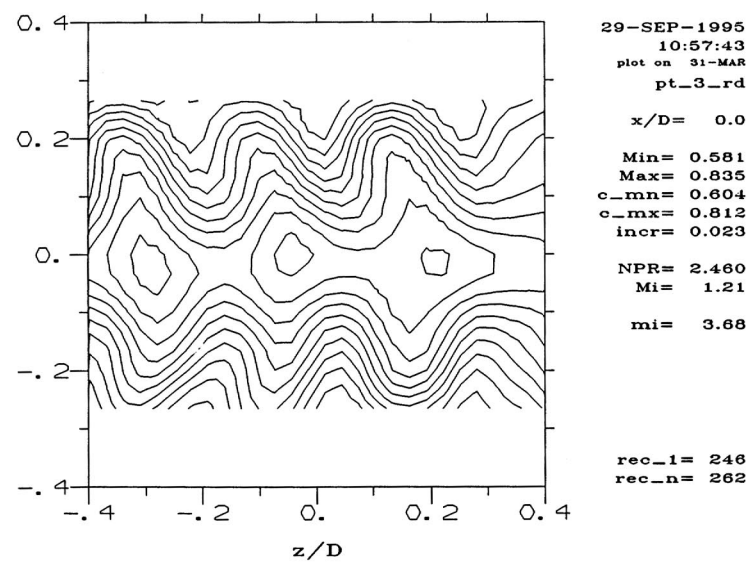

Figure B12

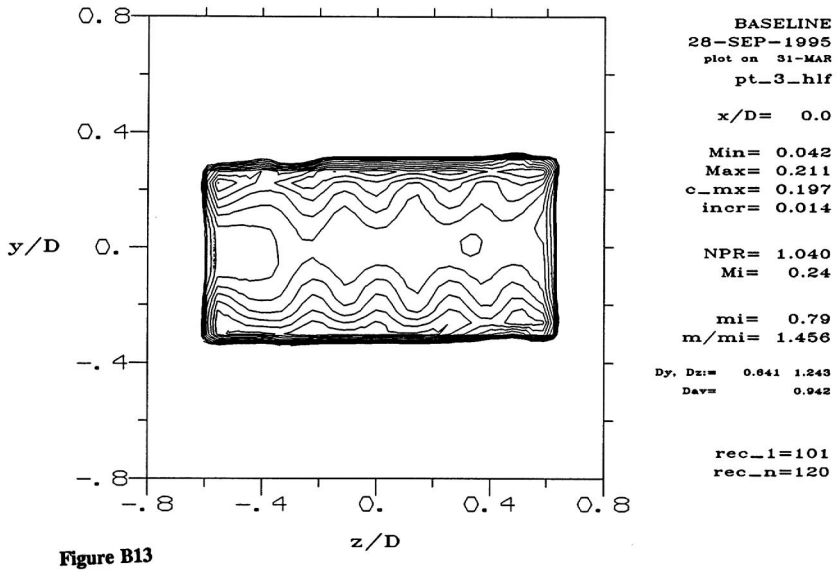

Figure B13

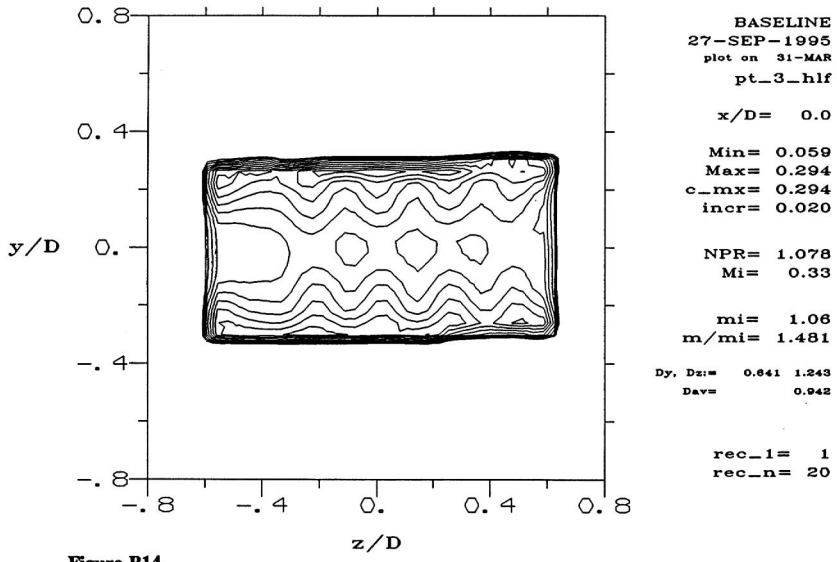

Figure B14

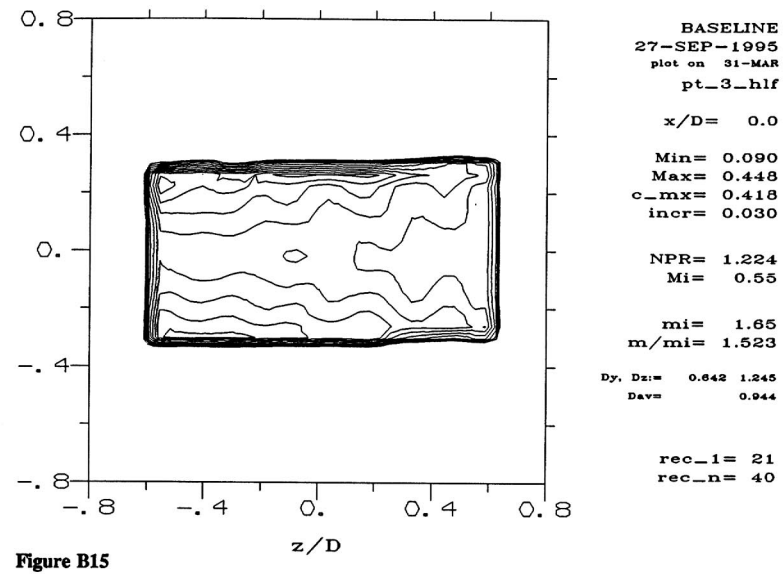

Figure B15

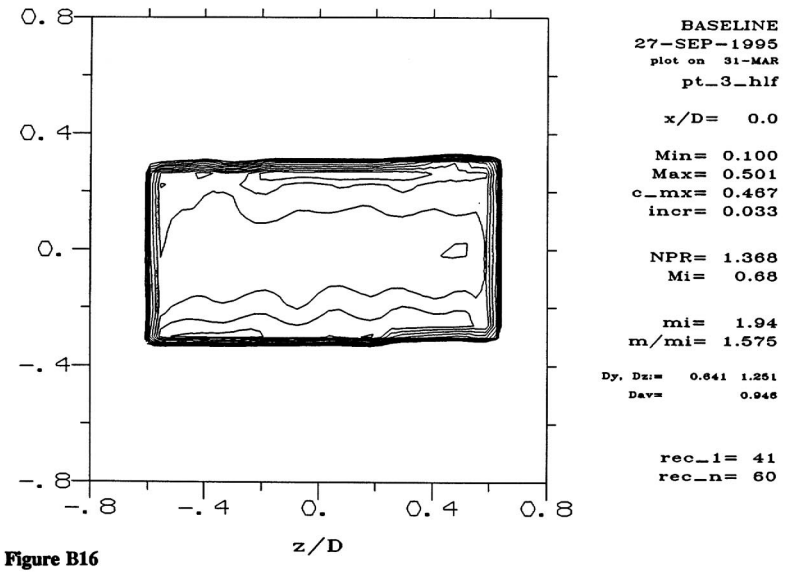

Figure B16

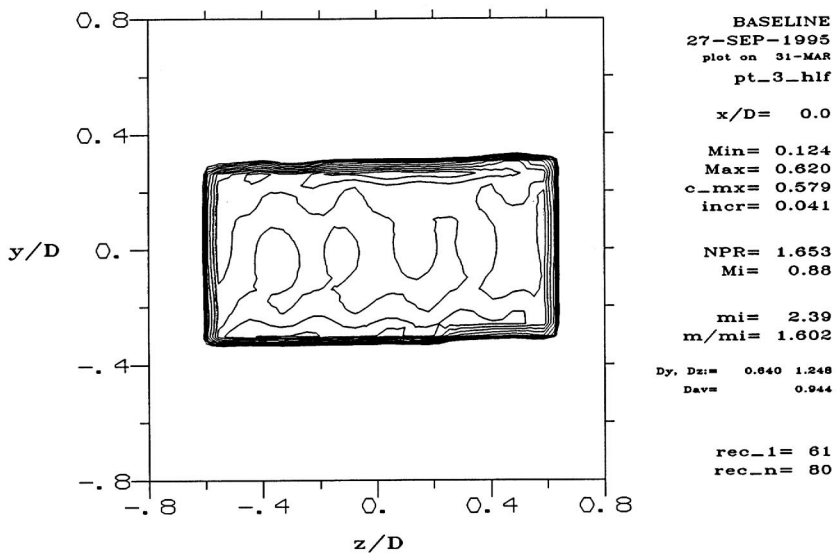

Figure B17

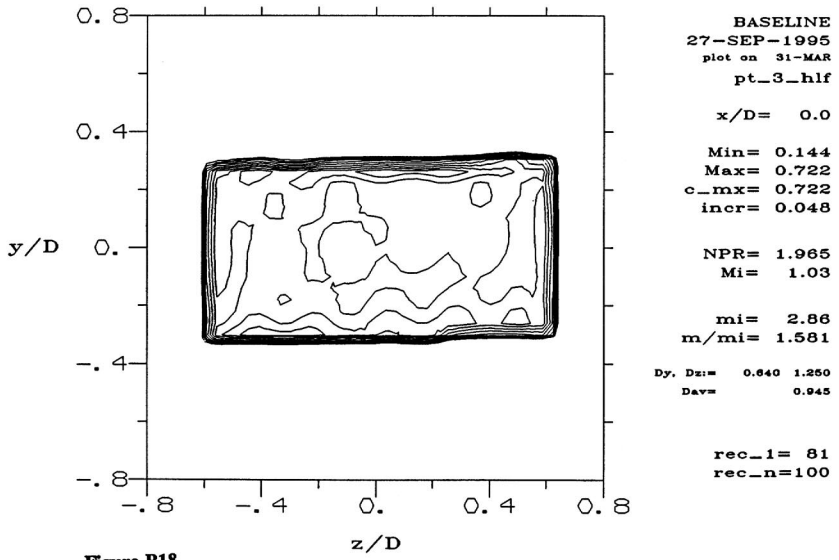

Figure B18

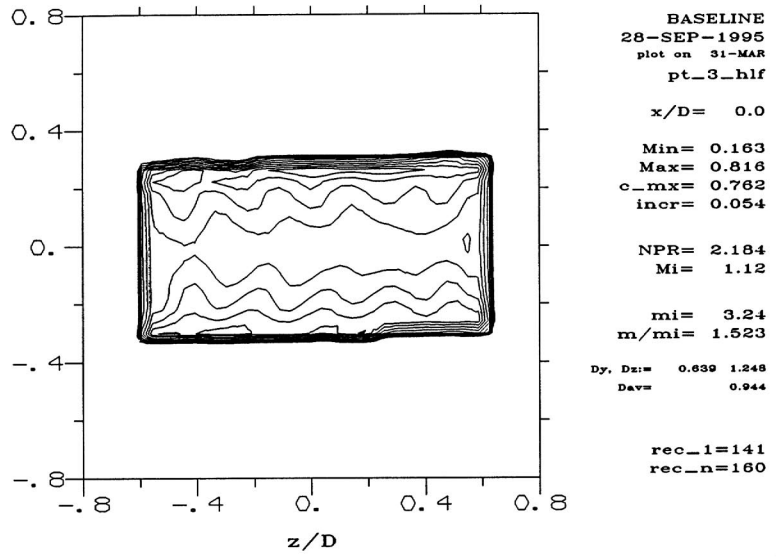

Figure B19

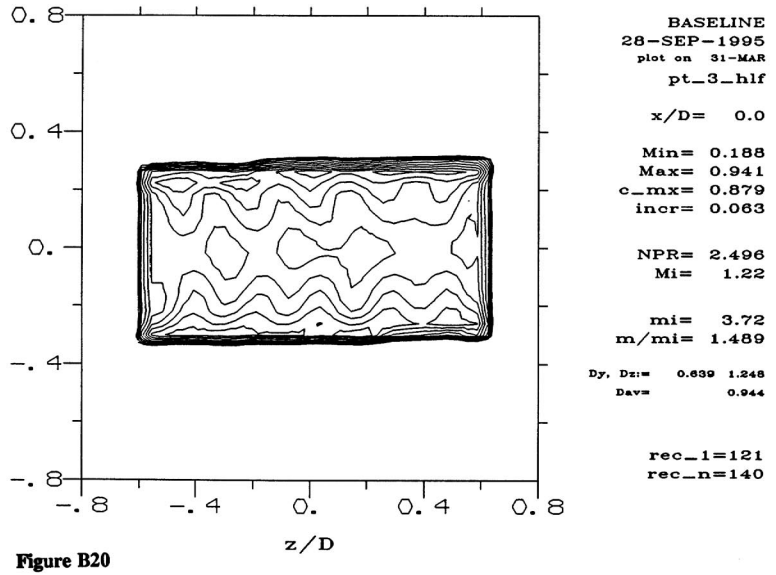

Figure B20

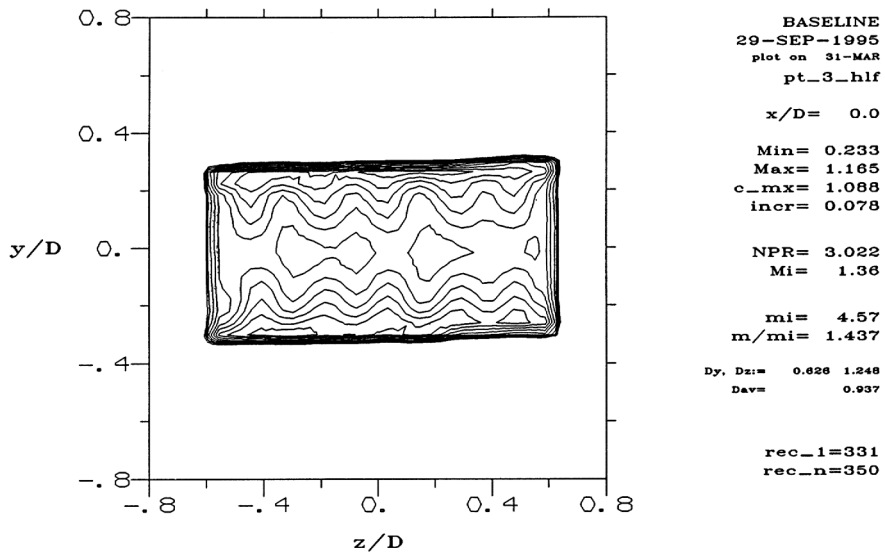

BASELINE
29-SEP-1995
plot on 31-MAR
pt_3_hlf

x/D= 0.0

Min= 0.233
Max= 1.165
c_mx= 1.088
incr= 0.078

NPR= 3.022
Mi= 1.36

mi= 4.57
m/mi= 1.437

Dy, Dz:= 0.626 1.248
Dav= 0.937

rec_1=331
rec_n=350

Figure B21

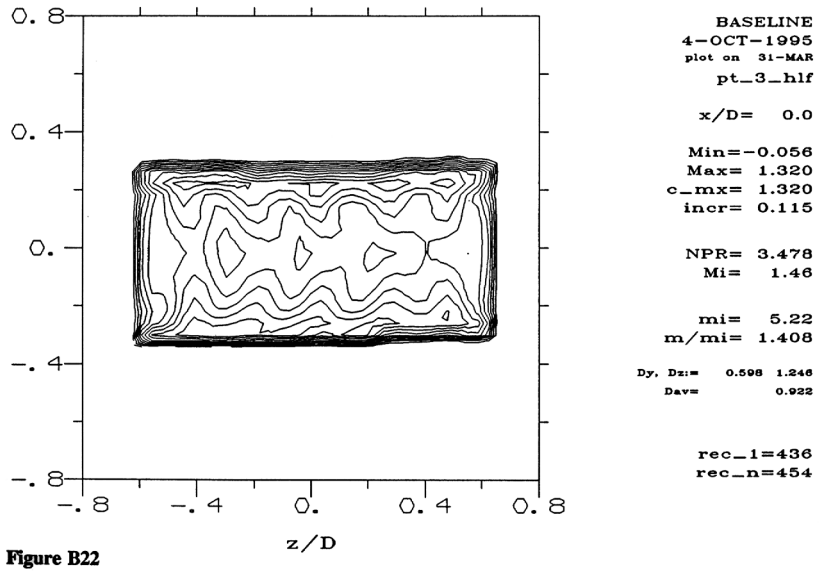

BASELINE
4-OCT-1995
plot on 31-MAR
pt_3_hlf

x/D= 0.0

Min=-0.056
Max= 1.320
c_mx= 1.320
incr= 0.115

NPR= 3.478
Mi= 1.46

mi= 5.22
m/mi= 1.408

Dy, Dz:= 0.598 1.246
Dav= 0.922

rec_1=436
rec_n=454

Figure B22

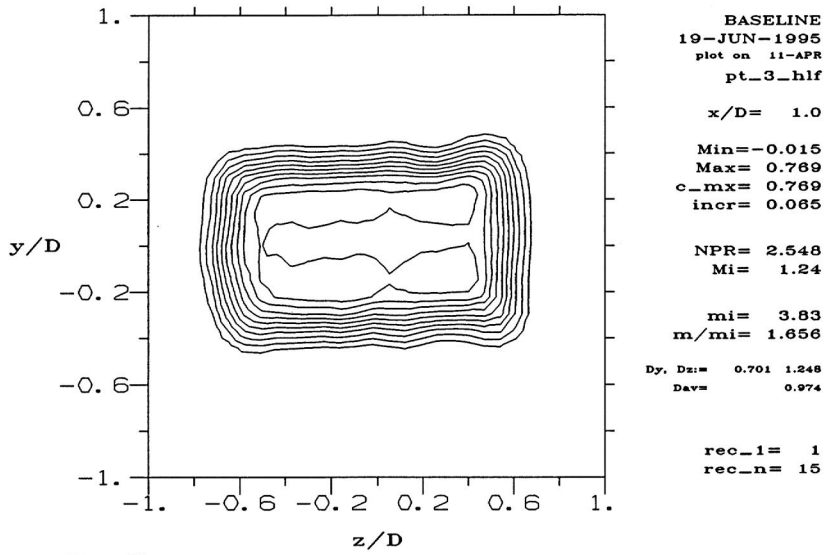

BASELINE
19-JUN-1995
plot on 11-APR
pt_3_hlf

x/D= 1.0

Min=-0.015
Max= 0.769
c_mx= 0.769
incr= 0.065

NPR= 2.548
Mi= 1.24

mi= 3.83
m/mi= 1.656

Dy, Dz:= 0.701 1.248
Dav= 0.974

rec_1= 1
rec_n= 15

Figure C1

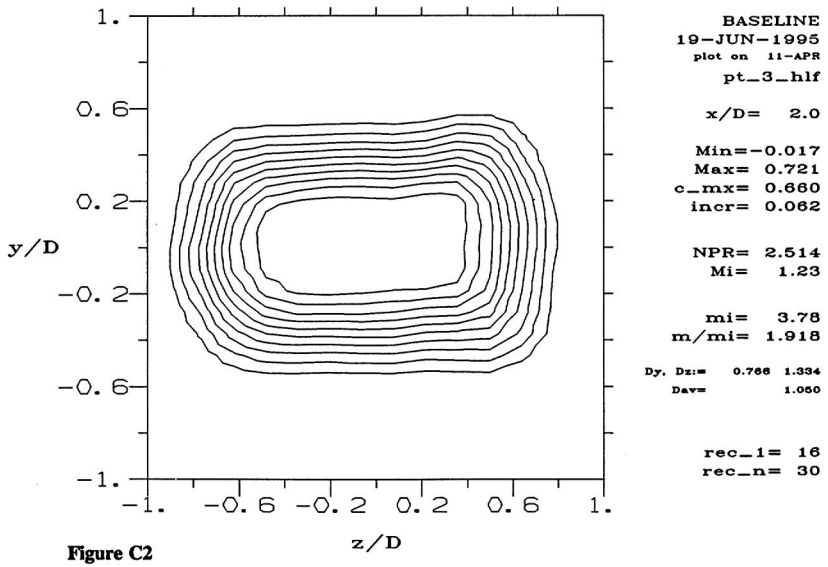

BASELINE
19-JUN-1995
plot on 11-APR
pt_3_hlf

x/D= 2.0

Min=-0.017
Max= 0.721
c_mx= 0.660
incr= 0.062

NPR= 2.514
Mi= 1.23

mi= 3.78
m/mi= 1.918

Dy, Dz:= 0.766 1.334
Dav= 1.050

rec_1= 16
rec_n= 30

Figure C2

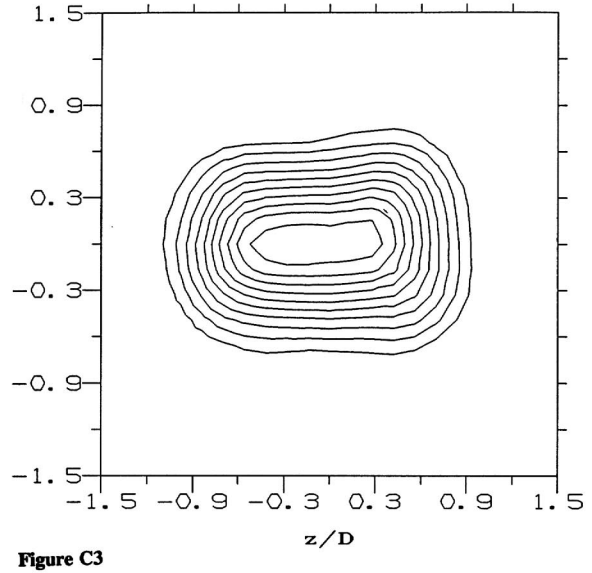

BASELINE
20-JUN-1995
plot on 11-APR
pt_3_hlf

x/D= 4.0

Min=-0.009
Max= 0.688
c_mx= 0.630
incr= 0.058

NPR= 2.513
Mi= 1.23

mi= 3.77
m/mi= 2.411

Dy, Dz:= 0.831 1.519
Dav= 1.175

rec_1= 31
rec_n= 43

Figure C3

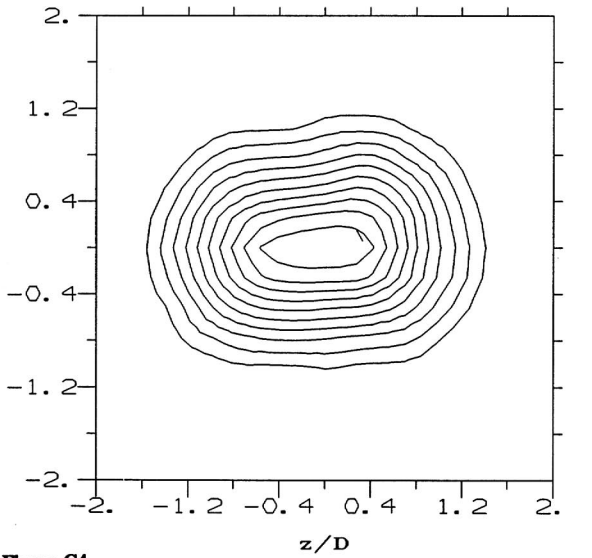

BASELINE
21-JUN-1995
plot on 11-APR
pt_3_hlf

x/D= 8.0

Min=-0.006
Max= 0.507
c_mx= 0.464
incr= 0.043

NPR= 2.510
Mi= 1.23

mi= 3.77
m/mi= 3.541

Dy, Dz:= 1.187 2.025
Dav= 1.606

rec_1= 44
rec_n= 56

Figure C4

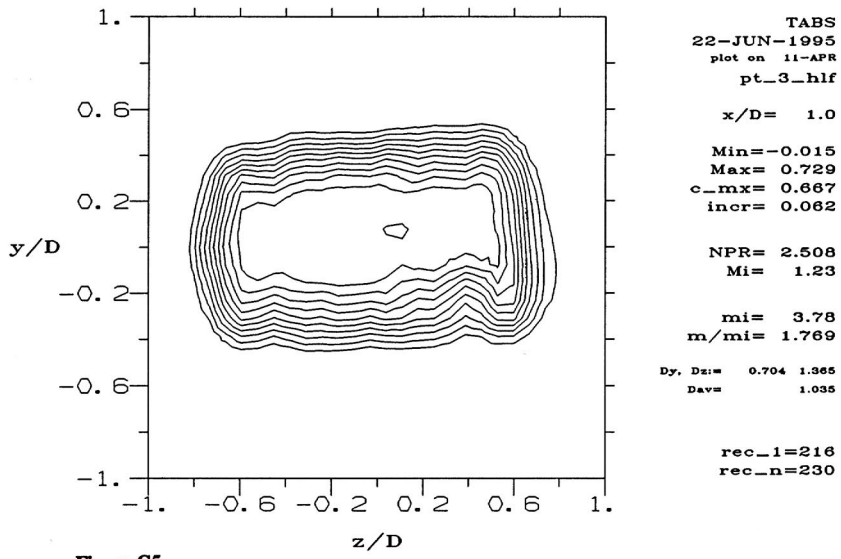

Figure C5

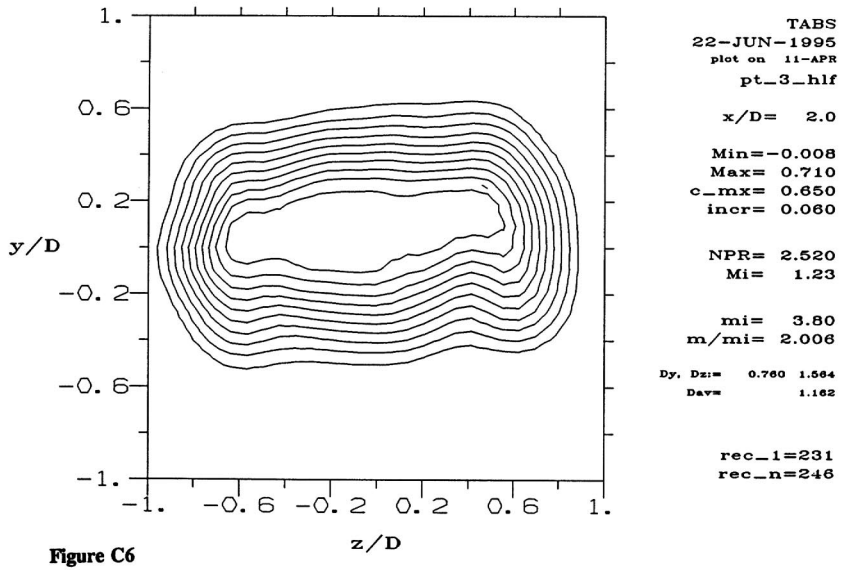

Figure C6

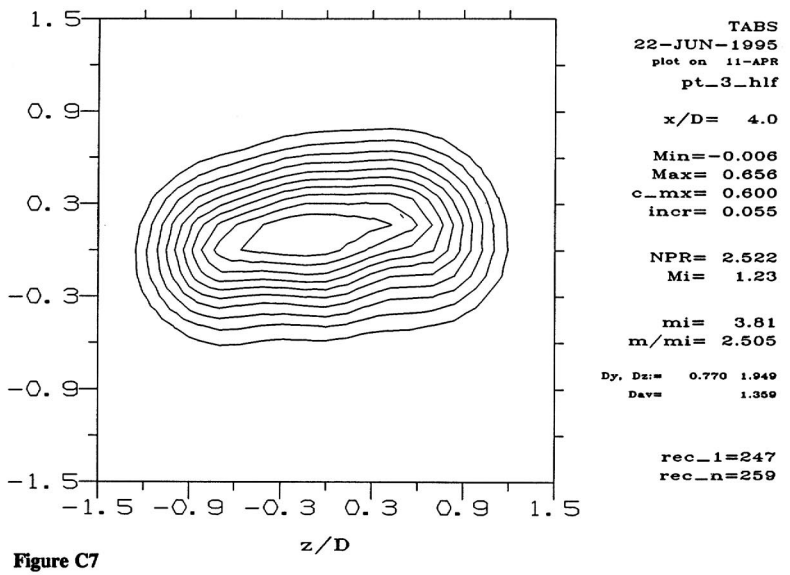

Figure C7

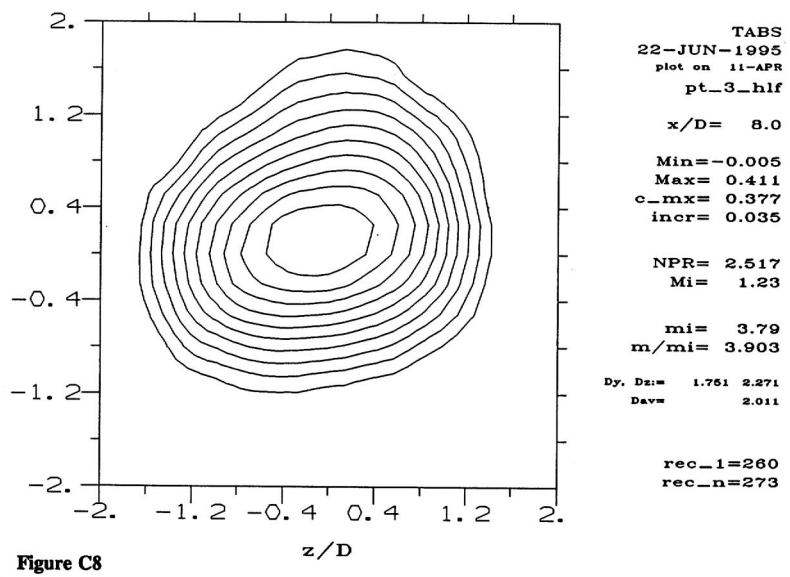

Figure C8

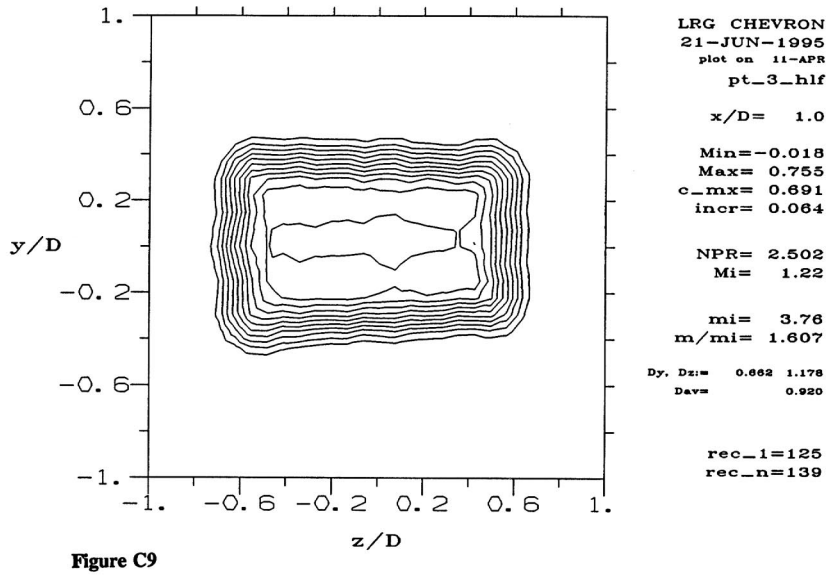

Figure C9

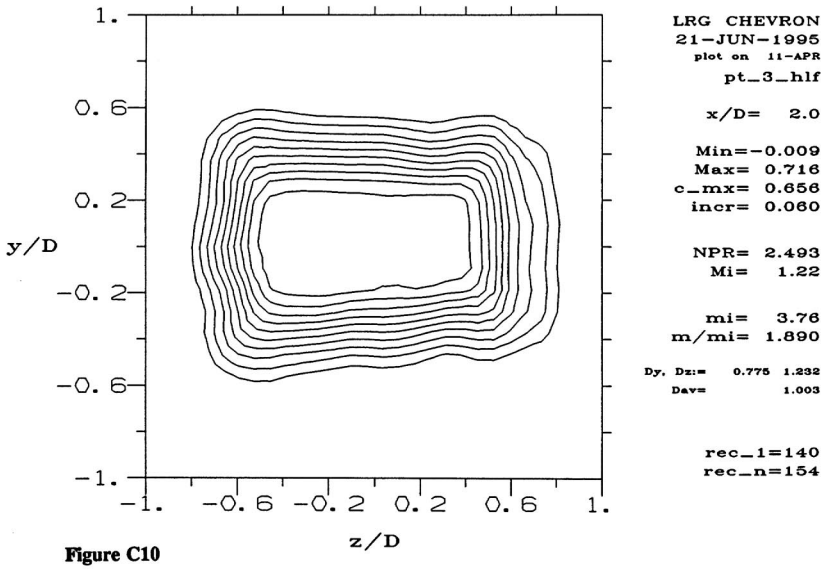

Figure C10

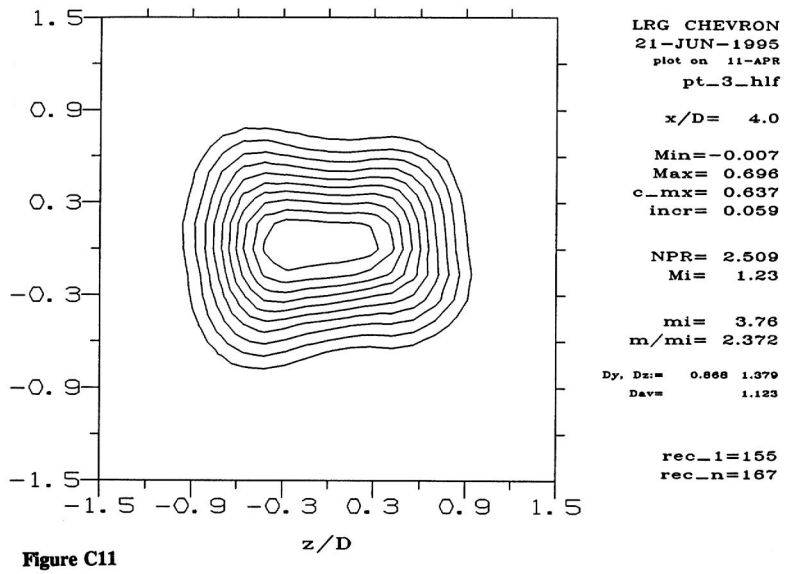

Figure C11

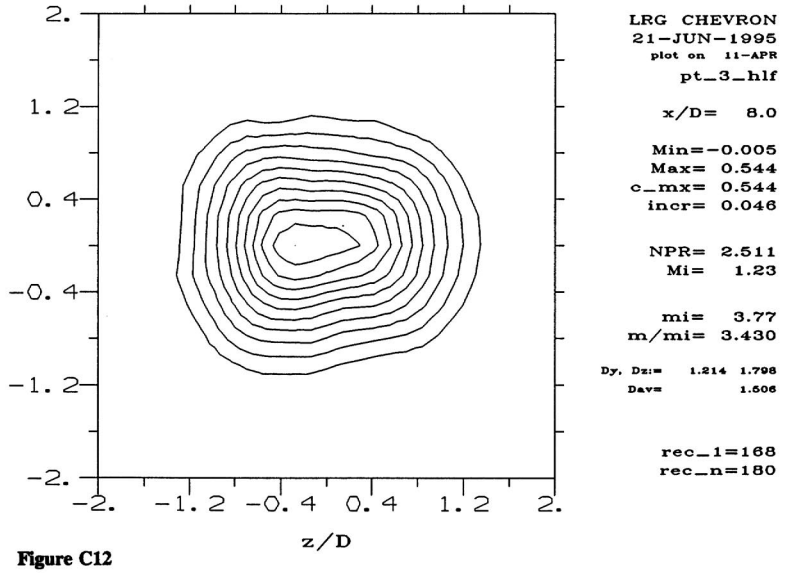

Figure C12

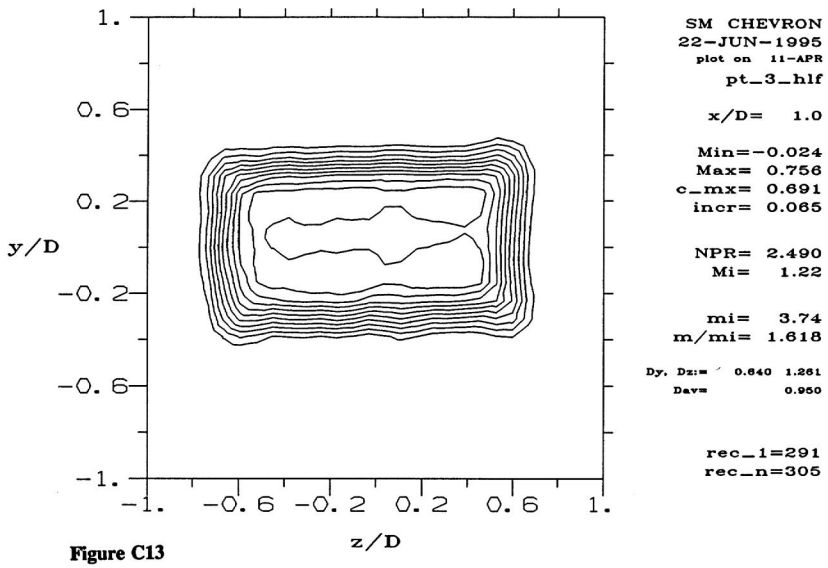

Figure C13

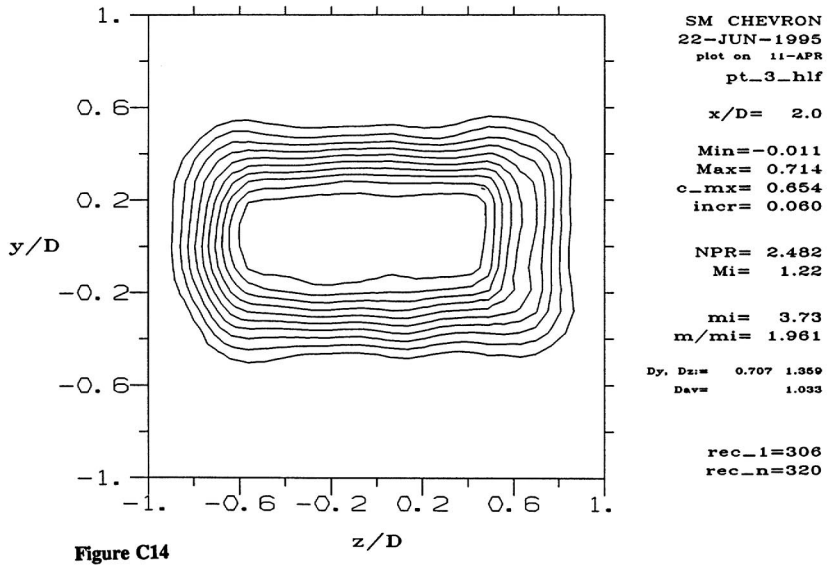

Figure C14

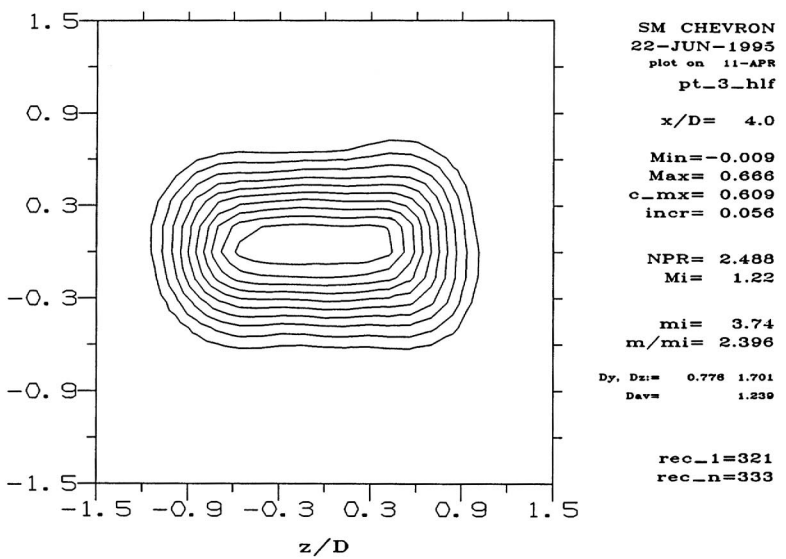

Figure C15

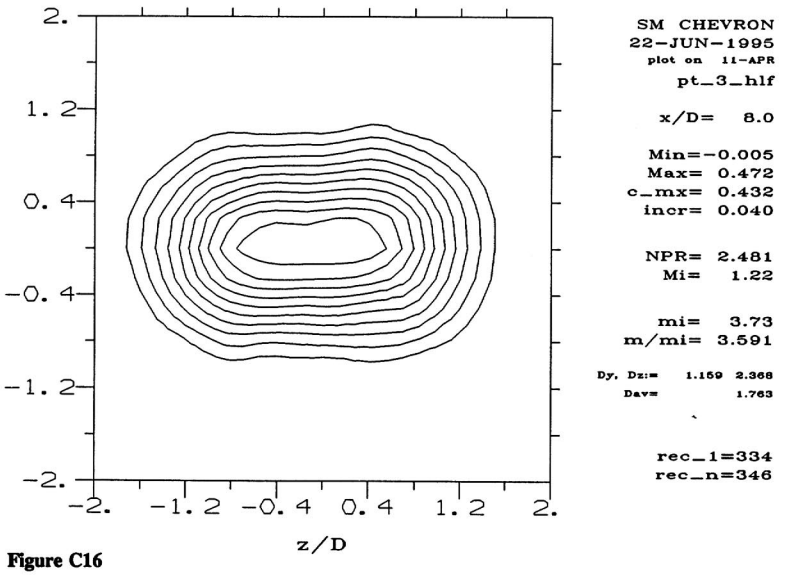

Figure C16

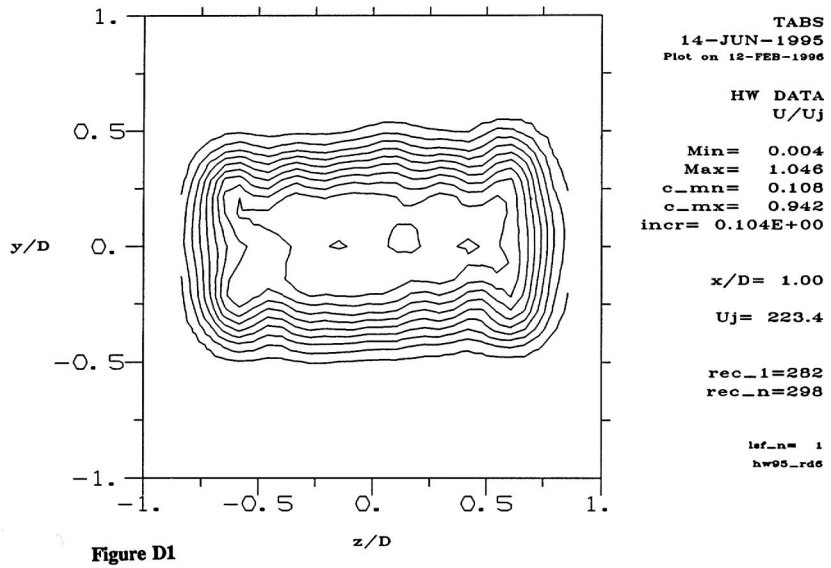

Figure D1

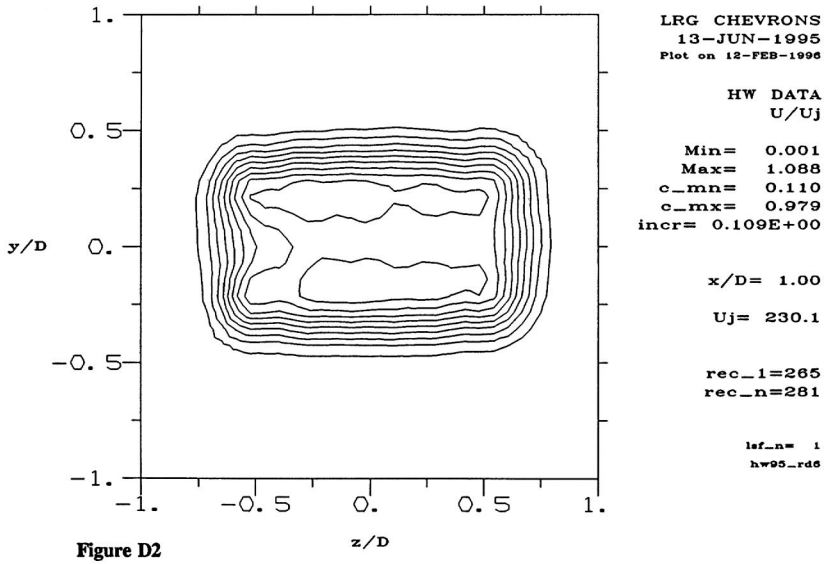

Figure D2

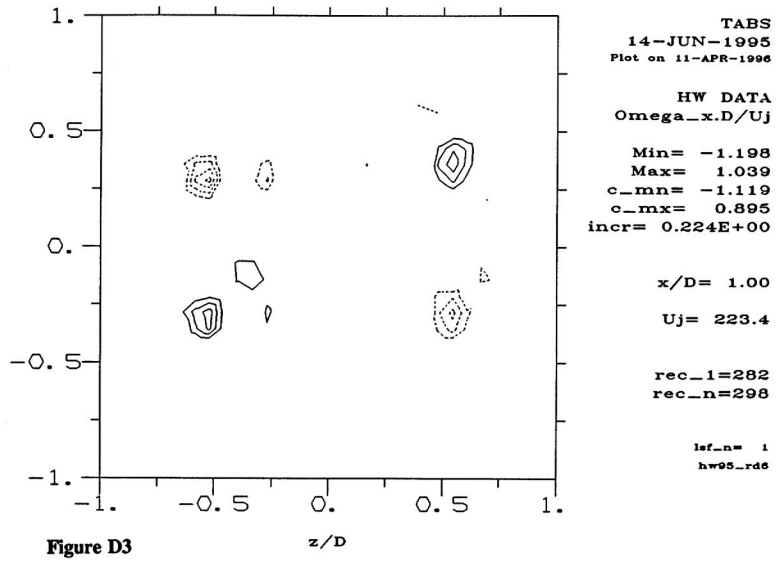

Figure D3

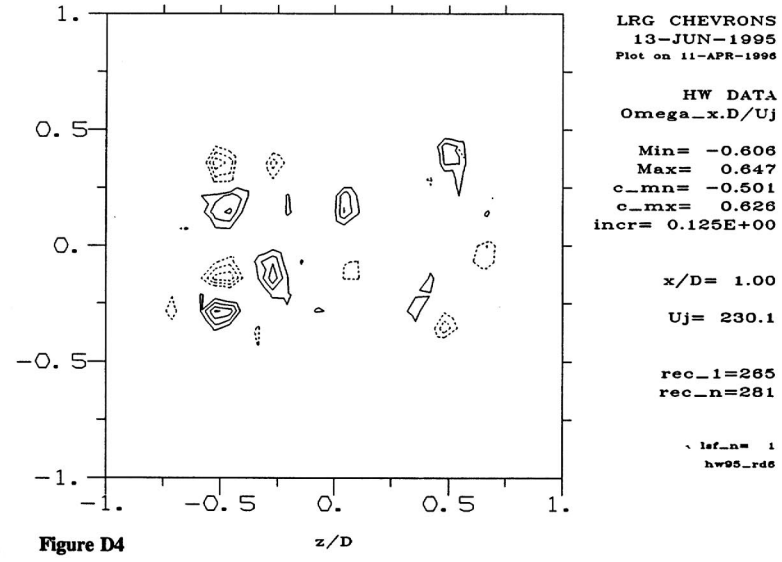

Figure D4

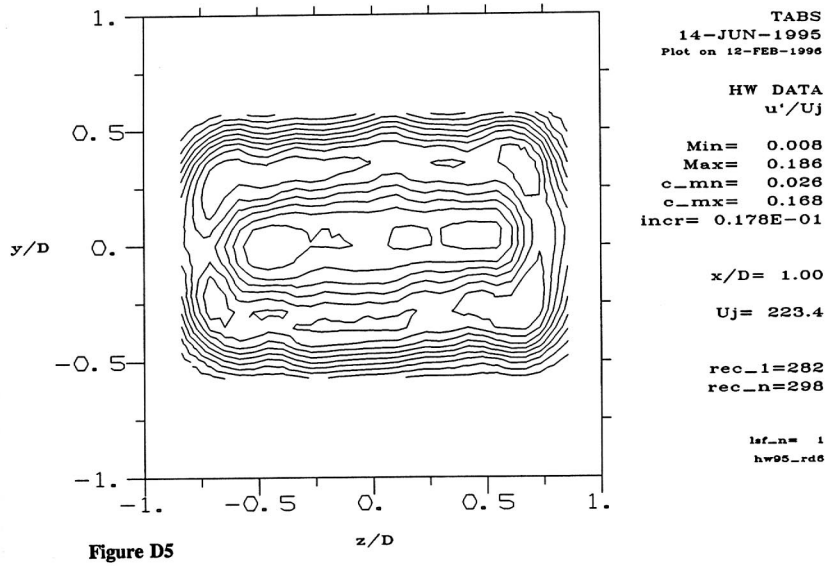

Figure D5

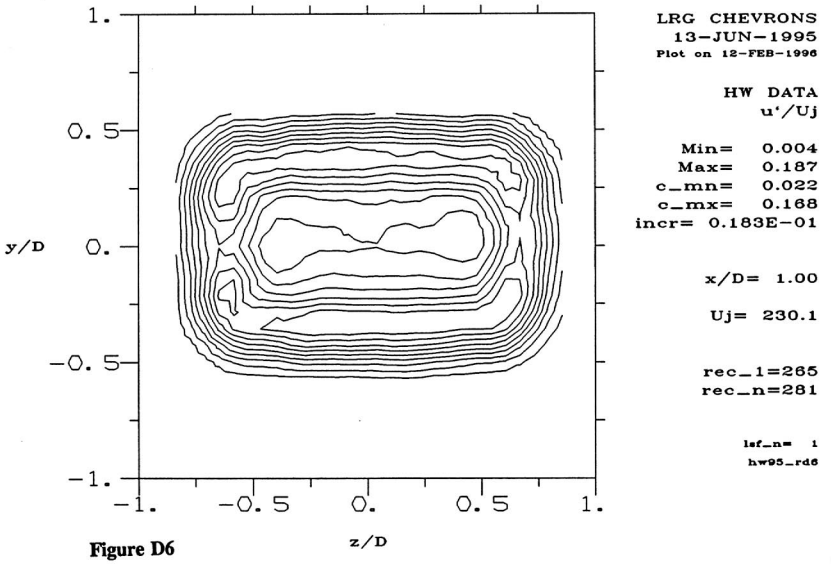

Figure D6

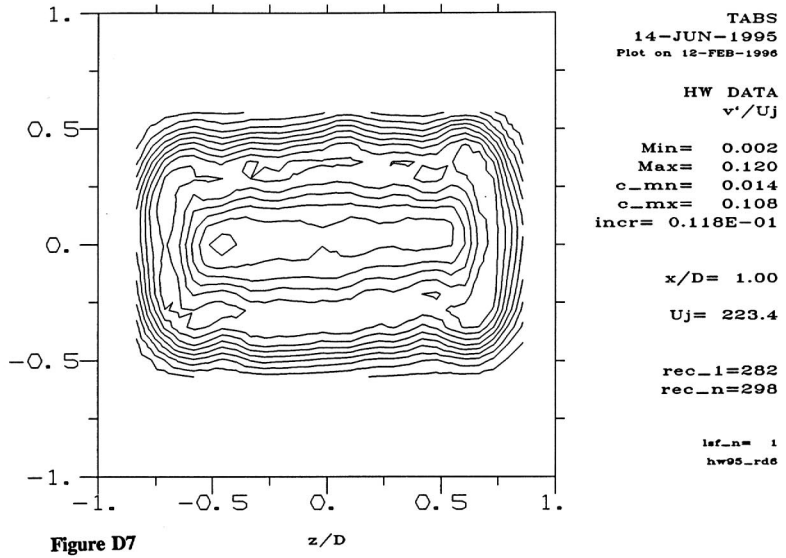

Figure D7

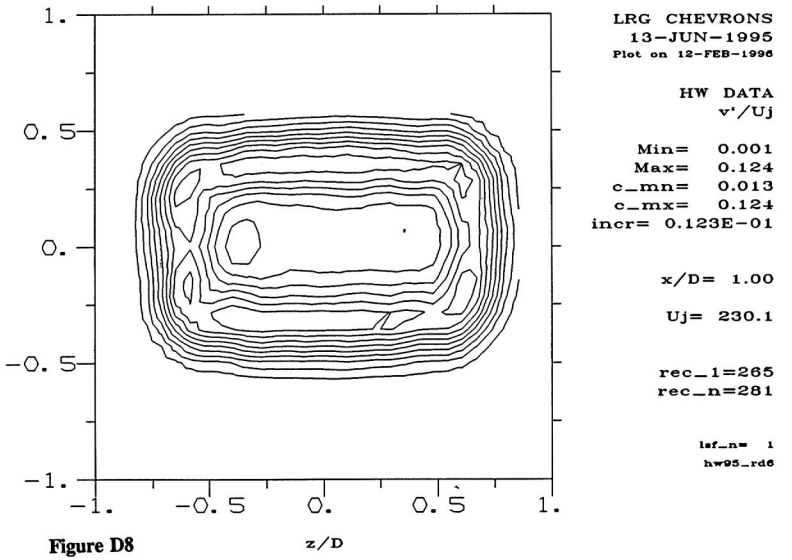

Figure D8

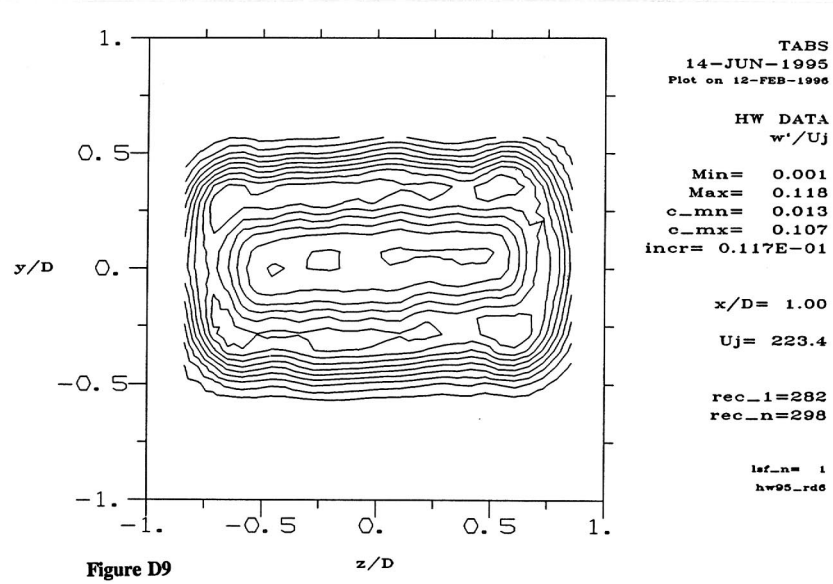

Figure D9

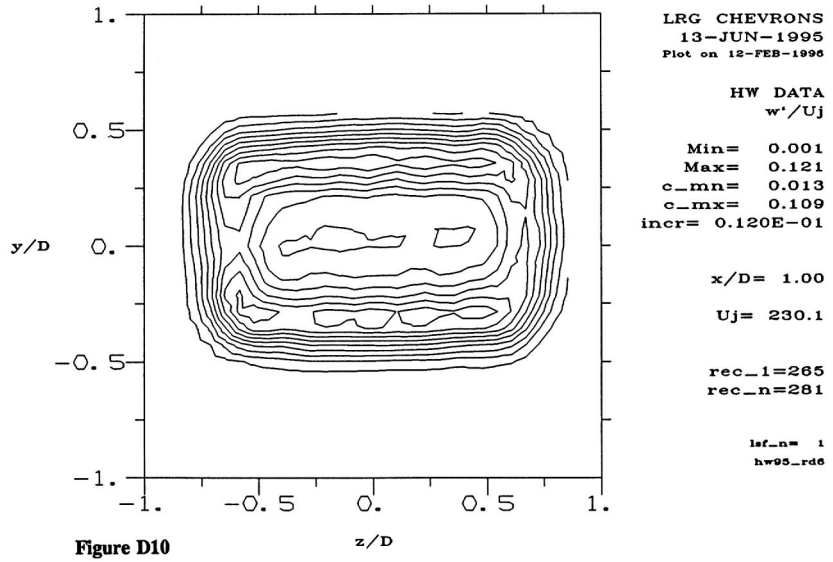

Figure D10

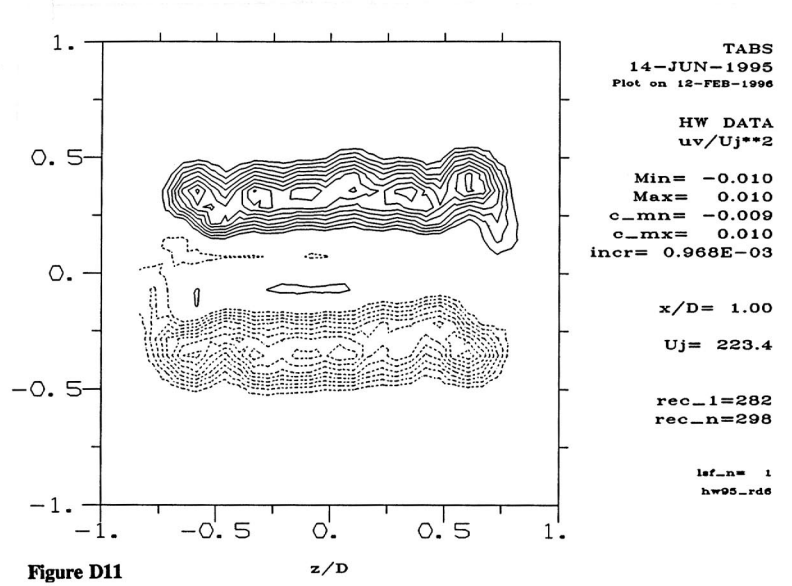

Figure D11

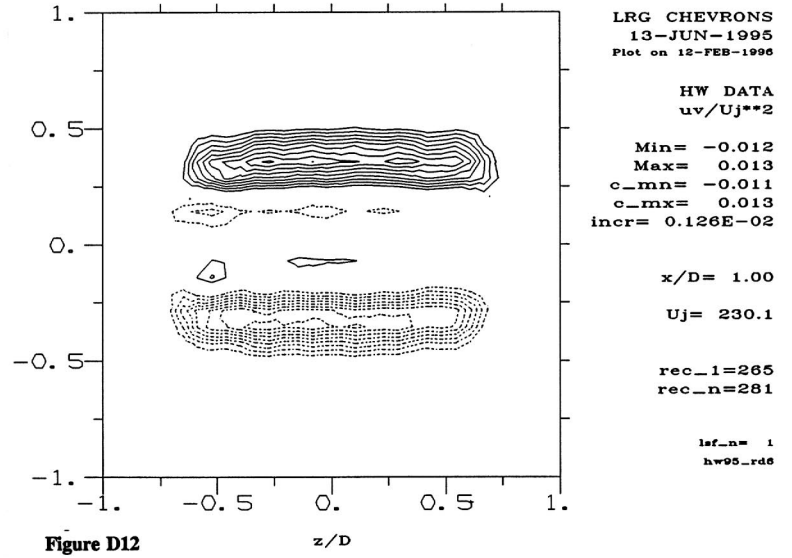

Figure D12

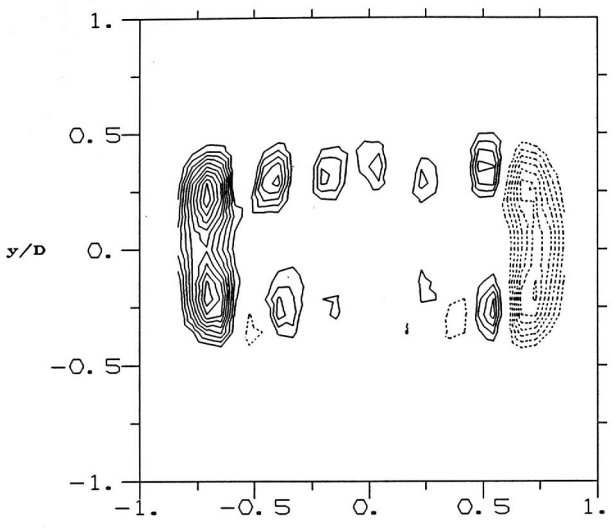

TABS
14-JUN-1995
Plot on 12-FEB-1996

HW DATA
uw/Uj**2

Min= -0.009
Max= 0.013
c_mn= -0.009
c_mx= 0.012
incr= 0.112E-02

x/D= 1.00

Uj= 223.4

rec_1=282
rec_n=298

lsf_n= 1
hw95_rd6

Figure D13

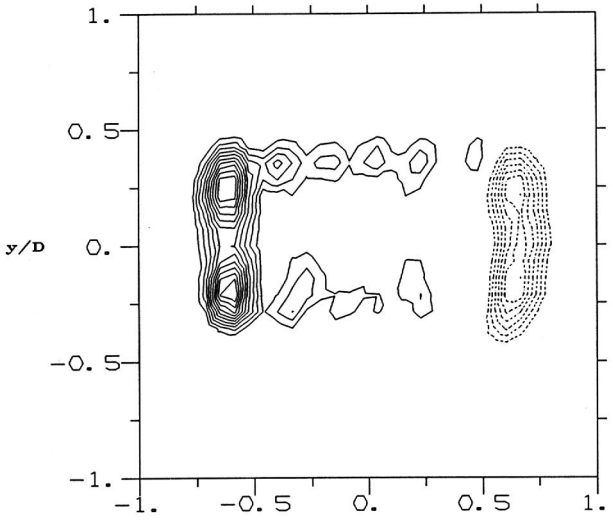

LRG CHEVRONS
13-JUN-1995
Plot on 12-FEB-1996

HW DATA
uw/Uj**2

Min= -0.007
Max= 0.011
c_mn= -0.007
c_mx= 0.010
incr= 0.894E-03

x/D= 1.00

Uj= 230.1

rec_1=265
rec_n=281

lsf_n= 1
hw95_rd6

Figure D14

REPORT DOCUMENTATION PAGE

Form Approved
OMB No. 0704-0188

1. AGENCY USE ONLY (*Leave blank*)	2. REPORT DATE	3. REPORT TYPE AND DATES COVERED
	July 2004	Technical Memorandum

4. TITLE AND SUBTITLE

An Experiment on the Near Flow Field of the GE/ARL Mixer Ejector Nozzle

5. FUNDING NUMBERS

WBS–22–714–09–46

6. AUTHOR(S)

K.B.M.Q. Zaman

7. PERFORMING ORGANIZATION NAME(S) AND ADDRESS(ES)

National Aeronautics and Space Administration
John H. Glenn Research Center at Lewis Field
Cleveland, Ohio 44135–3191

8. PERFORMING ORGANIZATION REPORT NUMBER

E–14589

9. SPONSORING/MONITORING AGENCY NAME(S) AND ADDRESS(ES)

National Aeronautics and Space Administration
Washington, DC 20546–0001

10. SPONSORING/MONITORING AGENCY REPORT NUMBER

NASA TM—2004-213113

11. SUPPLEMENTARY NOTES

This research was originally published internally as HSR040 in July 1996. Responsible person, K.B.M.Q. Zaman, organization code 5860, 216–433–5888.

12a. DISTRIBUTION/AVAILABILITY STATEMENT

Unclassified - Unlimited
Subject Categories: 02 and 07 Distribution: Nonstandard

Available electronically at http://gltrs.grc.nasa.gov

This publication is available from the NASA Center for AeroSpace Information, 301–621–0390.

12b. DISTRIBUTION CODE

13. ABSTRACT ***(Maximum 200 words)***

This report is a documentation of the results on flowfield surveys for the GE/ARL mixer-ejector nozzle carried out in an open jet facility at NASA Glenn Research Center. The results reported are for cold (unheated) flow without any surrounding co-flowing stream. Distributions of streamwise vorticity as well as turbulent stresses, obtained by hot-wire anemometry, are presented for a low subsonic condition. Pitot probe survey results are presented for nozzle pressure ratios up to 3.5. Flowfields both inside and outside of the ejector are considered. Inside the ejector, the mean velocity distribution exhibits a cellular pattern on the cross sectional plane, originating from the flow through the primary and secondary chutes. With increasing downstream distance an interchange of low velocity regions with adjacent high velocity regions takes place due to the action of the streamwise vortices. At the ejector exit, the velocity distribution is nonuniform at low and high pressure ratios but reasonably uniform at intermediate pressure ratios. The effects of two chevron configurations and a tab configuration on the evolution of the downstream jet are also studied. Compared to the baseline case, minor but noticeable effects are observed on the flowfield.

14. SUBJECT TERMS

Nozzles; Mixing; Ejector; Turbulence

15. NUMBER OF PAGES

57

16. PRICE CODE

17. SECURITY CLASSIFICATION OF REPORT	18. SECURITY CLASSIFICATION OF THIS PAGE	19. SECURITY CLASSIFICATION OF ABSTRACT	20. LIMITATION OF ABSTRACT
Unclassified	Unclassified	Unclassified	